An Investigation of Manganese Macro segregation in Cast Dual Phase Steels using Micro X-ray Fluorescence Spectroscopy

by

Tasneem Mahzabeen

A thesis
presented to the University of Waterloo
in fulfillment of the
thesis requirement for the degree of
Master of Applied Science
in
Mechanical and Mechatronics Engineering

Waterloo, Ontario, Canada, 2017

AUTHOR'S DECLARATION

I hereby declare that I am the sole author of this thesis. This is a true copy of the thesis, including any required final revisions, as accepted by my examiners.

I understand that my thesis may be made electronically available to the public.

Abstract

Advanced High Strength Steels with a high manganese content offer an exceptional balance of strength and ductility. However, the occurrence of segregation in these steels, particularly at the centerline, leads to quality control issues in continuous casting. Segregation, which is a non-uniform distribution of manganese in the as-cast structure, originates during solidification. Moreover, segregation of manganese during the continuous casting process can lead to the formation of detrimental martensite bands in subsequent manufacturing operations.

Traditionally, macro segregation, which occurs over large distances, has been measured using etching techniques that provide qualitative insights. As the attention on high Mn Advanced High Strength steels is increasing, it is imperative to develop more effective and quantitative methods of measurements. From literature, it is known that segregation is largely influenced by casting parameters such as casting speed and superheat. These parameters have a significant effect on the development and size of equiaxed and columnar zones in the as-cast structure.

This research investigates the effects of casting parameters such as the casting speed and superheat, nominal manganese concentration, and spatial orientation on the macro segregation present in as-cast Dual Phase 600 steels. A new analysis technique, using micro X-ray fluorescence, was used to quantitatively measure manganese macro segregation in industrially cast steels and create metrics to assess the macro segregation in the as-cast structure. This technique was validated against a current quantitative method.

To assess centerline segregation, four different metrics, using two distinct methods, were developed in this thesis. Each metric measures segregation in different ways, and ranges from calculating arithmetic means to determining segregation spatial sizes. The developed metrics shed light on the spatial behavior of manganese segregation as a function of the selected casting conditions and nominal manganese compositions.

Acknowledgements

I would like to thank my supervisor, Professor Mary Wells, for her guidance and support during my Master's degree. Her encouragements have been a key motivating factor to the completion of my thesis and the work it encompasses.

In addition, I would like to thank our industry partner, Arcelor Mittal Dofasco, and more specifically, from their R&D team in Hamilton, Dr. Joydeep Sengupta and Jackie Leung for access to their MXRF equipment, the procurement of materials, their recommendations regarding the experimental setup, as well as the direction of the overall project. Joydeep has been instrumental in this project, and I would like to thank him for all his input and industry experience to help guide the project. Additionally, I had the opportunity to work with three bright interns, Andrew D'Ziuba, Connie Pelligra and Amir Noorafkan. Each were involved in various stages of the project, from its inception to the final stages. In particular, I would like to thank Amir for procuring samples and conducting the experiments on my behalf. Overall, my thesis would not have been successfully complete without the help and dedication of the brilliant team from R&D Hamilton.

Also, I would like to thank Dr. Massimo DiCiano for all his contributions to this project. Massimo was always helpful whenever I needed advice, or just needed someone to discuss ideas with, and for that I am most grateful.

I would also like to acknowledge the Natural Sciences and Engineering Research Council of Canada for their financial support.

Finally, I'd like to thank Dr. John Wen and Dr. Norman Zhou for the time they took to read and evaluate my thesis, as well as their comments.

Dedication

I would like to dedicate this thesis to my parents, Matinur and Monowara Rahman. They have always encouraged me to do my best and keep moving through all the obstacles. They believed in me and saw my potential when I myself was unable to see it.

I will always be grateful to have you as parents.

Table of Contents

AUTHOR'S DECLARATION ii
Abstract iii
Acknowledgements iv
Dedication v
Table of Contents vi
List of Figures viii
List of Tables xv
Chapter 1 : Introduction 1
1.1 Motivation 4
1.2 Scope and Outline of Thesis 5
Chapter 2 : Literature Review 6
2.1 Continuous Casting 6
2.2 Solidification during Continuous Casting 8
2.3 Segregation and Casting 10
2.4 Key Casting Parameters 11
2.5 Current macro segregation evaluation techniques 12
2.6 Effect of Manganese in Dual Phase Steels 13
2.7 Segregation and Hot Rolling 14
2.7.1 Martensite Banding 15
Chapter 3 : Experimental Methodology 17
3.1 Sample Selection and Extraction 17
3.2 X-Ray Fluorescence Spectroscopy 18
3.2.1 Micro X-Ray Fluorescence Experimental Device 19
Chapter 4 : Results and Discussions 24
4.1 Typical Measured Data (Centerline and Far Field) 24
4.1.1 Comparison to a current technique 25
4.2 Centerline 27
4.2.1 Metrics Overview 27
4.2.2 Metric Development 28
4.2.3 Effects of Spatial Orientation 31
4.2.4 Effect of Casting Speed 33

4.2.5 Effect of Superheat 39
4.2.6 Effect of Nominal Mn Composition 44
4.3 Far Field 49
4.3.1 Metric Overview 49
4.3.2 Effect of Spatial Orientation 50
4.3.3 Effect of Casting Speed 51
4.3.4 Effect of Superheat 51
4.3.5 Effect of Nominal Mn Composition 52
4.4 Factors to Consider 53
4.4.1 Centerline 53
4.4.2 Far Field 62
Chapter 5 : Conclusions and Recommendations 63
References 64
Appendix A : Effect of Spatial Orientation on CL Segregation 68
Appendix B : Effect of Casting Speed on CL Segregation 74
Appendix C : Effect of Superheat on CL Segregation 82
Appendix D : Effect of Nominal Mn Composition on CL Segregation 93
Appendix E : Effect of Spatial Orientation on FF Segregation 113
Appendix F : Extended Factors to Consider 115

List of Figures

Figure 1: Comparison of tensile strength and elongation of AHSS grades [5] 1
Figure 2: Micrograph of a DP steel microstructure [15] 2
Figure 3: Schematic of a continuous casting process [19] 6
Figure 4: Schematic of in-mold phenomena [19] 7
Figure 5: Dimensions of slabs, blooms and billets [22] 8
Figure 6: Grain structure after solidification [25] 9
Figure 7: Schematic of dendritic solidification. The dark regions have higher solute concentrations [7] .. 10
Figure 8: a. Microstructure of the as-received steel b. Mn concentration map where the Mn concentration is greater in the regions indicated by white ovals [9] 14
Figure 9: Martensite bands seen in DP 780 on a longitudinal cross section at the center [36] 15
Figure 10: MXRF sample locations with respect to original steel slab 18
Figure 11: Schematic of main components in x-ray spectroscopy [39] 19
Figure 12: Schematic of scan area (red square box) and dimensional specifications 20
Figure 13: Effect of dwell time on Mn wt% detection 21
Figure 14: Frequency distributions of centerline data at different dwell times for Standard 1 22
Figure 15: Frequency distributions of centerline data at different dwell times for Standard 2 22
Figure 16: Repeatability results for 3000 ms on Standard 1 and 2 23
Figure 17: Schematic of three major modes of measurements available in MXRF systems 24
Figure 18: Example of a subset of normalized data 25
Figure 19: A comparison between current qualitative methods and quantitative method using the experimental data; surface etched using an ammonium cupric chloride after annealing; 1.5 Mn wt% and High Vc and High ΔT 26
Figure 20: Comparison between an element composition map and the corresponding segregation profile 28
Figure 21: Creation of segregation profile; red dash line indicates Row 4 while blue dash line locates Row 58; Note that standard deviation error bars have been excluded for clarity purposes 29
Figure 22: Development of Metrics A and C 30
Figure 23: Example of a 3 value system 31
Figure 24: Metrics A and C as a function of spatial orientation for a High V_c and High ΔT condition 32
Figure 25: Metrics A, B and D as a function of spatial orientation for a High Vc and High ΔT casting condition; Metric A and B uses a 1.09x filter and 3 value system 33
Figure 26: Metric A as a function of casting speed for 1.5 Mn wt% for a. a high ΔT and b. a low ΔT 34

Figure 27: Metric C as a function of casting speed for 1.5 Mn wt% a. Maximum normalized Mn for a high ΔT b. Maximum normalized Mn for a low ΔT c. 90th Percentile for a high ΔT d. 90th percentile for a low ΔT 34
Figure 28: Frequency distribution of normalized Mn at centerline of Sample A with High Vc and High ΔT casting condition 35
Figure 29: Metric A as a function of casting speed for 1.5 Mn wt% using a 3 value system 37
Figure 30: Metric B as a function of casting speed for 1.5 Mn wt% using factors 1.03x, 1.06x, 1.09x and a 3 value system 37
Figure 31: Metric D as a function of casting speed for 1.5 Mn wt% using factors 1.03x, 1.06x, 1.09x 38
Figure 32: Method 1 and Metrics A and C as a function of superheat for 1.5 Mn wt% 39
Figure 33: Metric A as a function of superheat for 1.5 Mn wt% using factors 1.03x, 1.06x, 1.09x and 2 and 3 value systems 41
Figure 34: Metric B as a function of superheat for 1.5 Mn wt% using factors 1.03x,1.06x, 1.09x and 2 and 3 value systems 42
Figure 35: Metric D as a function of superheat for 1.5 Mn wt% using factors 1.03x, 1.06x, 1.09x 43
Figure 36: Metrics A and C as a function of 1.5 and 1.85 Mn wt% 44
Figure 37: Metrics A and C as a function of 1.5 and 2.1 Mn wt% 45
Figure 38: Metric A as a function of nominal composition of 1.5, 1.85 and 2.1 Mn wt% using a 3 value system 47
Figure 39: Metric B as a function of nominal composition of 1.5, 1.85 and 2.1 Mn wt% using factors 1.03x,1.06x, 1.09x and a 3 value system 48
Figure 40: Metric D as a function of nominal composition of 1.5, 1.85 and 2.1 Mn wt% using factors 1.03x, 1.06x, 1.09x 49
Figure 41: Fixed area used to calculate far field average 50
Figure 42: Far field average of the normalized Mn as a function of spatial orientation for a High Vc and High ΔT casting condition 50
Figure 43: Effect of Vc in the far field for a. a high ΔT b. a low ΔT 51
Figure 44: Effect of ΔT in the far field 52
Figure 45: Effect of Nominal Mn composition in the far field 52
Figure 46: Comparison between 1 mm and 0.5 mm spatial resolutions 54
Figure 47: An overlap of centerline frequency distributions of 1 and 0.5 mm spatial resolution scans of Sample A with High Vc and high ΔT casting condition 54

Figure 48: Comparison of a. Metric A b. Metric C for Sample A with High V_c and High ΔT casting condition 55
Figure 49: Metric A on 1 mm and 0.5 mm spatial resolution scans 56
Figure 50: Metric B on 1 mm and 0.5 mm spatial resolution scans 57
Figure 51: Metric D on 1 mm and 0.5 mm spatial resolution scans 58
Figure 52: Metric A using 4 value system and 1.03x, 1.06x and 1.2x factors 60
Figure 53: Metric A using 1 vs 4 value system using a 1.09x factor 61
Figure 54: Segregation profile for medium casting speed and high superheat condition 62
Figure 55: Method 1 and Metrics A and C as a function of spatial orientation for a High Vc and Low ΔT condition 68
Figure 56: Method 1 and Metrics A and C as a function of spatial orientation for a Medium Vc and High ΔT condition 69
Figure 57: Method 1 and Metrics A and C as a function of spatial orientation for a Medium Vc and Low ΔT condition 69
Figure 58: Method 1 and Metrics A and C as a function of spatial orientation for a Low Vc and High ΔT condition 70
Figure 59: Method 1 and Metrics A and C as a function of spatial orientation for a Low Vc and Low ΔT condition 70
Figure 60: Method 2 and Metric A as a function of spatial orientation for five casting conditions using 1.09x and a 3 value system 71
Figure 61: Metric B as a function of spatial orientation for five casting conditions using 1.09x and a 3 value system 72
Figure 62: Metric D as a function of spatial orientation for five casting conditions using 1.09x 73
Figure 63: Method 2 and Metric A as a function of casting speed for 1.5 Mn wt% using factors 1.03x, 1.06x, 1.09x and a 1 value system 74
Figure 64: Method 2 and Metric A as a function of casting speed for 1.5 Mn wt% using factors 1.03x, 1.06x, 1.09x and a 2 value system 74
Figure 65: Method 2 and Metric A as a function of casting speed for 1.5 Mn wt% using factors 1.03x, 1.06x, 1.09x and a 4 value system 75
Figure 66: Metric B as a function of casting speed for 1.5 Mn wt% using factors 1.03x, 1.06x, 1.09x and a 1 value system 75

Figure 67: Metric B as a function of casting speed for 1.5 Mn wt% using factors 1.03x, 1.06x, 1.09x and a 2 value system 76
Figure 68: Metric B as a function of casting speed for 1.5 Mn wt% using factors 1.03x, 1.06x, 1.09x and a 4 value system 76
Figure 69: Metric B as a function of casting speed for 1.5 Mn wt% using factors 1.04x, 1.05x, 1.07x and a 1 value system 77
Figure 70: Metric B as a function of casting speed for 1.5 Mn wt% using factors 1.04x, 1.05x, 1.07x and a 2 value system 77
Figure 71: Metric B as a function of casting speed for 1.5 Mn wt% using factors 1.04x, 1.05x, 1.07x and a 3 value system 78
Figure 72: Metric B as a function of casting speed for 1.5 Mn wt% using factors 1.04x, 1.05x, 1.07x and a 4 value system 78
Figure 73: Metric B as a function of casting speed for 1.5 Mn wt% using factors 1.08x, 1.1x, 1.2x and a 1 value system 79
Figure 74: Metric B as a function of casting speed for 1.5 Mn wt% using factors 1.08x, 1.1x, 1.2x and a 2 value system 79
Figure 75: Metric B as a function of casting speed for 1.5 Mn wt% using factors 1.08x, 1.1x, 1.2x and a 3 value system 80
Figure 76: Metric B as a function of casting speed for 1.5 Mn wt% using factors 1.08x, 1.1x, 1.2x and a 4 value system 80
Figure 77: Metric D as a function of casting speed for 1.5 Mn wt% using factors 1.04x, 1.05x and 1.07x 81
Figure 78: Metric D as a function of casting speed for 1.5 Mn wt% using factors 1.08x, 1.1x and 1.2x 81
Figure 79: Method 2 and Metric A as a function of superheat for 1.5 Mn wt% using factors 1.03x, 1.06x, 1.09x and 1 and 4 value systems 82
Figure 80: Method 2 and Metric A as a function of superheat for 1.5 Mn wt% using factors 1.04x, 1.05x, 1.07x and 1 and 4 value systems 83
Figure 81: Method 2 and Metric A as a function of superheat for 1.5 Mn wt% using factors 1.04x, 1.05x, 1.07x and 2 and 3 value systems 84
Figure 82: Method 2 and Metric A as a function of superheat for 1.5 Mn wt% using factors 1.08x, 1.1x, 1.2x and 1 and 4 value systems 85

Figure 83: Method 2 and Metric A as a function of superheat for 1.5 Mn wt% using factors 1.08x, 1.1x, 1.2x and 2 and 3 value systems 86
Figure 84: Metric B as a function of superheat for 1.5 Mn wt% using factors 1.03x, 1.06x, 1.09x and 1 and 4 value systems 87
Figure 85: Metric B as a function of superheat for 1.5 Mn wt% using factors 1.04x, 1.05x, 1.07x and 1 and 4 value systems 88
Figure 86: Metric B as a function of superheat for 1.5 Mn wt% using factors 1.04x, 1.05x, 1.07x and 2 and 3 value systems 89
Figure 87: Metric B as a function of superheat for 1.5 Mn wt% using factors 1.08x, 1.1x, 1.2x and 1 and 4 values 90
Figure 88: Metric B as a function of superheat for 1.5 Mn wt% using factors 1.08x, 1.1x, 1.2x and 2 and 3 values 91
Figure 89: Metric D as a function of superheat for 1.5 Mn wt% using factors 1.04x, 1.05x, 1.07x, 1.08x, 1.1x and 1.2x 92
Figure 90: Metric A as a function of nominal composition of 1.5, 1.85 and 2.1 Mn wt% using factors 1.03x, 1.06x and 1.09x and a 1 value system 93
Figure 91: Metric A as a function of nominal composition of 1.5, 1.85 and 2.1 Mn wt% using factors 1.03x, 1.06x and 1.09x and a 2 value system 94
Figure 92: Metric A as a function of nominal composition of 1.5, 1.85 and 2.1 Mn wt% using factors 1.03x, 1.06x and 1.09x and a 4 value system 95
Figure 93: Metric A as a function of nominal composition of 1.5, 1.85 and 2.1 Mn wt% using factors 1.04x, 1.05x and 1.07x and a 1 value system 96
Figure 94: Metric A as a function of nominal composition of 1.5, 1.85 and 2.1 Mn wt% using factors 1.04x, 1.05x and 1.07x and a 2 value system 97
Figure 95: Metric A as a function of nominal composition of 1.5, 1.85 and 2.1 Mn wt% using factors 1.04x, 1.05x and 1.07x and a 3 value system 98
Figure 96: Metric A as a function of nominal composition of 1.5, 1.85 and 2.1 Mn wt% using factors 1.04x, 1.05x and 1.07x and a 4 value system 99
Figure 97: Metric B as a function of nominal composition of 1.5, 1.85 and 2.1 Mn wt% using factors 1.03x, 1.06x and 1.09x and a 1 value system 100
Figure 98: Metric B as a function of nominal composition of 1.5, 1.85 and 2.1 Mn wt% using factors 1.03x, 1.06x and 1.09x and a 2 value system 101

Figure 99: Metric B as a function of nominal composition of 1.5, 1.85 and 2.1 Mn wt% using factors 1.03x, 1.06x and 1.09x and a 4 value system..... 102
Figure 100: Metric B as a function of nominal composition of 1.5, 1.85 and 2.1 Mn wt% using factors 1.04x, 1.05x and 1.07x and a 1 value system..... 103
Figure 101: Metric B as a function of nominal composition of 1.5, 1.85 and 2.1 Mn wt% using factors 1.04x, 1.05x and 1.07x and a 2 value system..... 104
Figure 102: Metric B as a function of nominal composition of 1.5, 1.85 and 2.1 Mn wt% using factors 1.04x, 1.05x and 1.07x and a 3 value system..... 105
Figure 103: Metric B as a function of nominal composition of 1.5, 1.85 and 2.1 Mn wt% using factors 1.04x, 1.05x and 1.07x and a 4 value system..... 106
Figure 104: Metric B as a function of nominal composition of 1.5, 1.85 and 2.1 Mn wt% using factors 1.08x, 1.1x and 1.2x and a 1 value system..... 107
Figure 105: Metric B as a function of nominal composition of 1.5, 1.85 and 2.1 Mn wt% using factors 1.08x, 1.1x and 1.2x and a 2 value system..... 108
Figure 106: Metric B as a function of nominal composition of 1.5, 1.85 and 2.1 Mn wt% using factors 1.08x, 1.1x and 1.2x and a 3 value system..... 109
Figure 107: Metric B as a function of nominal composition of 1.5, 1.85 and 2.1 Mn wt% using factors 1.08x, 1.1x and 1.2x and a 4 value system..... 110
Figure 108: Metric D as a function of nominal composition of 1.5, 1.85 and 2.1 Mn wt% using factors 1.04x, 1.05x, 1.07x..... 111
Figure 109: Metric D as a function of nominal composition of 1.5, 1.85 and 2.1 Mn wt% using factors 1.08x, 1.1x, 1.2x..... 112
Figure 110: Far field average of the normalized Mn as a function of spatial orientation for 1.5 Mn wt% 113
Figure 111: A comparison of the far field average as a function of spatial orientation for 1.5, 1.85 and 2.1 Mn wt%..... 114
Figure 112: Metric A using 1 mm and 0.5 mm spatial resolution scans with factors 1.03x, 1.06x, 1.09x and 1 and 4 value system 115
Figure 113: Metric B using 1 mm and 0.5 mm spatial resolution scans with factors 1.03x, 1.06x, 1.09x and 1 and 4 value system 116
Figure 114: Method 2 and Metric A as a function of superheat for 1.5 Mn wt% using factors 1.03x, 1.06x, 1.09x and 1 and 4 value systems..... 117

Figure 115: Method 2 and Metric A as a function of superheat for 1.5 Mn wt% using factors 1.04x, 1.05x, 1.07x and 1 and 4 value systems 118
Figure 116: Method 2 and Metric A as a function of superheat for 1.5 Mn wt% using factors 1.04x, 1.05x, 1.07x and 2 and 3 value systems 119
Figure 117: Method 2 and Metric A as a function of superheat for 1.5 Mn wt% using factors 1.08x, 1.1x, 1.2x and 1 and 4 value systems 120
Figure 118: Method 2 and Metric A as a function of superheat for 1.5 Mn wt% using factors 1.08x, 1.1x, 1.2x and 2 and 3 value systems 121
Figure 119: Metric B as a function of superheat for 1.5 Mn wt% using factors 1.03x, 1.06x, 1.09x and 1 and 4 value systems 122
Figure 120: Metric B as a function of superheat for 1.5 Mn wt% using factors 1.04x, 1.05x, 1.07x and 1 and 4 value systems 123
Figure 121: Metric B as a function of superheat for 1.5 Mn wt% using factors 1.04x, 1.05x, 1.07x and 2 and 3 value systems 124
Figure 122: Metric B as a function of superheat for 1.5 Mn wt% using factors 1.08x, 1.1x, 1.2x and 1 and 4 values 125
Figure 123: Metric B as a function of superheat for 1.5 Mn wt% using factors 1.08x, 1.1x, 1.2x and 2 and 3 values 126
Figure 124 Metric D as a function of superheat for 1.5 Mn wt% using factors 1.04x, 1.05x, 1.07x, 1.08x, 1.1x and 1.2x 127

List of Tables

Table 1: Effect of common alloying elements in DP grades [15] 3
Table 2: Equilibrium Partition Ratios for Various Elements in Steel [7] 11
Table 3: Typical DP600 alloy chemistry 17
Table 4: Variation in Vc and ΔT 17
Table 5: Overview of Metrics A – D to evaulate centreline segregation 27
Table 6: P values for statistical tests (1.5 Mn wt%) 36
Table 7: P values for statistical tests on superheat results (1.5 Mn wt%) 40
Table 8: P values for statistical tests (1.5 vs 1.85 vs 2.1 Mn wt%) 46

Chapter 1: Introduction

Presently, a significant interest has been expressed by the steel industry for the development of the next generation of high manganese, Mn, Advanced High Strength Steels, AHSS [1] [2] [3] [4] [5]. AHSS products meet the competitive requirements for excellent combinations of mechanical properties such as strength, formability, etc. [5].

AHSS steels comprise of complex, multiple constituents which provide a blend of strength and ductility. Phases such as martensite, bainite and ultrafine grained ferrite provide high strength, while constituents such as austenite and ferrite promote high ductility [5]. The type of microstructure present and final mechanical properties relies on the specific grade of AHSS and processing routes taken. Figure 1 shows an overview of the tensile strengths and elongation of current AHSS grades, compared to conventional steel grades. The mechanical properties of AHSS steels are heavily influenced by the overall Mn composition. Traditionally, Mn is used in steels for the stabilization of sulphur, solid solution strengthening and avoidance of hot shortness [6]. However, Mn is also known to be an austenite stabilizer [7] [6] [8] [9] [10] [11]. This alloying effect of Mn is used extensively in AHSS grades to obtain a mix of strength and ductility [6]. Thus, Mn is an important alloying element for the design of AHSS grades. The effects of Mn as an alloying element, and the consequences surrounding its addition will be explored in later chapters.

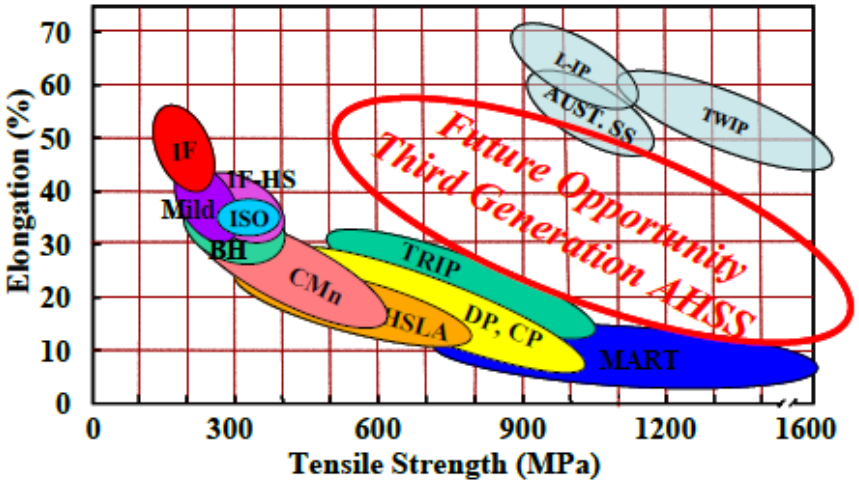

Figure 1: Comparison of tensile strength and elongation of AHSS grades [5]

As seen in Figure 1, mild steels such as Interstitial Free, IF, steels, have low strength and high formability. IF steels contain low amounts of carbon, resulting in lower strength, and yet, they were once the leading material used in vehicle bodies. On the other hand, high strength low alloy, HSLA, steels offer higher tensile strengths. This is due to the addition of micro alloying elements such as titanium, vanadium, niobium, etc. However, as seen in Figure 1, this increase in strength compromises elongation significantly. HSLA was one of the first high strength steels used in the automotive industry. However, due to the better combination of strength and elongation, AHSS grades such as Dual Phase, DP, steels are replacing HSLA grades in energy absorbing areas [12] [13] [14].

DP steel microstructures mainly comprise of ferrite and martensite, as shown in Figure 2, with small amounts of retained austenite and bainite [15]. The final microstructure is dependent on the processing routes taken such as hot rolling, cold rolling, and hot dip galvanized [5]. Improved strength and formability, good weldability, easy processing and availability are some of the many benefits offered by DP steels. Thus, there is an interest in producing DP steels with superior mechanical properties [5]. DP steels are currently the primary AHSS grades being utilized in the automotive industry [5] [4].

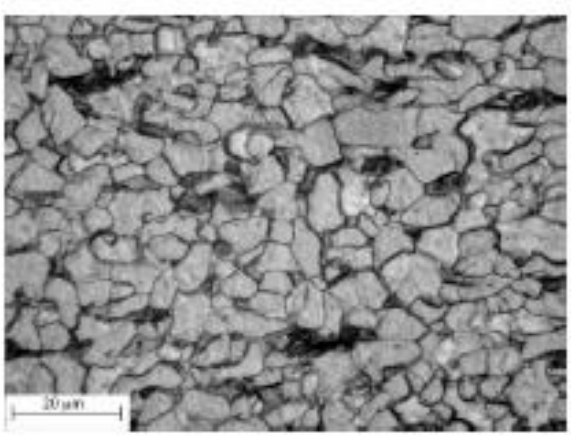

Figure 2: Micrograph of a DP steel microstructure [15]

Strength in DP steels is controlled by the volume fraction of martensite, which is typically around 10 to 40% [5] [15]. Additionally, the size and distribution of martensite influences the amount of ductility

[5] [15]. The addition of Mn helps produce martensite upon cooling. A summary of the main alloying elements and their effects are shown in the Table 1 below [15].

Table 1: Effect of common alloying elements in DP grades [15]

Alloying Element	Effect
C (0.06 – 0.15%)	• Stabilizes austenite • Strengthens martensite • Determines phase distribution
Mn (1.5 – 2.5%)	• Stabilizes austenite • Strengthens ferrite solid solutioning • Retards ferrite formation
Si	• Promotes ferritic transformation
Cr, Mo (up to 4%)	• Stabilizes austenite • Retards formation of pearlite and bainite
V (up to 0.06%)	• Stabilizes austenite • Strengthens precipitation • Refines microstructure
Nb (up to 0.04%)	• Stabilizes austenite • Reduces M_s temperature • Refines microstructure and promotes transformation of non-recrystallized austenite to ferrite

Another AHSS grade, call Transformation-Induced Plasticity, TRIP, steels also make use of high Mn contents [4]. TRIP steels have multi-phase microstructures, with retained austenite, ferrite, bainite and martensite. During deformation, the applied strain or stress can induce transformations in the retained austenite, leading to the formation of martensite. This results in higher ductility [15] [16]. TRIP steels typically contain up to 15 to 20 Mn weight percent, wt%. A second group of high Mn steels, known as

Twinning Induced Plasticity, TWIP, contains above 25 Mn wt%, to obtain high ductility with the use of extensive mechanical twinning [16].

It is well known that mechanical properties are greatly affected by the processing routes and parameters that were applied to the material. DP, TRIP and TWIP steels undergo numerous processes, starting from continuous casting, to hot or cold rolling to hot galvanizing. For all grades, numerous technological issues, which begins with continuous casting, have hindered the use of high Mn contents, despite the benefits [3]. More specifically, during continuous casting, macro and micro segregation of Mn occurs as the solidification process ensues. This results in local inhomogeneities of Mn in the solidified as-cast structure and affects microstructural development and mechanical properties during subsequent forming operations [4]. The control of segregation will improve quality control in current AHSS grades and pave the path for practical casting and steelmaking of higher Mn AHSS grades. In addition to segregation, other difficulties include the susceptibility to tear or high cracking during solidification, effects of aluminum interaction with mold powder, and effects of alloying elements such as aluminum, manganese and silicon on solidification characteristics [17] [18].

1.1 Motivation

As mentioned, the segregation of Mn during continuous casting has hindered the production and development of AHSS grades. The aim to enhance quality control on current AHSS grades and widen the scope to casting AHSS grades with much larger Mn contents led to the realization that a better understanding of Mn macro segregation in the as-cast structure is required to fully understand and control the casting of these steels.

A comprehensive analysis on the effects of various factors such as slab spatial orientation, casting parameters and nominal Mn composition on the as-cast structure is thus required. This understanding will provide a means of enhancing quality control during and after casting. It will also lay the foundation for subsequent examinations related to the formation of martensite bands and their implications on the mechanical properties and quality of AHSS steels during and after forming processes such as hot and cold rolling.

1.2 Scope and Outline of Thesis

This thesis will focus on the quantitative measurement of Mn segregation and the development and assessment of metrics to observe the effects of slab spatial orientation, casting parameters and nominal Mn compositions on Mn macro segregation in the as-cast structure of DP steels.

Results from this thesis can be used by in the steel making industry and the broader steel research community to better understand and quantify factors affecting macro segregation and improve castability of high Mn AHSS grades.

Chapter 2: Literature Review

2.1 Continuous Casting

Continuous casting is a widely used commercial steelmaking process through which a majority of the 750 million tons of annual steel produced worldwide is created [19]. The implementation of this process was advised in 1856 by Henry Bessemer. During the 1930s and 1940s, this type of casting was used for nonferrous material, and then in the 1960s, its application was extended to steels. Continuous casting provided several benefits over traditional ingot casting methods, including improvements in steel quality, through-puts, energy usage and manpower [20].

The principle governing continuous casting is relatively simple. A schematic of the commonly used vertical curved caster and the overall process is shown in Figure 3.

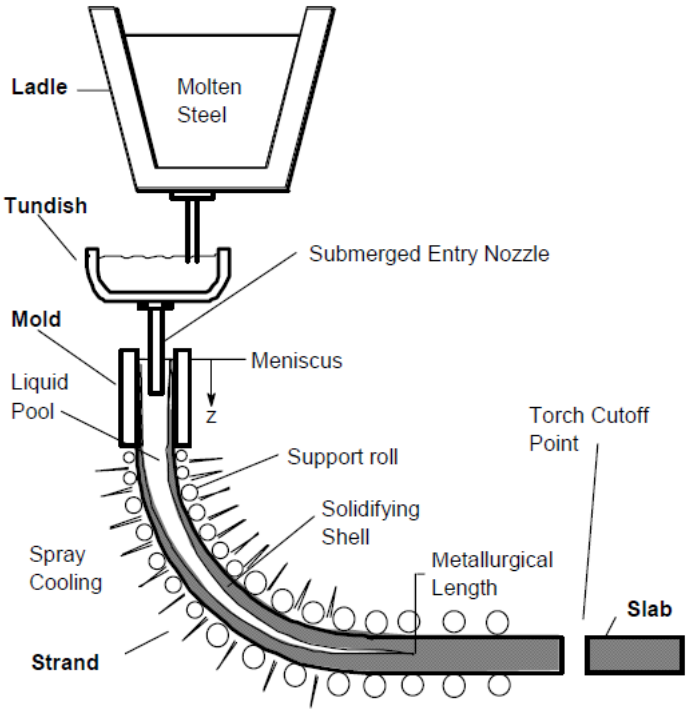

Figure 3: Schematic of a continuous casting process [19]

Liquid steel, heated above the liquidus temperature, is tapped in to a ladle from an electric or basic oxygen furnace [21]. A turret then rotates the ladle and transfers the liquid from the ladle to the tundish. A nozzle at the bottom of the ladle is opened to allow the molten steel to enter the tundish. This submerged entry nozzle controls the flow rate as the liquid fills one or multiple water-cooled copper molds. Once in the mold, solidification first begins at the mold and metal interface. The liquid then solidifies against the mold walls to form a solid shell [20] [21]. The solidification process will be explained in the following section. A schematic of the complex and intricate phenomena that occur in the melt as it begins to solidify, is shown in Figure 4.

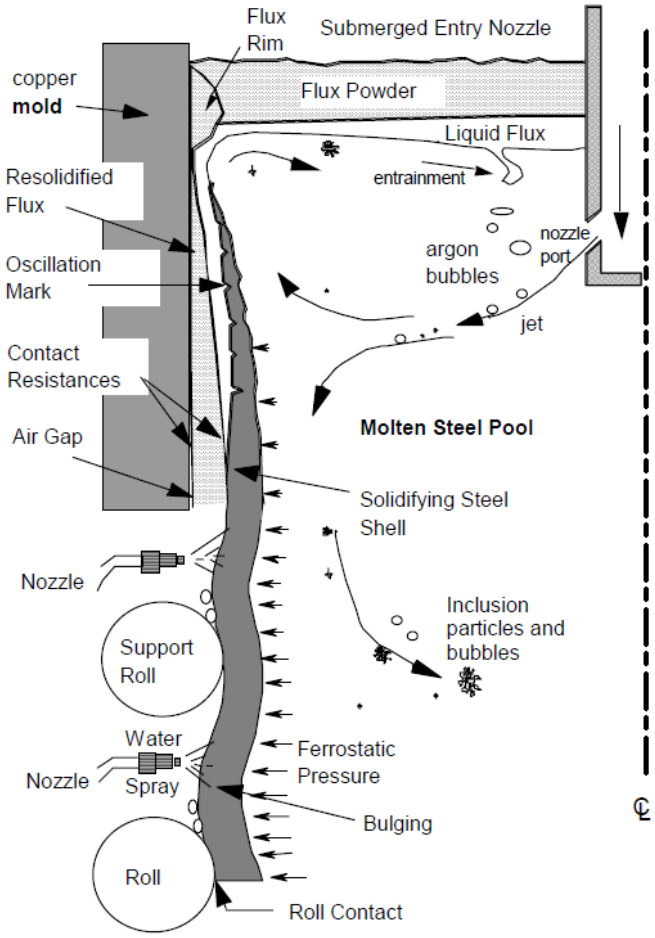

Figure 4: Schematic of in-mold phenomena [19]

The mold's main function is to form a solid shell that can contain the still liquid core once it is withdrawn. Cool water within the molds is used to transfer heat away from the liquid, aiding in the process of solidification [20] [21]. A few key factors to monitor in the mold are, shell shape and thickness, temperature distribution, and internal and surface quality to minimize non-metallic inclusions and, porosity [19].

When the solid shell has reached an appropriate thickness, the shell is gradually removed from the mold and guided through a curved arrangement of support rolls. It is then cooled by spraying water and air in between supporting rolls while being aligned horizontally. After the center has fully solidified, the strand is then torch cut into, depending on the size and shape, slabs, billets or blooms [20] [21]. See Figure 5.

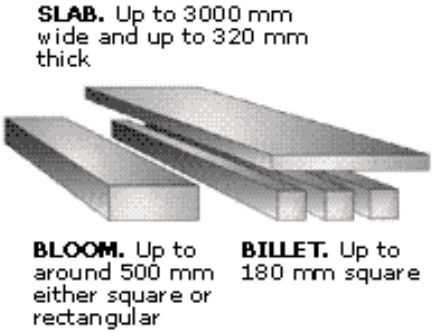

Figure 5: Dimensions of slabs, blooms and billets [22]

2.2 Solidification during Continuous Casting

Crystallization begins with the formation of large amounts of stable nuclei and the removal of latent heat and superheat. These two conditions are met at the liquid and metal interface. A series of small, equiaxed grains form at this interface, and create the chill zone. As the steel solidifies, latent heat is released in to the surrounding melt, leading to a decrease in undercooling and a reduction of rapid grain growth. Eventually, fractions of the small equiaxed grains which have favorable growth axis begin to grow outward from the chill zone and in the opposite direction of heat flow. This leads to the formation of columnar grains. The columnar zone ends when the temperature of the adjacent fluid increases

sufficiently due to the release of latent heat. Next, larger equiaxed grains form in the central region [23] [24]. A schematic of the different grain zones is shown in Figure 6.

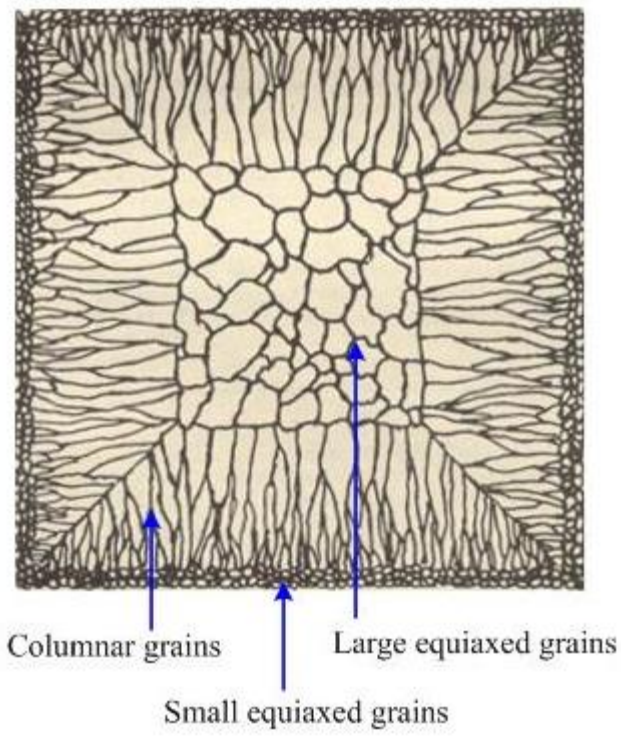

Figure 6: Grain structure after solidification [25]

Akin to most commercial steels, both equiaxed and columnar zones are dendritic. The word dendrite is derived from the Greek word for tree, and evidently it is named appropriately as its structure is tree-like. Dendrites grow opposite to the direction of heat flow and typically consists of primary, secondary and even tertiary arms. The surface energy in most metals is anisotropic and favors growth in specific direction. Thus, dendritic growth is encouraged. The driving force for dendritic growth, and hence the growth of equiaxed and columnar zones, is the undercooling of the melt. As the undercooling increases, the Gibbs free energy difference between liquid and solid state increases as well, making it favorable for solidification and the formation of equiaxed and columnar zones [24] [25].

2.3 Segregation and Casting

The solidification process during continuous casting causes macroscopic and microscopic segregation of elements [7]. This segregation leads to a non-uniform distribution of elements in the as-cast steel.

Macroscopic segregation refers to non-uniform chemical composition of elements over a macroscopic distance [26]. It is seen most prevalently at the centerline of as-cast steels [7]. Macroscopic segregation is primarily caused by mass flow of the solute rich liquid away from the growing solidification front [27]. Mass movement can be caused by convection forces, the motion of the liquid during pouring, and gravitational forces on growing crystals [27]. The macroscopic level of this type of segregation makes it impossible to obtain chemical homogeneity despite extended heat treatments [26].

Microscopic segregation occurs in between dendrites as liquid steel solidifies. During solidification, columnar dendrites grow outward from the chill zone, and eject solutes in to the liquid portion, as shown in Figure 7.

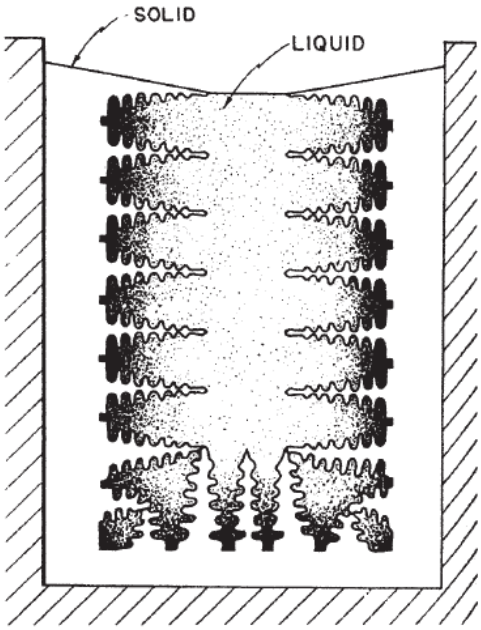

Figure 7: Schematic of dendritic solidification. The dark regions have higher solute concentrations [7]

The size of columnar zones, more specifically, the secondary dendrite arm spacing, largely controls the amount of micro segregation present at the end of the solidification process [7]. The ejection of solutes in to the liquid is driven by equilibrium partitioning of elements within the liquid and solid phase field. Equilibrium partitioning constants, k, of several elements are shown in Table 2.

Table 2: Equilibrium Partition Ratios for Various Elements in Steel [7]

Element	k
P	0.14
Nb	0.23
Cr	0.33
Mn	0.71
Ni	0.83

Solutes with low k values tend to segregate more. However, the concentration of the solute also plays a vital role. From Table 2, it appears that in alloy steels with phosphor and manganese, phosphor solutes will segregate more than manganese solutes. Yet, in most low carbon alloy steels, the concentration of manganese is much greater than phosphor. Hence, regardless of a low k value, manganese tends to segregate the most [7].

2.4 Key Casting Parameters

Controlling the size of the columnar zone can greatly affect the amount of segregation, especially at the centerline [26]. To suppress the growth of the columnar zone, it is necessary that a sufficient amount of equiaxed crystals are present ahead of the columnar front. Contrary to columnar dendrites, equiaxed crystals eject solutes uniformly within the mushy zone, resulting in a significant reduction in segregation [26] [28]. Casting parameters such as low superheats, and slow casting speeds, along with the addition of electromagnetic stirring have been investigated to accelerate the columnar to equiaxed zone transition [7] [26] [29].

It is well established in literature that low superheats can help reduce centerline segregation [28]. Less segregation occurs if there are more equiaxed grains present, as opposed to columnar grains. Newly nucleated crystals can develop to become equiaxed grains if the liquid surrounding them is at a temperature that is lower than the melting temperature [28]. At low superheats, the crystals can sink down the mold and become deposited in front of the columnar grain front. This results in a smaller columnar zone. At high superheats, fewer nuclei are seen due to the higher temperature of the surrounding bulk liquid. Thus, a larger columnar grain section is seen, resulting in a larger level of segregation [28]. However, one of the major issues with using low superheats is nozzle clogging [29]. The effectiveness of in-mold electromagnetic stirring has been correlated to its ability to remove superheat and allow for a larger quantity of equiaxed crystals [28].

Casting speed is another well-known casting parameter that can affect segregation during continuous casting. Increasing the casting speed reduces the amount of time in the mold, and thereby limiting the amount of heat transfer occurring and the solidification rate. This reduction of in-mold time leads to a longer time required for the removal of superheat. This in turn delays the nucleation and growth of equiaxed crystals, which plays a vital role in arresting the columnar growth front. Furthermore, it is also imperative to acknowledge the effect of casting speed on the solid shell thickness below the mold. The solid shell must be stable enough to prevent break-outs and withstand bulging [27]. Bulging can also result in an increase of macro segregation. During bulging a weak solid shell expands, and causes the solute rich interdendritic liquid to be drawn to the center because of ferrostatic forces. The solute rich liquid cools within the center, and results in centerline macro segregation. Bulging may occur if the support rolls are too far apart, and is promoted at higher casting speeds due to a weaker solid shell after the mold [27]. Other machine factors that can affect bulging are improper roll alignment, improper roll pitch, etc. [30].

2.5 Current macro segregation evaluation techniques

Currently, segregation investigation in the as-cast structure is predominantly qualitative. These techniques typically comprise of an initial visual inspection of a macro etched surface, followed by the application of internal rating systems, applied on digital images of the macrostructure. Macrostructures are typically revealed using chemical etchants such as sulphur or Baumann prints, Oberhoffer reagent and

hydrochloric acid [26] [31] [32]. The results from initial inspections, etching treatments, image quality, and subsequent severity ratings differ not just from one steelmaker to another, but it also varies from plant to plant. Thus, current practices lead to labor intensive procedures, limitations on sample sizes and more importantly, introduces subjectivity in quality control. Likewise, qualitative techniques offer no numerical insights into the segregation.

In response to this lack of standardization and data collection, efforts have been made to shift towards more quantitative methods of assessing segregation. Studies have investigated segregation using quantitative methods such as Optical Electron Spectroscopy, OES, Energy Dispersive x-ray, Electron Probe Micro Analysis, and X-ray fluorescence, XRF [26] [33] [34] [2] [35]. However, a comprehensive characterization of the as-cast structure of DP steels and a corresponding assessment of macro segregation at the centerline has yet to be undertaken.

2.6 Effect of Manganese in Dual Phase Steels

As an alloying element, Mn stabilizes austenite by lowering the Ar_3 temperature at which austenite transforms to ferrite upon cooling [7] [8] [9] [10] [11]. Steels with segregation often have lean and rich areas of local Mn concentrations [7]. Solute rich regions have a lower Ar_3 temperature than solute lean regions [7]. Upon cooling, ferrite first forms in the low solute areas of austenite, causing carbon to be ejected in to the rich solute areas [7]. These rich Mn areas eventually form pearlite, and upon accelerated cooling, martensite and bainite, as shown in Figure 8 [7] [9] [10].

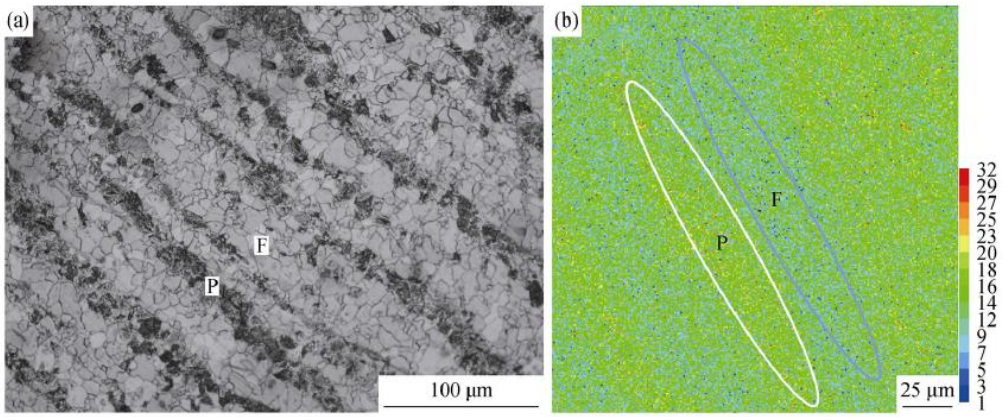

Figure 8: a. Microstructure of the as-received steel b. Mn concentration map where the Mn concentration is greater in the regions indicated by white ovals [9]

Mn also inhibits carbon activity in austenite, and thereby trapping carbon in Mn rich zones [7] [11].

2.7 Segregation and Hot Rolling

Although the origin of chemical segregation is from solidification, hot rolling and heat treatments cause further chemical partitioning during diffusion controlled solid state transformations [7]. Furthermore, deformation during hot rolling aligns solute lean and rich zones into bands parallel to the rolling direction. This produces alternating bands of high and low concentrations of various solute elements. Thus, the combined segregation from solidification and solid-state phase transformations lead to banded structures in semi-finished and finished steel products [7].

Studies reveal that long holding times and high temperatures are needed to reduce, or eliminate micro segregation. Substitutional elements with low diffusion coefficients, such as Mn, react slowly to the homogenizing effects of hot rolling. Therefore, the holding times and temperatures found in these studies are incompatible with modern steel mill productivity [7].

The underlying cause of banding can be primarily attributed to the residual interdendritic micro and larger scale macro segregation, and can be controlled during the casting process [7]. The

microstructural appearance of banding, in the form of equilibrium and non-equilibrium constituents, can be controlled through hot rolling parameters such as cooling rate, coiling temperature, deformation strain, finish roll temperature, inter-critical annealing temp, etc. [7].

2.7.1 Martensite Banding

Banding is a phenomenon present in all types of steels, to some degree [7]. In most low carbon alloy steels, it is evident primarily in the form of ferrite and pearlite. Within DP steels, banding is seen in the form of ferrite and bainite, pearlite and/or martensite. Moreover, in DP steels, martensite is present as bands in the centerline, as opposed to the preferred randomly dispersed islands, as shown in Figure 9.

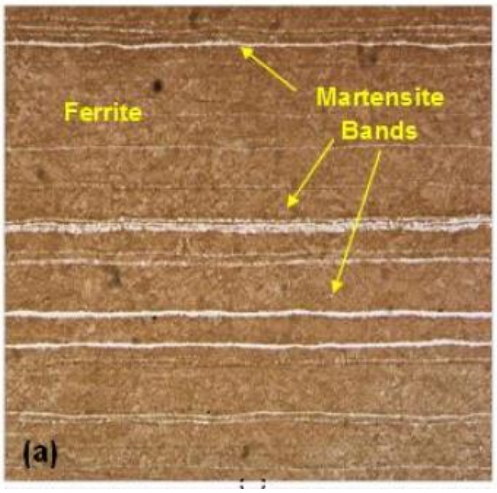

Figure 9: Martensite bands seen in DP 780 on a longitudinal cross section at the center [36]

Martensite morphology and distribution has a significant effect on accumulated damage on semi-finished and finished steel products, and is seen as a precursor to potential failure [37] [38]. Steels with martensite banding present in the centerline have been found to exhibit faster damage growth [37]. Furthermore, highly banded structures are unfavorable for steel products which will be subject to thermal cycles because the strain anisotropy from heating and cooling transformations may induce stress fields [38]. Therefore, banding prevention can greatly improve mechanical properties of semi-finished and finished steel products.

Banding typically appears in the microstructure after forming operations such as hot or cold rolling. However, the underlying cause of banding can be primarily attributed to residual Mn micro and macro segregation, and can be controlled during the casting process [7].

Chapter 3: Experimental Methodology

The primary experimental method applied in this thesis is Micro X-Ray Fluorescence Spectroscopy, MXRF. The following section outlines the sampling process, includes a background on the principles governing MXRF and describes the validation work that was completed for the MXRF device.

3.1 Sample Selection and Extraction

A total of twenty-four samples, casted using a range of casting speed, Vc and superheat, ΔT, were extracted from industrial, continuously casted DP600 slabs. The chemical composition is shown in Table 3.

Table 3: Typical DP600 alloy chemistry

Element	C	Mn	P	S	Si	Cr	Ti	N	Al
Weight Percentage [wt%]	0.10	1.51	0.01	0.00	0.17	0.21	0.02	0.00	0.05

A combination of high and low ΔT, and high, medium and low Vc were selected to provide variations in the casting parameters and are shown in Table 4.

Table 4: Variation in Vc and ΔT

Slab Number	**Vc**	**ΔT**	**Vc [m/s]**	**ΔT [^{O}C]**
1	Low	Low	0.8	23
2	Low	High	0.8	35
3	Medium	Low	1	26
4	Medium	High	1.1	35
5	High	Low	1.3	29
6	High	High	1.2	37

Four samples were extracted from each slab; Sample A and B were taken along the slab length, while Sample C and D were taken along the slab width. These samples were 0.5 meters, m, apart from one another. All sample were taken at steady state. The extraction process is outlined in Figure 10.

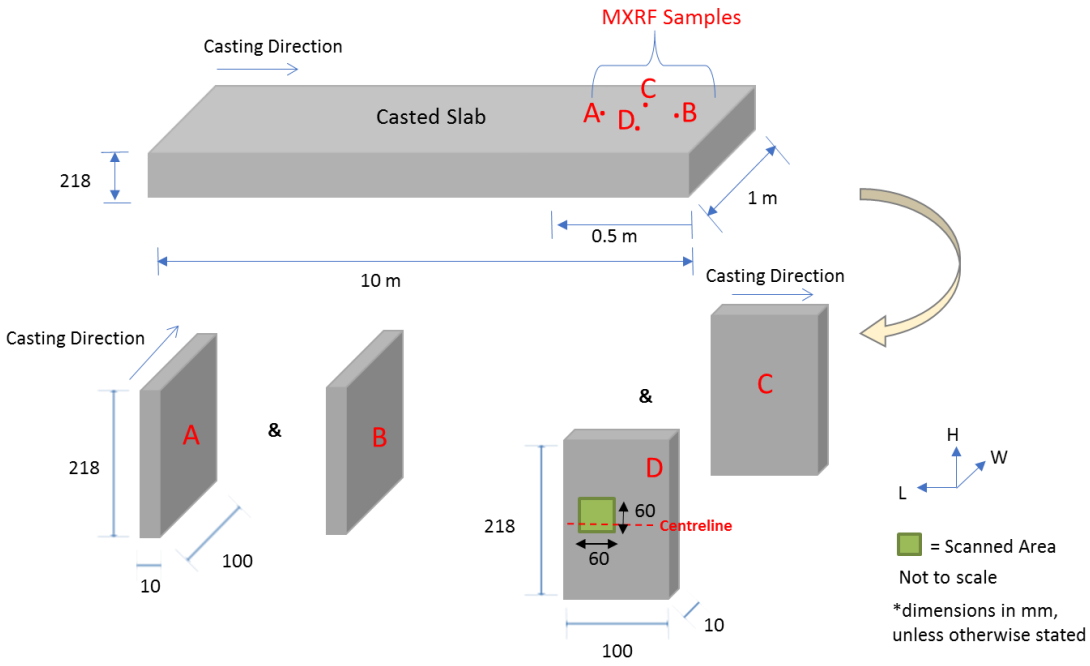

Figure 10: MXRF sample locations with respect to original steel slab

Additional DP600 alloy slabs, with 1.85 nominal Mn wt% (medium Vc and low ΔT) and 2.1 nominal Mn wt% (high Vc and high ΔT), were also examined. Samples from these slabs were extracted in the same manner as shown in Figure 10.

3.2 X-Ray Fluorescence Spectroscopy

In X-Ray Fluorescence Spectroscopy, XRF, samples are irradiated with high energy X-rays. The incident X-rays tend to have sufficient energy to expel electrons from one of the atom's inner, lower energy orbital shells. To regain stability, the atom replenishes the vacant electron spot with an electron from a higher energy orbital shells. The selected electron then moves to a lower energy shell orbital and releases a fluorescent X-ray. This fluorescent X-ray is equal to the difference in energy between the two quantum states, and is characteristic to each element. The fluorescent X-rays result in characteristic lines

in the X-ray emission spectrum. Thus, the measurement and identification of all fluorescent X-rays provides quantitative and qualitative insights in to the elements that are present within irradiated samples. This is the foundation of XRF analysis [39] [40].

There are two detection systems that are general used to measure the fluorescent X-rays, Wavelength Dispersive Detection, WDXRF, and Energy Dispersive Detection, EDXRF. WDXRF uses a single crystal or multilayer optic to select and diffract narrow X-ray energy ranges which can correspond to fluorescent X-rays of elements. This offers great signal to background ratio, leading to high elemental sensitivity [40]. On the other hand, EDXRF simultaneously detects a wider range of X-ray energies. A distinct EDXRF technique makes use of poly-capillary optics to focus incident beams ranging in diameters from micrometers to millimeters, allowing for smaller sections to be analyzed [39]. A schematic highlighting the main components of typical x-ray spectroscopy is shown in Figure 11.

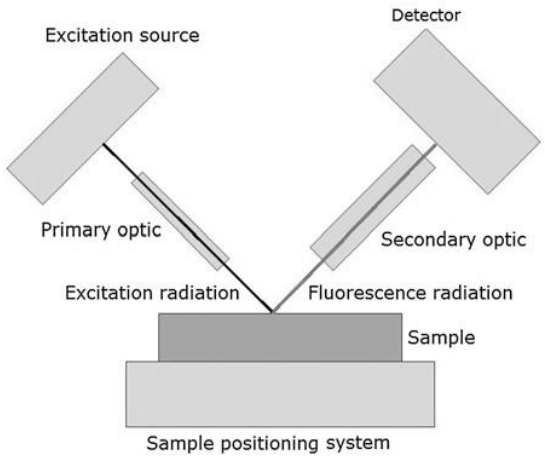

Figure 11: Schematic of main components in x-ray spectroscopy [39]

3.2.1 Micro X-Ray Fluorescence Experimental Device

The experiments were conducted using a bench-top EDX MXRF device, located at Arcelor-Mittal Dofasco's Research and Development Laboratory in Hamilton, Canada. Generally, benchtop devices comprise of a chamber with a xyz stage, an excitation source and a silicon-drift detector. These devices are also connected to an in-built software which provides data acquisition and spectral processing

for single point, line and area scans. The area scanned for this thesis is shown in Figure 12. Key scan parameters consisted of a 50 micrometer spot size, a dwell time of 3000 milliseconds, ms, and a spatial resolution of 1 millimeter, mm.

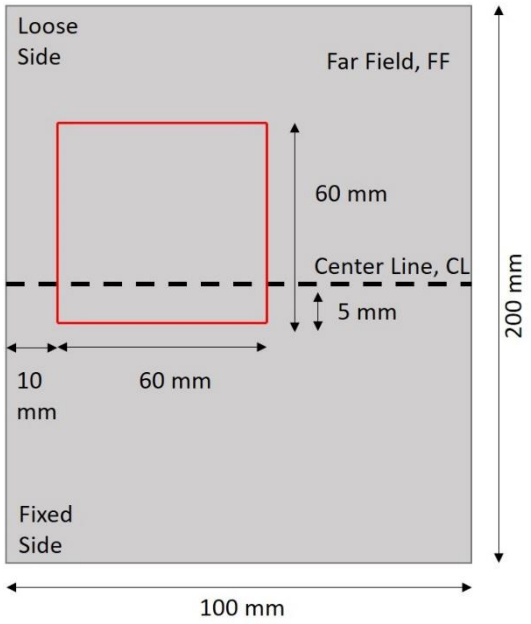

Figure 12: Schematic of scan area (red square box) and dimensional specifications

A preliminary parametric study was conducted to validate this device and method, and select an appropriate dwell time for the experiments. Dwell time refers to the time, typically in milliseconds, that the incoming x-rays are held per pixel. Using a pixel size or spatial resolution of 1 mm, multiple scans using the MXRF equipment were conducted on OES samples with known Mn compositions. The following dwell times were tested: 1050 ms, 1650 ms, 3000 ms and 6000 ms. Due to the keen interest on macro segregation, a coarse spatial resolution of 1 mm was selected. Some studies, which have used XRF to investigate macro segregation have used much coarser resolutions [33] [34]. The results are presented in Figure 13.

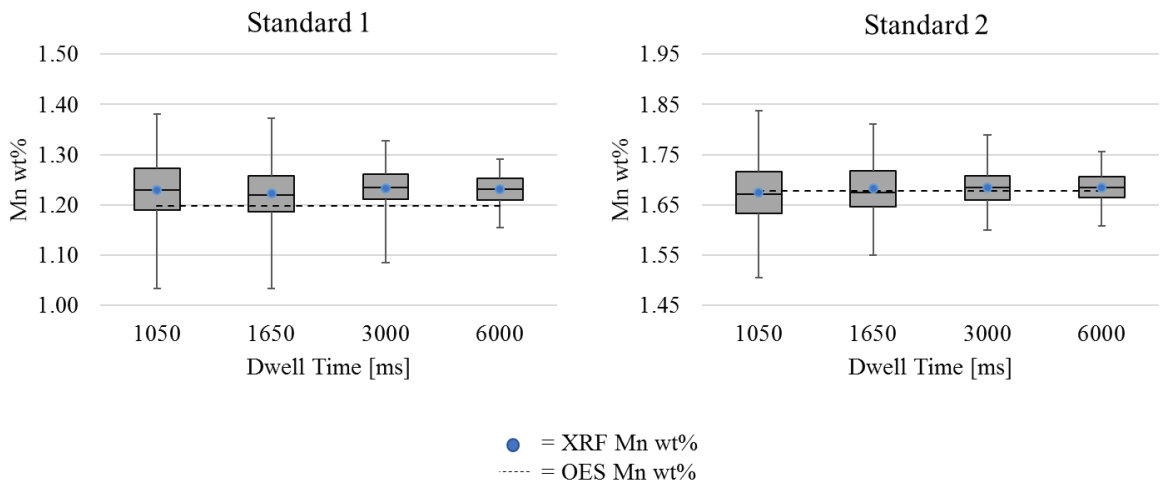

Figure 13: Effect of dwell time on Mn wt% detection

The MXRF scans consistently reported values similar to the OES standards, attaining measurements with a 1 percent error. Moreover, it was found that a dwell time of 3000 ms was a suitable parameter. This dwell time provided a great balance between accuracy in measurement, variation in dataset and total scan time. As seen in Figure 14 and Figure 15, a 3000 ms dwell time reported Mn wt% values with more accuracy at the higher Mn wt%. The samples used for the thesis had a Mn wt% closer to Standard 2 than to Standard 1, and thus, making this dwell time an appropriate parameter. Furthermore, the 3000 ms dwell time showed the least amount of variability, as evident in Figure 14 and Figure 15.

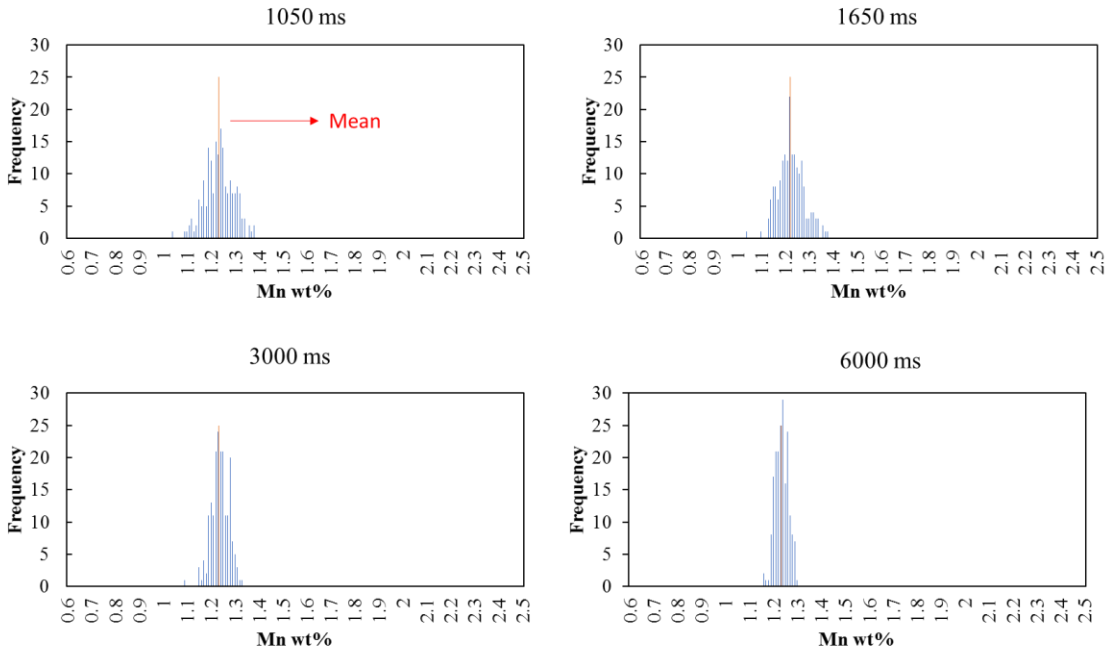

Figure 14: Frequency distributions of centerline data at different dwell times for Standard 1

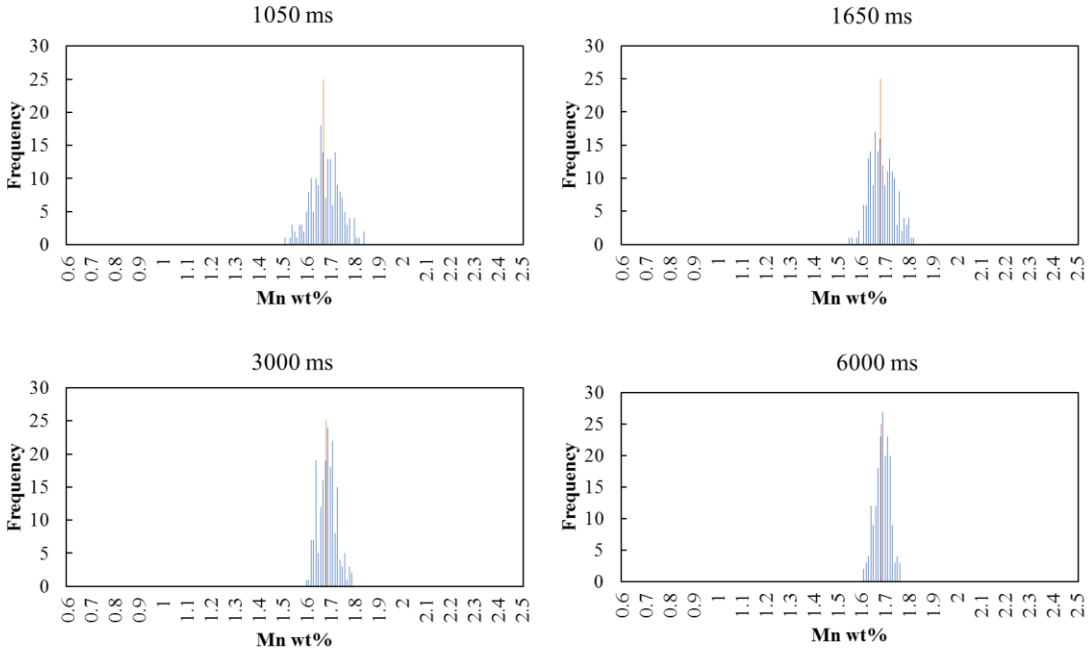

Figure 15: Frequency distributions of centerline data at different dwell times for Standard 2

As the dwell time increased, a slimmer distribution, i.e. less noise, was found. Moreover, from Figure 15, the interquartile range, which is a measure of spread in boxplots, reveals values that also decreased as dwell time increased. A smaller variation in the dataset is better suited to reliably and consistently detect a range of low, mid and high Mn wt%, making it beneficial for detection of centerline macro segregation. Both 3000 ms and 6000 ms dwell times provided a smaller spread, and yet, it was evident that the interquartile range of the higher dwell times, 3000 ms and 6000 ms, were similar to one another. In addition, the 3000 ms dwell time allowed for a reasonable scan time of 4 hours per sample, as opposed to 8 hours per sample. Hence, a dwell time of 3000 ms was selected.

To further gauge the reliability of the selected dwell time and MXRF method, a repeatability test was also conducted. A fixed area of 15 by 15 mm was scanned three times successively for both standards. The findings are presented in Figure 16.

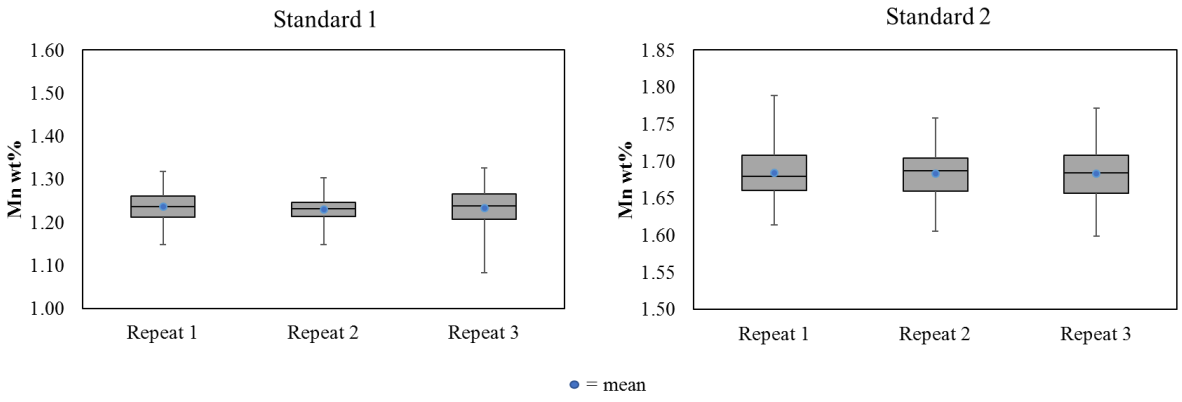

Figure 16: Repeatability results for 3000 ms on Standard 1 and 2

The findings show that there is negligible variation in measurements taken by the MXRF equipment, under the same conditions. Standard 2 reported consistent mean Mn wt% measurements and spread, in between repeats.

Chapter 4: Results and Discussions

4.1 Typical Measured Data (Centerline and Far Field)

MXRF techniques have three common modes of measurements, single point, line and area scans [39]. Single point scans, as evident by its name, scan small spots on the sample that are akin to the laser spot size, and return the intensity count and corresponding wt% of the element of interest. Line scans provide one dimensional arrays of data at numerous points that are equally set apart. Area scans operate in a similar fashion, except in two dimensions instead [39]. A schematic of the three modes are shown in Figure 17.

Single Point Scan:

Data 1

Line Scan:

Data 1	Data 2	Data 3	Data 4

Area Scan:

Data 1	Data 2	Data 3	Data 4
Data 5	Data 6	Data 7	Data 8
Data 9	Data 10	Data 11	Data 12
Data 13	Data 14	Data 15	Data 16

Figure 17: Schematic of three major modes of measurements available in MXRF systems

As mentioned in 3.1, 60 mm by 60 mm area scans were conducted on the as-cast samples. The area included both the centerline and the far field, and its size and location was fixed for each sample. Figure 18 shows a subset (5 mm by 60 mm) of the larger dataset (60 mm by 60 mm) from a 1 mm spatial resolution scan. Typically, raw data comes in the form of elemental intensity counts and wt%. However, for confidentiality purposes, all raw data was normalized using an average from a 60 mm by 10 mm area in the far field, prior to any analysis.

The experimental data was manipulated in numerous ways to reveal and analyze Mn macro segregation in both the centerline and far field of the as-cast structure.

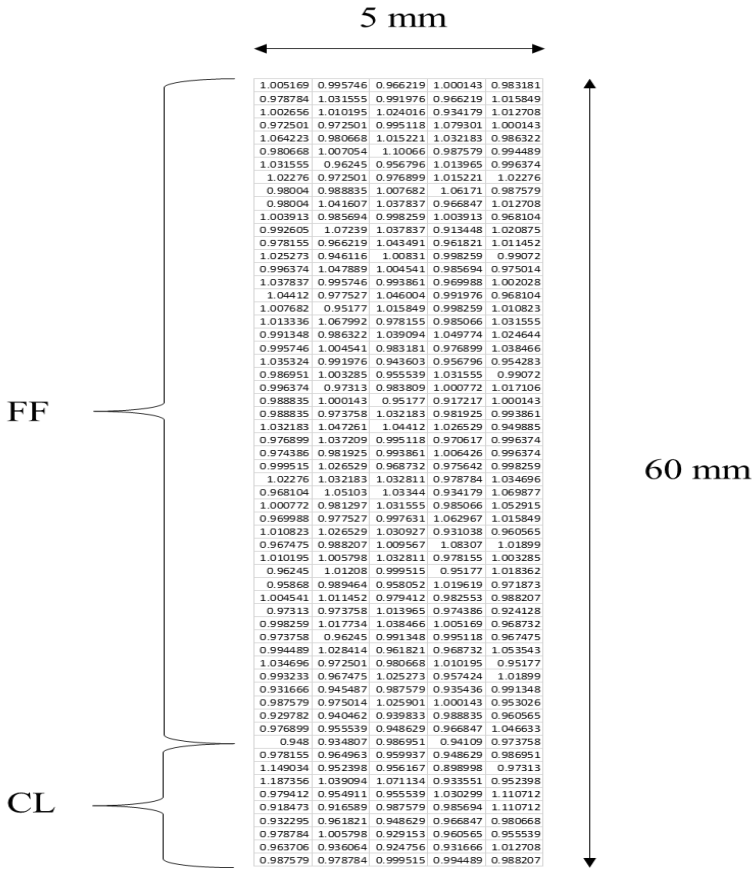

1.005169	0.995746	0.966219	1.000143	0.983181
0.978784	1.031555	0.991976	0.966219	1.015849
1.002656	1.010195	1.024016	0.934179	1.012708
0.972501	0.972501	0.995118	1.079301	1.000143
1.064223	0.980668	1.015221	1.032183	0.986322
0.980668	1.007054	1.10066	0.987579	0.994489
1.031555	0.96245	0.956796	1.013965	0.996374
1.02276	0.972501	0.976899	1.015221	1.02276
0.98004	0.988835	1.007682	1.06171	0.987579
0.98004	1.041607	1.037837	0.966847	1.012708
1.003913	0.985694	0.998259	1.003913	0.968104
0.992605	1.07239	1.037837	0.913448	1.020875
0.978155	0.966219	1.043491	0.961821	1.011452
1.025273	0.946116	1.00831	0.998259	0.99072
0.996374	1.047889	1.004541	0.985694	0.975014
1.037837	0.995746	0.993861	0.969988	1.002028
1.04412	0.977527	1.046004	0.991976	0.968104
1.007682	0.95177	1.015849	0.998259	1.010823
1.013336	1.067992	0.978155	0.985066	1.031555
0.991348	0.986322	1.039094	1.049774	1.024644
0.995746	1.004541	0.983181	0.976899	1.038466
1.035324	0.991976	0.943603	0.956796	0.954283
0.986951	1.003285	0.955539	1.031555	0.99072
0.996374	0.97313	0.983809	1.000772	1.017106
0.988835	1.000143	0.95177	0.917217	1.000143
0.988835	0.973758	1.032183	0.981925	0.993861
1.032183	1.047261	1.04412	1.026529	0.949885
0.976899	1.037209	0.995118	0.970617	0.996374
0.974386	0.981925	0.993861	1.006426	0.996374
0.999515	1.026529	0.968732	0.975642	0.998259
1.02276	1.032183	1.032811	0.978784	1.034696
0.968104	1.05103	1.03344	0.934179	1.069877
1.000772	0.981297	1.031555	0.985066	1.052915
0.969988	0.977527	0.997631	1.062967	1.015849
1.010823	1.026529	1.030927	0.931038	0.960565
0.967475	0.988207	1.009567	1.08307	1.01899
1.010195	1.005798	1.032811	0.978155	1.003285
0.96245	1.01208	0.999515	0.95177	1.018362
0.95868	0.989464	0.958052	1.019619	0.971873
1.004541	1.011452	0.979412	0.982553	0.988207
0.97313	0.973758	1.013965	0.974386	0.924128
0.998259	1.017734	1.038466	1.005169	0.968732
0.973758	0.96245	0.991348	0.995118	0.967475
0.994489	1.028414	0.961821	0.968732	1.053543
1.034696	0.972501	0.980668	1.010195	0.95177
0.993233	0.967475	1.025273	0.957424	1.01899
0.931666	0.945487	0.987579	0.935436	0.991348
0.987579	0.975014	1.025901	1.000143	0.953026
0.929782	0.940462	0.939833	0.988835	0.960565
0.976899	0.955539	0.948629	0.966847	1.046633
0.948	0.934807	0.986951	0.94109	0.973758
0.978155	0.964963	0.959937	0.948629	0.986951
1.149034	0.952398	0.956167	0.898998	0.97313
1.187356	1.039094	1.071134	0.933551	0.952398
0.979412	0.954911	0.955539	1.030299	1.110712
0.918473	0.916589	0.987579	0.985694	1.110712
0.932295	0.961821	0.948629	0.966847	0.980668
0.978784	1.005798	0.929153	0.960565	0.955539
0.963706	0.936064	0.924756	0.931666	1.012708
0.987579	0.978784	0.999515	0.994489	0.988207

Figure 18: Example of a subset of normalized data

4.1.1 Comparison to a current technique

Figure 19 displays a comparison between a conventional macro etched surface, and a quantitative examination using an element composition map. This comparison illustrates the MXRF technique's ability to effectively reveal the Mn variation in the as-cast structure, and more specifically in this case, at the centerline.

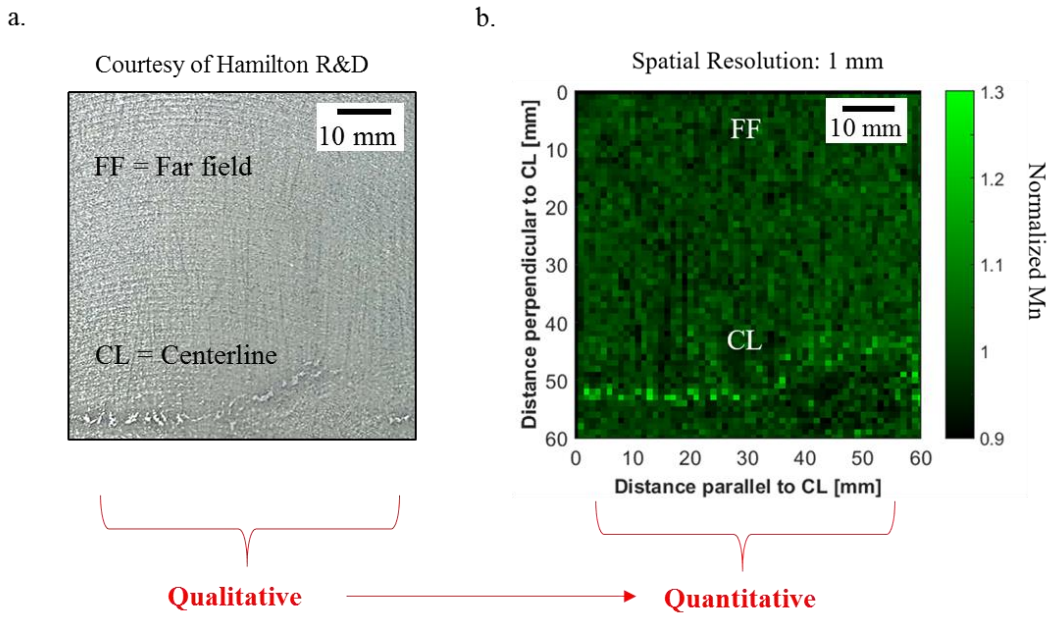

Figure 19: A comparison between current qualitative methods and quantitative method using the experimental data; surface etched using an ammonium cupric chloride after annealing; 1.5 Mn wt% and High Vc and High ΔT

As mentioned, the prime focus of the thesis was to assess segregation. The first step to accomplish this lies in the creation and observation of element composition maps. As shown in Figure 19, these maps reveal the encompassing segregation in a visual, yet quantitative manner.

In the process of assessing segregation, the composition maps provide a quick look at the overall scanned area and highlight any abnormalities. Abnormalities could be present in the form of manganese sulfide inclusions and in the quality of the segregation or scan. All these factors can potentially influence subsequent analysis. As shown by the V segregation in Figure 19, segregation at the centerline may be nonlinear. This nonlinearity is the result of instantaneous changes in casting conditions. Thus, the composition maps provide a rapid means of observing the scanned surface for any oddities prior to the application of the various metrics presented in this thesis.

4.2 Centerline

4.2.1 Metrics Overview

As mentioned previously, the focus of this thesis is to develop quantitative ways to reveal and assess Mn macro segregation at the centerline and far field of as-cast structures. To achieve this, an emphasis was placed on generating an array of numerical metrics. A description of each of the four metrics is provided in Table 5. Each metric is uniquely defined and developed.

Table 5: Overview of Metrics A – D to evaulate centreline segregation

Metric	Description
A – Band Thickness	This metric assesses the band thickness, which refers to the portion of Mn segregation at the centerline. Note that centerline segregation occurs along the entire width of the 1 m wide slab. Thus, the band thickness, and not area, was chosen.
B – Average of Normalized Mn	This metric evaluates the arithmetic average of the normalized Mn values in the identified segregation region. The segregation region is defined using a 1, 2, 3 or 4 value system.
C – Maximum and 90^{th} Percentile of Normalized Mn	This metric evaluates the maximum and 90^{th} percentile of the normalized Mn values in the segregation band.
D – Area Percentage	This metric focuses on the percentage of area that is found to contain specific levels of segregation, given a fixed, 60 by 10 mm, area.

4.2.2 Metric Development

Two separate mathematical methods, Method 1 and Method 2, were used to develop Metrics A – D. The following section describes the creation of these two methods, and the subsequent metrics.

4.2.2.1 Method 1

Method 1 analyses the experimental data through measurements of central tendency such as the arithmetic means or averages. This method relies on segregation profiles, similar to the one shown in Figure 20, to develop Metrics A and C.

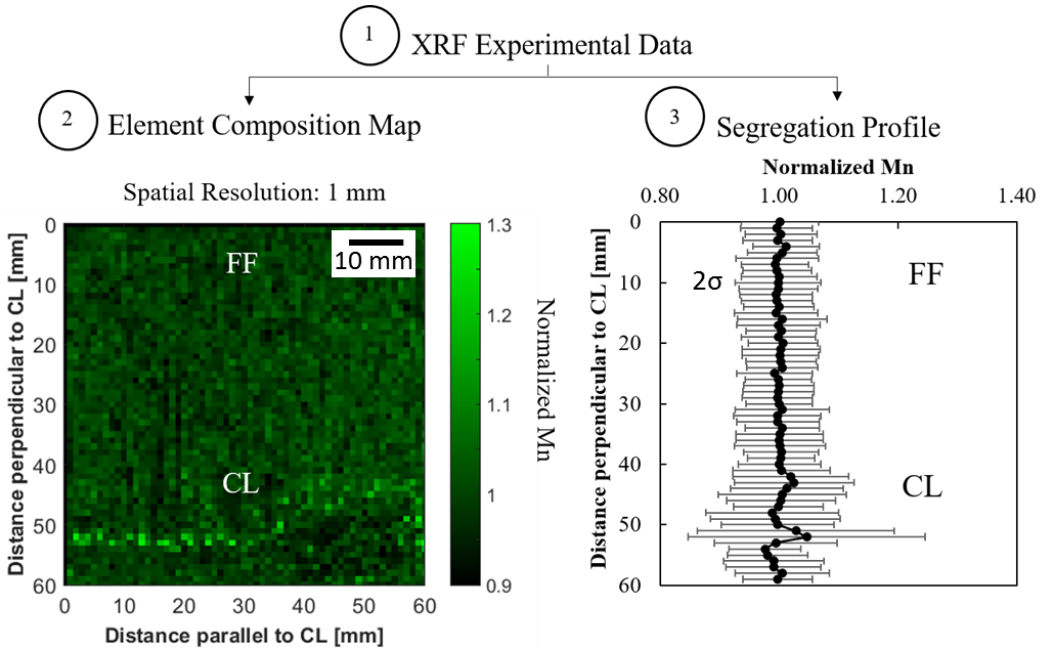

Figure 20: Comparison between an element composition map and the corresponding segregation profile

Segregation profiles are a numerical representation of the Mn variation in the scanned area. These profiles are essentially a consolidation of expansive data into singular values. The profiles were created by calculating and plotting an average of the normalized values for each row of data. See Figure 21. There

is a total of 59 normalized values per row, and there are 59 rows in total. This corresponds to the 60 mm by 60 mm scanned area.

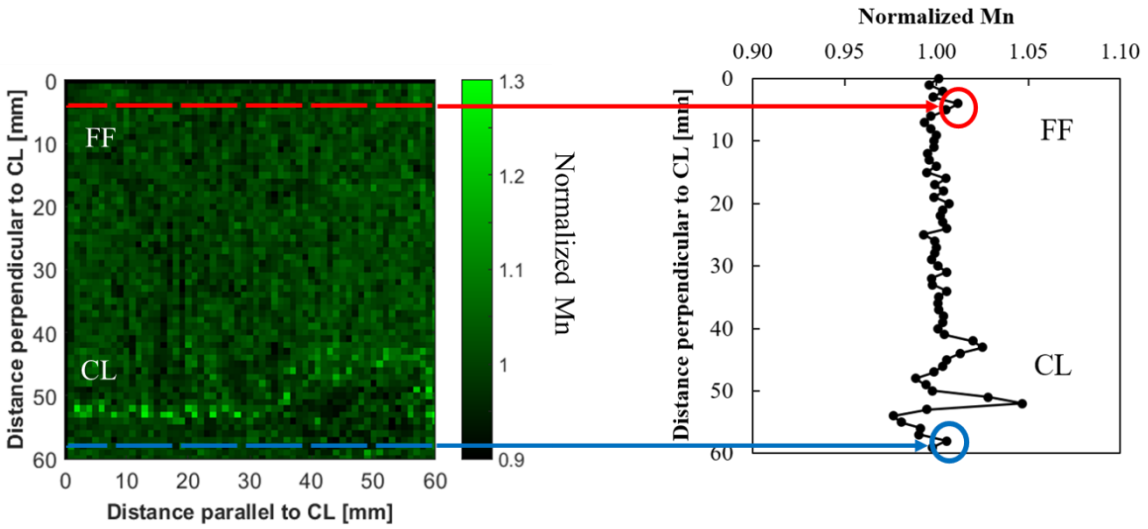

Figure 21: Creation of segregation profile; red dash line indicates Row 4 while blue dash line locates Row 58; Note that standard deviation error bars have been excluded for clarity purposes

Subsequently, Metrics A and C can be calculated from the centerline of the segregation profile. See Figure 22. As the centerline of the as-cast structure is approached, all segregation profiles reveal a pattern; the normalized values reach a minimum, then a maximum, and finally another minimum, before returning to unity. This pattern is a characteristic feature present in all scanned samples. Thus, Metric A, or the band thickness, was equated to be the spatial difference between the two minima. The centerline of the segregation profile is also used to evaluate Metric C, which is both the maximum and 90th percentile of the normalized Mn values. The maximum value, although an indicator of the level of Mn present, is a singular value which overlooks the presence of a range of medium to high Mn values in the segregated region. Thus, in addition to the maximum, the 90th percentile was also considered. The 90th percentile is the value that is greater than or equal to 90% of the measurements in the frequency distribution [41]. All average values in the segregation band was rearranged in ascending and then the top 10% was removed, revealing the 90th percentile. Essentially, this is the value that 90% of the data points are smaller than and 10% of data points are larger than. Examining this value decreases errors that are associated with using discrete measurements as standards for comparison.

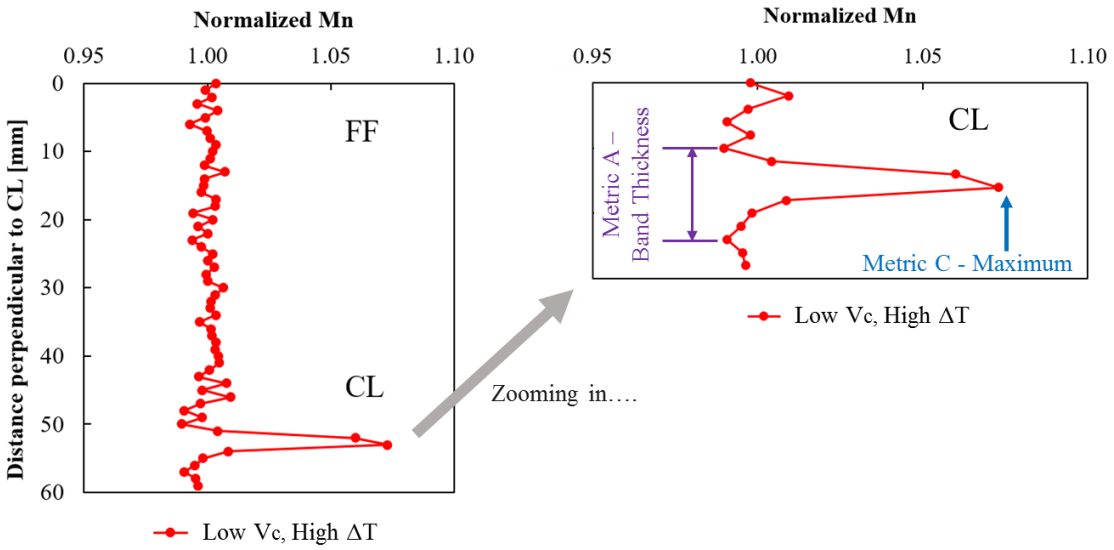

Figure 22: Development of Metrics A and C

4.2.2.2 Method 2

Method 2 analyzes distinct normalized Mn values at the centerline. In a fixed, 10 by 60 mm area which contains the centerline, the segregated Mn is highlighted by filtering the experimental data. Each discrete data point was filtered by checking to see if it was greater than unity, indicating a higher level of Mn or segregation by the following factors, 1.03, 1.04, 1.05, 1.06, 1.07, 1.08, 1.09, 1.1 and 1.2. Unity is defined as the far field average (over a 10 mm by 60 mm area) specific to each normalized dataset and is akin to the nominal Mn composition.

After filtration, the segregated portion, within the 10 by 60 mm fixed area, needed to be identified. This was done by implementing a value system, which identifies the beginning and end of segregated areas. The value system cycles through each row of data and counts the total number of data points found to be greater than the specified factor. The system will then identify the start and beginning of the segregation by comparing the total number of counts per row to the selected value, which ranges from one to four. For example, using a 3 value system and a factor of 1.03, a segregated area would begin when a total of three normalized values in a row of data are filtered to be greater than 1.03. Similarly, the

segregated area would also end when three normalized values in a row of data are found to be greater than 1.03. This process is shown in Figure 23.

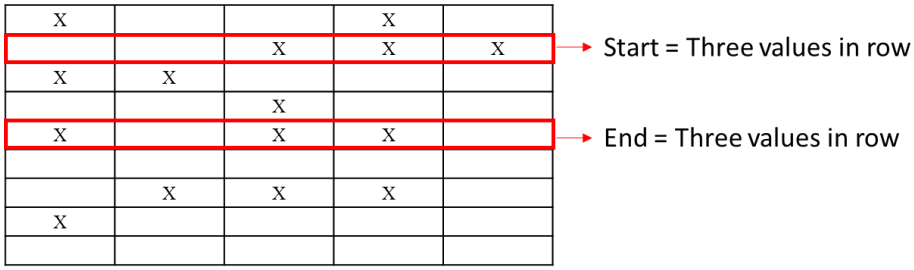

Figure 23: Example of a 3 value system

If, from one row to another, there are discontinuities in the filtered data i.e. a total count of zero, then the beginning and/or end of the segregated area is automatically delegated to the row with the selected value system, in this case three, prior to the discontinuity. See Figure 23. Once the experimental data is filtered using the appropriate factor and the segregated portion is identified using the optimal value system, Metrics A, B and D can be established.

Metric A, or the band thickness, is simply the spatial difference between the start and end of the segregation. Metric B calculates the arithmetic average of the normalized Mn values in the identified segregation section. Metric D calculates the percentage of the fixed area of 10 by 60 mm that contains normalized values that are greater than the selected factor.

4.2.3 Effects of Spatial Orientation

As mentioned in 3.1, four samples, A, B, C and D, were extracted per casting condition. These samples were taken to reveal the differences in segregation along the slab length and width.

The results using Method 1 and Metric A (band thickness) and C (maximum and 90th percentile) are shown in Figure 24.

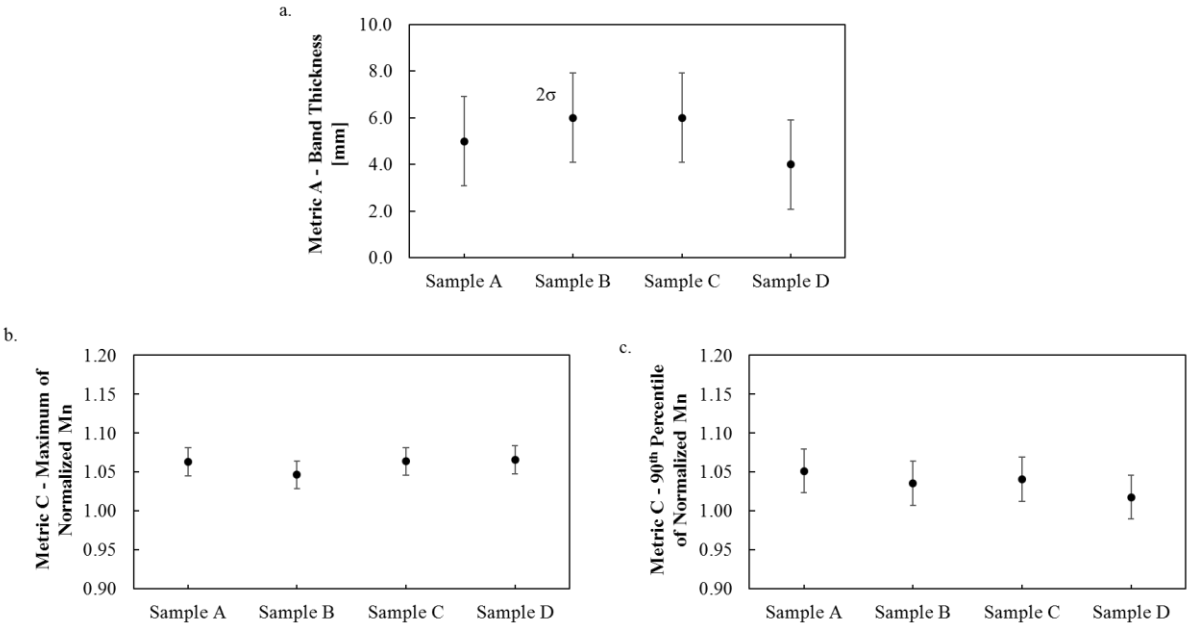

Figure 24: Metrics A and C as a function of spatial orientation for a High V_c and High ΔT condition

Figure 24a reveals that from sample to sample, the band thickness and corresponding two sigma standard deviations are comparable to one another. This trend is found in all six casting conditions. See Appendix A. Likewise, Figure 24b and c shows that the maximums and 90th percentiles are also alike, in between samples. Once again, this trend is seen for all casting conditions. See Appendix A. Thus, using Method 1 and Metrics A and C, it was found that samples which were taken 0.5 m apart in the slab width and length have minimal differences in centerline macro segregation.

The results using Method 2 and Metric A (band thickness), B (average of the normalized Mn) and D (area %) are shown in Figure 25.

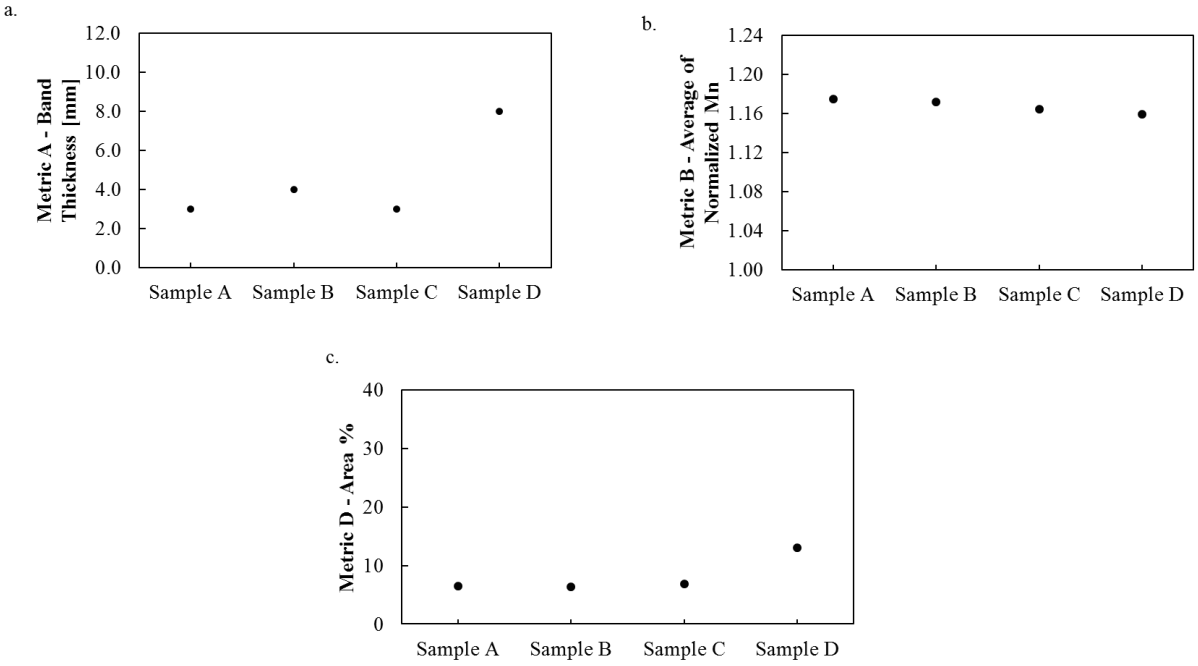

Figure 25: Metrics A, B and D as a function of spatial orientation for a High Vc and High ΔT casting condition; Metric A and B uses a 1.09x filter and 3 value system

Figure 25 reveals that from sample to sample, all three metrics appear unresponsive to the changes in segregation as the spatial orientation varies. This trend is found in all six casting conditions. See Appendix A. Hence, using Metrics A, B and D, it was found that samples which were taken 0.5 m apart in the slab width and length have little differences in centerline macro segregation.

4.2.4 Effect of Casting Speed

Due to the similarities in the band thickness, maximum and 90th percentiles (Method 1) between Samples A to D, an arithmetic average of each was used as representatives for each casting condition. Metrics A, as a function of the casting speed, is plotted in Figure 26.

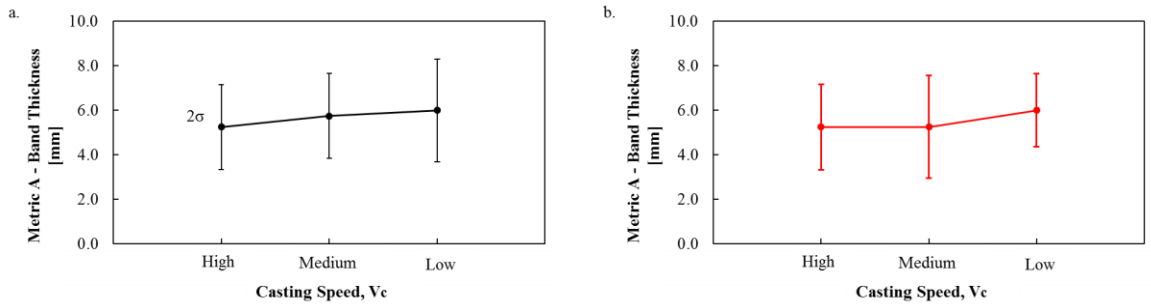

Figure 26: Metric A as a function of casting speed for 1.5 Mn wt% for a. a high ΔT and b. a low ΔT

Figure 26 reveals that the band thickness and corresponding two sigma standard deviations are consistent between samples from different casting speeds. This suggests that this metric is not a strong function of the tested ranges of casting speeds.

Moreover, as shown in Figure 27, the maximums and 90th percentiles also appear to be constant amidst the varied casting speeds. However, the maximum values for the low superheat conditions were found to have larger two sigma standard deviations than the high superheat conditions.

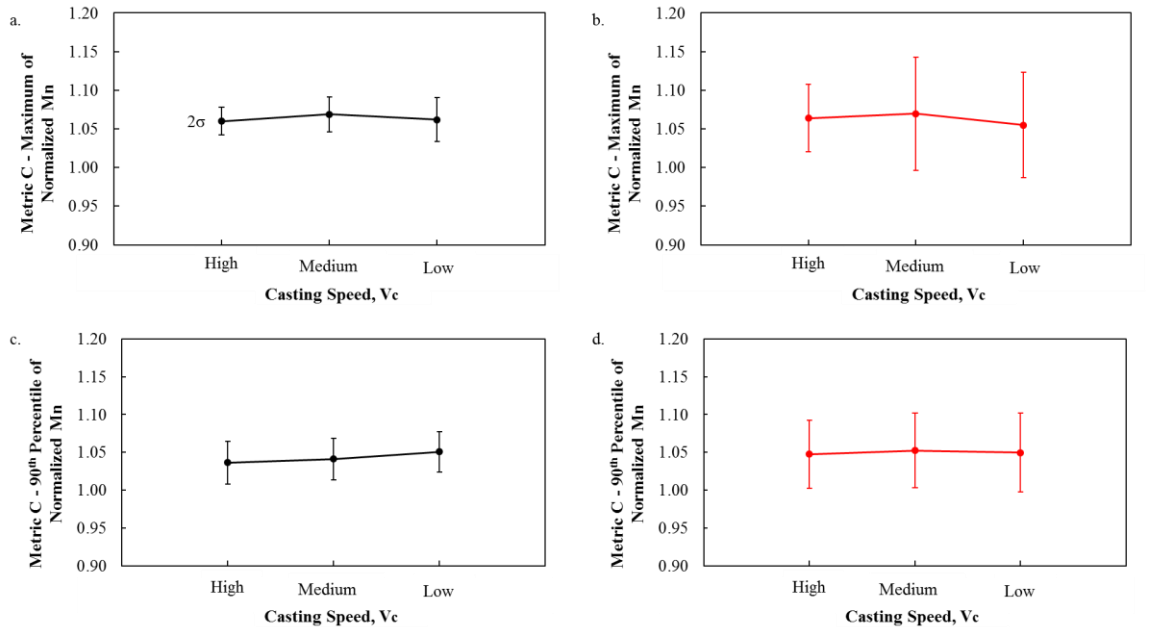

Figure 27: Metric C as a function of casting speed for 1.5 Mn wt% a. Maximum normalized Mn for a high ΔT b. Maximum normalized Mn for a low ΔT c. 90th Percentile for a high ΔT d. 90th percentile for a low ΔT

Overall, both Metrics A (band thickness) and C (maximum and 90th percentile), using Method 1, appear to be insensitive to changes in macro segregation within samples from the tested casting speeds.

Non-parametric statistical tests were used conducted to verify the statistical significance of the results. All centerline data was found to be have a positively skewed distribution, as shown in Figure 28.

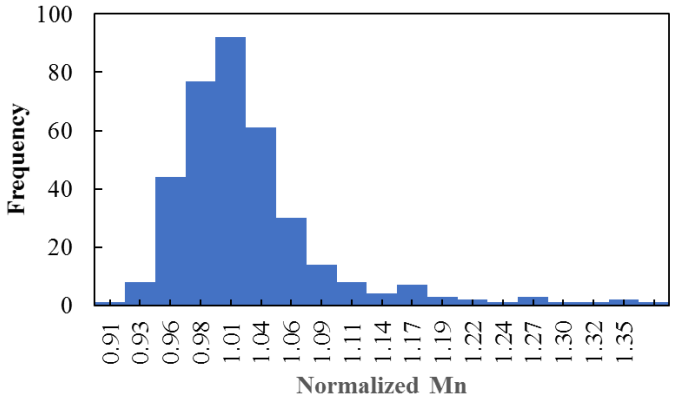

Figure 28: Frequency distribution of normalized Mn at centerline of Sample A with High Vc and High ΔT casting condition

Although t-tests and ANOVA tests are quite robust, alternative non-parametric tests such as Kruksal-Wallis and Mann-Whitney test were conducted instead. A summary of the p-values for Method 1 and Metrics A and C is shown in Table 6.

.

Table 6: P values for statistical tests (1.5 Mn wt%)

Test Type	Casting Conditions	Metric	p - value
Kruksal - Wallis	Vc - High vs Medium vs Low ΔT - High	A – Band Thickness	0.997
		C – Maximum	0.632
		C – 90th Percentile	0.563
	Vc - High vs Medium vs Low ΔT - Low	A – Band Thickness	0.999
		C – Maximum	0.159
		C – 90th Percentile	0.056

The p-values, which were all found to be above 0.05, reveal that the results from Method 1 and Metrics A and C are statistically insignificant from condition to condition. This further verifies the indifference of Metrics A and C to the changes in segregation regarding the selected casting speeds.

Figure 29 plots the results for varying casting speed using Method 2 and Metric A. Once again, no statistically significant trend is found amongst the tested casting speeds. See Appendix B for results regarding the remaining factors and value systems.

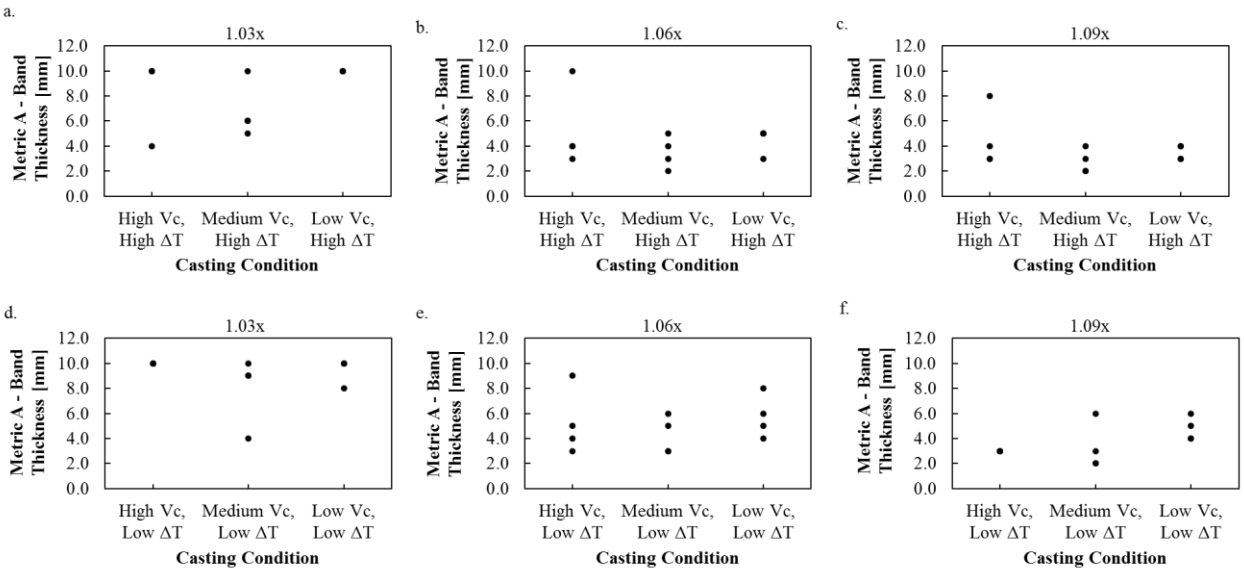

Figure 29: Metric A as a function of casting speed for 1.5 Mn wt% using a 3 value system

Method 2 and Metric B was also used to assess segregation between high, medium and low casting speeds. The results were plotted in Figure 30 and reveal no statistically significant trend as the casting speed varied. See Appendix B.

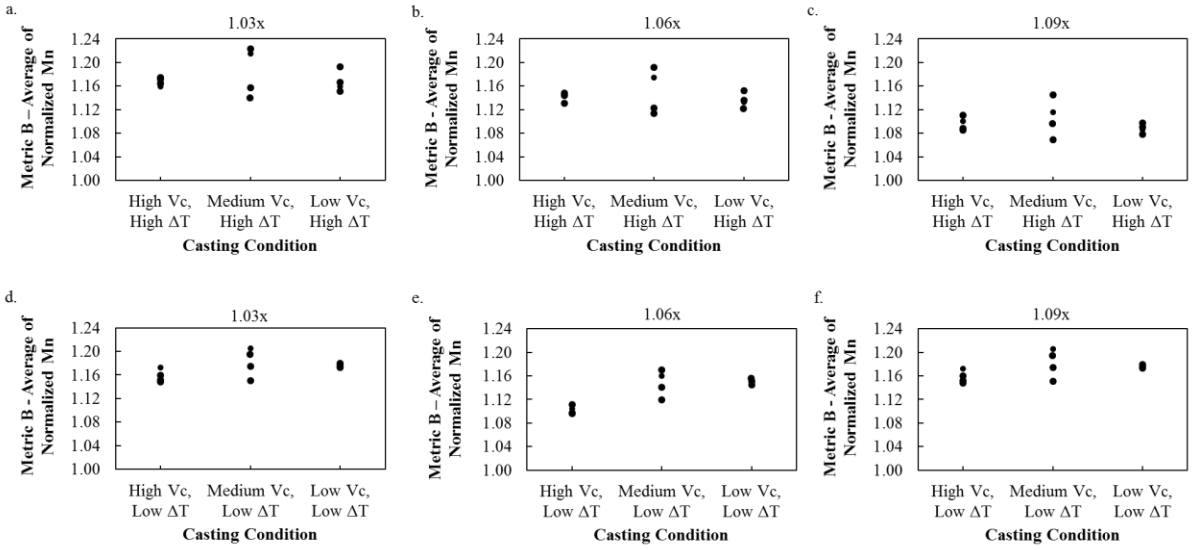

Figure 30: Metric B as a function of casting speed for 1.5 Mn wt% using factors 1.03x, 1.06x, 1.09x and a 3 value system

Likewise, Metric D (area percentage), as a function of varying casting speeds, is shown in Figure 31.

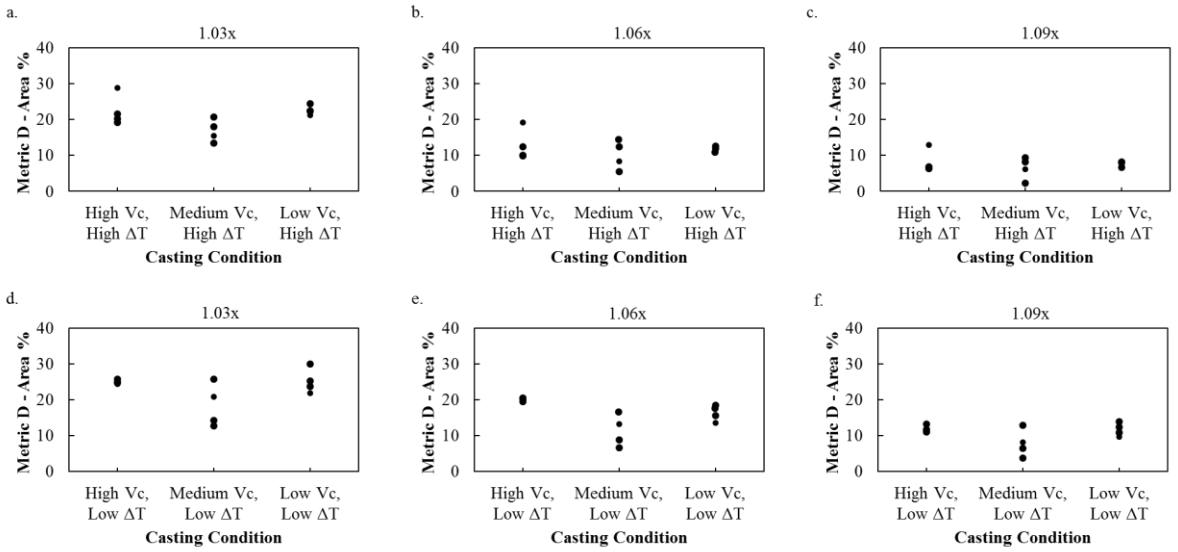

Figure 31: Metric D as a function of casting speed for 1.5 Mn wt% using factors 1.03x, 1.06x, 1.09x

The plots reveal that the percentage of area which contains normalized values greater than 1.03, 1.06 and 1.09, remains constant. Comparable results are seen for the remaining factors and can be found in Appendix B. Thus, Method D appears to be indifferent to the tested casting speeds as well.

The results using both Methods 1 and 2, and all four metrics (A, B, C and D) are not in accordance to literature. Typically, increasing the casting speed reduces the amount of time in the mold, which in turn, minimizes the amount of heat transfer that occurs and as well as the solidification rate. Reduction of in-mold time results in the slower removal of superheat. This delays the nucleation and growth of equiaxed crystals, which play a vital role in arresting the columnar growth front. Since columnar dendrites eject solutes in a non-uniform manner, this increases the level of segregation during solidification [26] [28]. Furthermore, the casting speed also influences the solid shell thickness below the mold. The solid shell must be stable enough to withstand bulging [27]. Bulging can increase the level of macro segregation present. Expansions in weak shells cause solute rich interdendritic liquid to be drawn towards the center because of ferrostatic forces [27]. Thus, increasing Vc negatively affects segregation. Yet, the results, with regards to the effects of Vc, do not align with literature.

4.2.5 Effect of Superheat

Due to the similarities in Method 1 and the band thickness, maximum and 90th percentiles between Samples A to D, an arithmetic average of each was used as representatives for each casting condition. Metrics A and C, as a function of the superheat, is plotted in Figure 32.

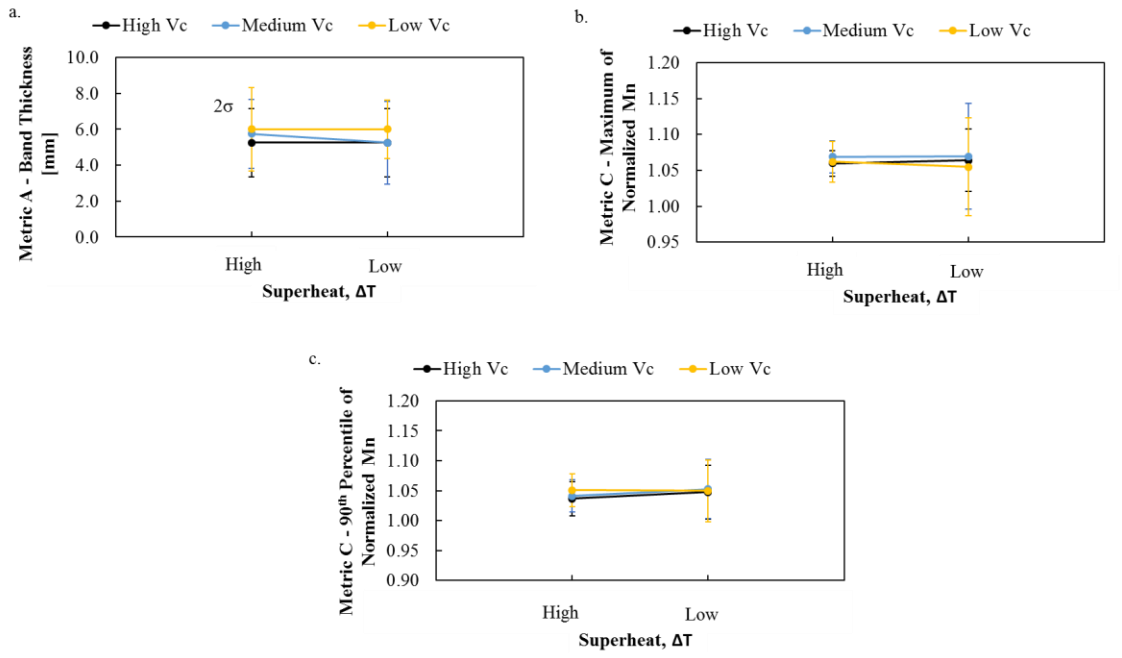

Figure 32: Method 1 and Metrics A and C as a function of superheat for 1.5 Mn wt%

Metric A reveals that the band thickness and two sigma standard deviations from a high to low superheat, at each casting speed, do not differ significantly. Similar results are seen for the maximum and 90th percentiles as well. However, low superheat conditions were found to have larger deviations than their counterparts. Overall, both Metrics A (band thickness) and C (maximum and 90th percentile), using Method 1, appear to be indifferent to changes in segregation within samples from the tested superheats.

A summary of the p-values for Method 1 and Metrics A and C is shown in Table 7.

Table 7: P values for statistical tests on superheat results (1.5 Mn wt%)

Test Type	Casting Conditions	Metric	p - value
Mann - Whitney	Vc - High ΔT – High vs Low	A – Band Thickness	0.500
		C – Maximum	0.386
		C – 90th Percentile	0.876
	Vc - Medium ΔT – High vs Low	A – Band Thickness	0.500
		C – Maximum	0.614
		C – 90th Percentile	0.876
	Vc - Low ΔT – High vs Low	A – Band Thickness	0.718
		C – Maximum	0.614
		C – 90th Percentile	0.614

Similar to the casting speed, all p-values were found to be above 0.05. Thus, the results from Method 1 and Metrics A and C are statistically insignificant from condition to condition. This further confirms the indifference of Method 1 and Metrics A and C to the changes in macro segregation regarding the selected superheats.

A comparison using Method 2 and Metric A (band thickness) for factors 1.03, 1.06 and 1.09 and the 2 and 3 value system is plotted in Figure 33 for low and high superheats.

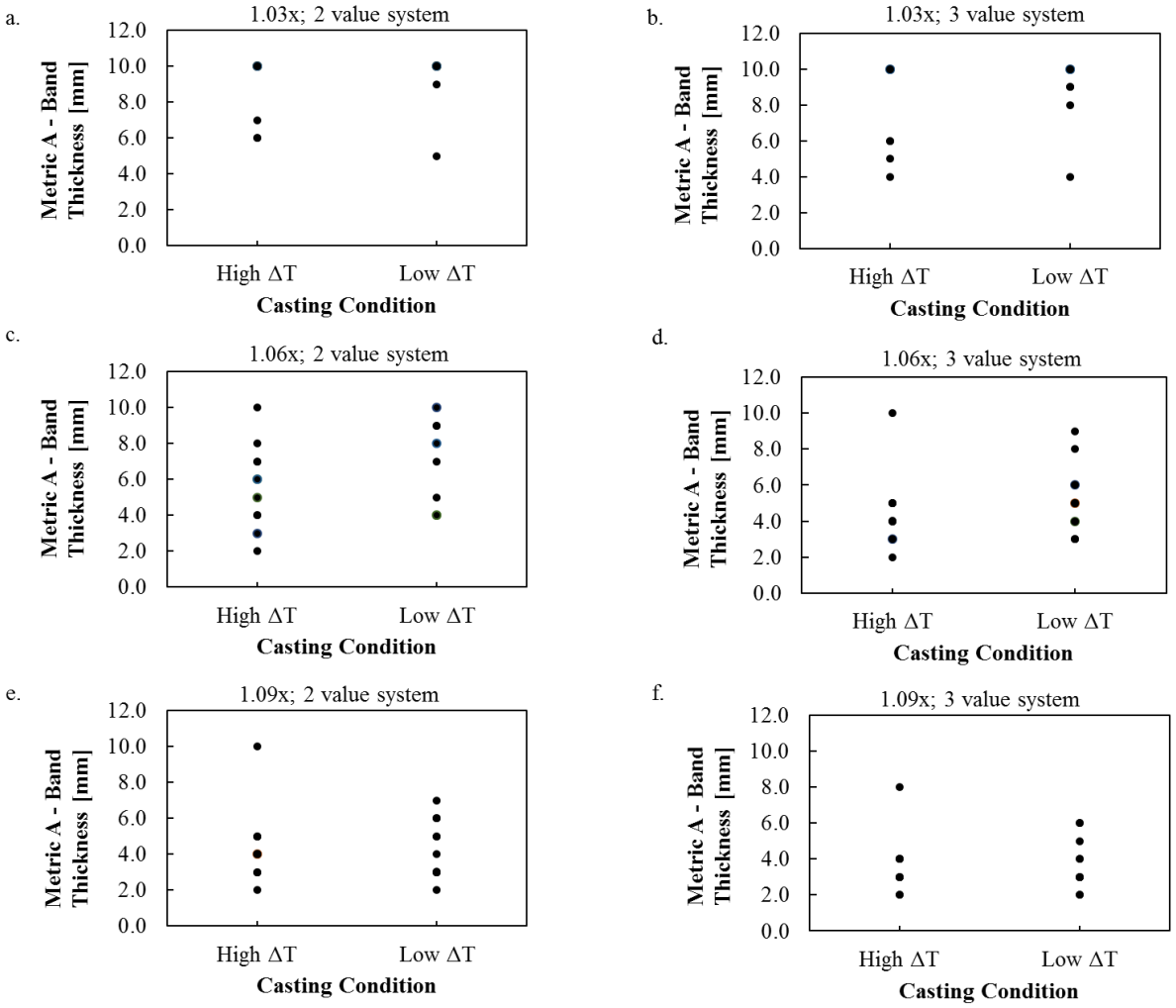

Figure 33: Metric A as a function of superheat for 1.5 Mn wt% using factors 1.03x, 1.06x, 1.09x and 2 and 3 value systems

From Figure 33, there is no evidence of a statistically significant trend as the superheat varies. For results regarding the full spectrum of factors and value systems, see Appendix C.

Metric B (average of normalized Mn) was also used to assess segregation between low and high superheat. The results were plotted in Figure 34. It is evident that the average normalized Mn remains consistent as superheat varies.

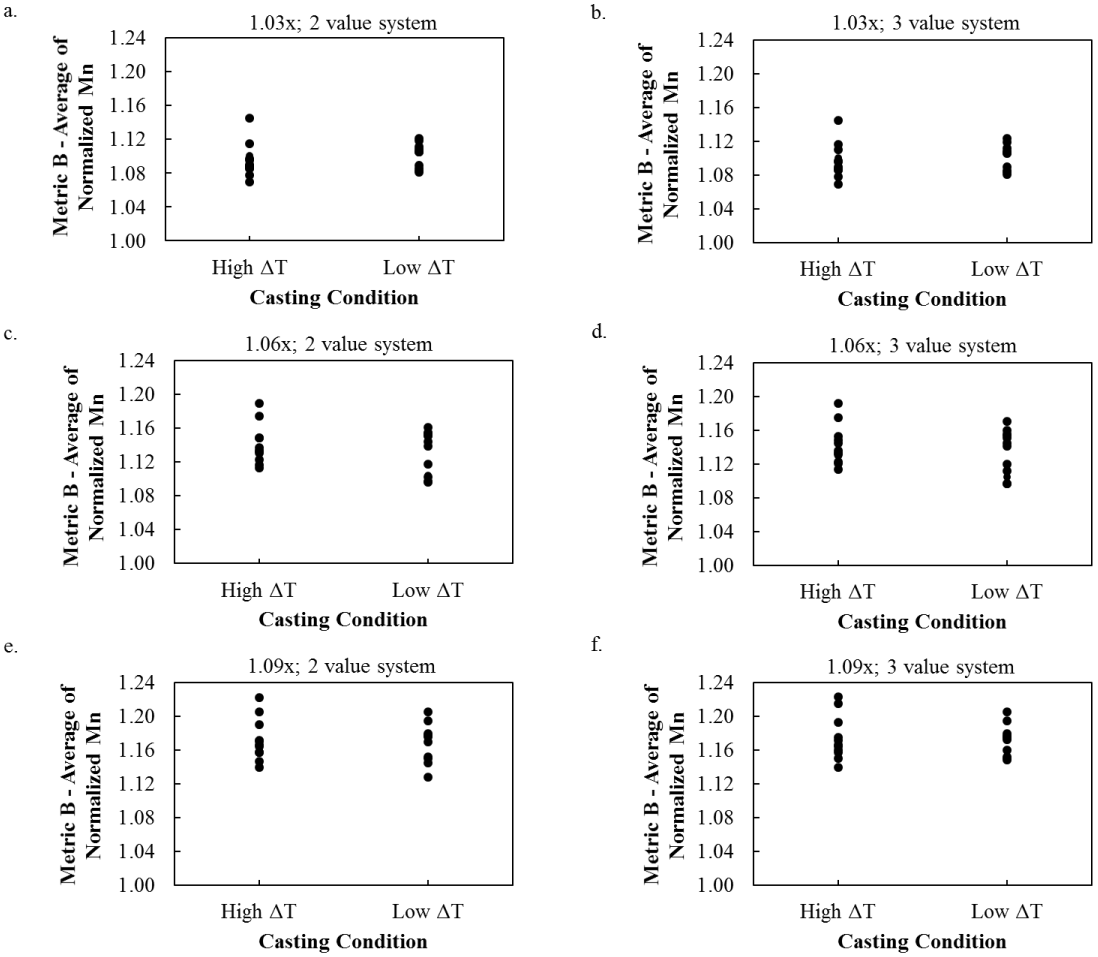

Figure 34: Metric B as a function of superheat for 1.5 Mn wt% using factors 1.03x,1.06x, 1.09x and 2 and 3 value systems

Method D (area %), as a function of superheat, is shown in Figure 35.

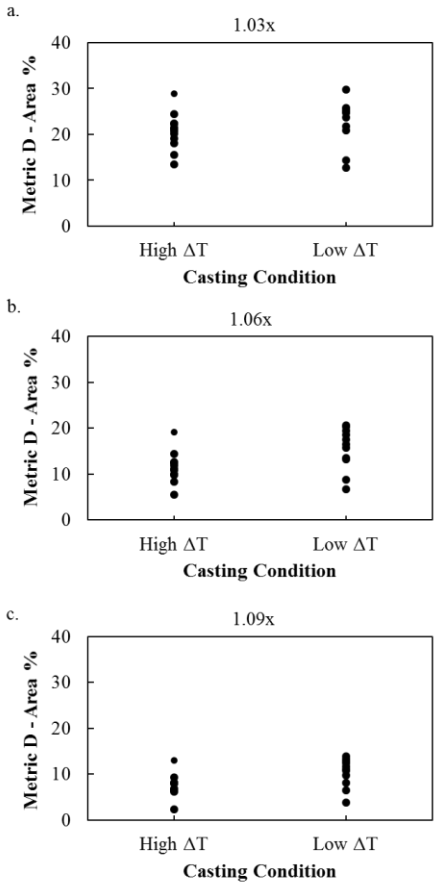

Figure 35: Metric D as a function of superheat for 1.5 Mn wt% using factors 1.03x, 1.06x, 1.09x

The plots reveal that the percentage of area which contains normalized values greater than 1.03, 1.06 and 1.06, remains constant. Similar results are seen for the remaining factors and can be found in Appendix C. Thus, Method D appears to be insensitive to the tested superheats.

Contrary to the results, as the superheat varied, a prominent difference in all metrics using both methods was anticipated. From literature, the superheat affects segregation via the size of columnar zones, making it a key factor to control during solidification. Columnar zones can greatly affect the amount of segregation present, especially at the centerline [26] [28]. Growth of columnar zones can be suppressed by ensuring that a sufficient amount of equiaxed crystals are present ahead of the columnar

front. As mentioned before, contrary to columnar dendrites, equiaxed crystals eject solutes uniformly within the mushy zone, which results in a significant reduction in segregation [26] [28]. Low superheats enable more equiaxed crystals to survive, sink down the mold and become deposited in front of the columnar grain front, resulting in smaller columnar zones and smaller levels of segregation [28]. On the other hand, high superheats minimize the amount of equiaxed crystals, due to the higher temperature of the surrounding bulk liquid. Therefore, larger columnar sections are formed, resulting in larger levels of segregation [28]. However, no correlation was found between the tested ΔT and developed metrics.

4.2.6 Effect of Nominal Mn Composition

The effects of varying nominal Mn composition on segregation, using Method 1 and Metric A and C, are plotted in Figure 36 and Figure 37.

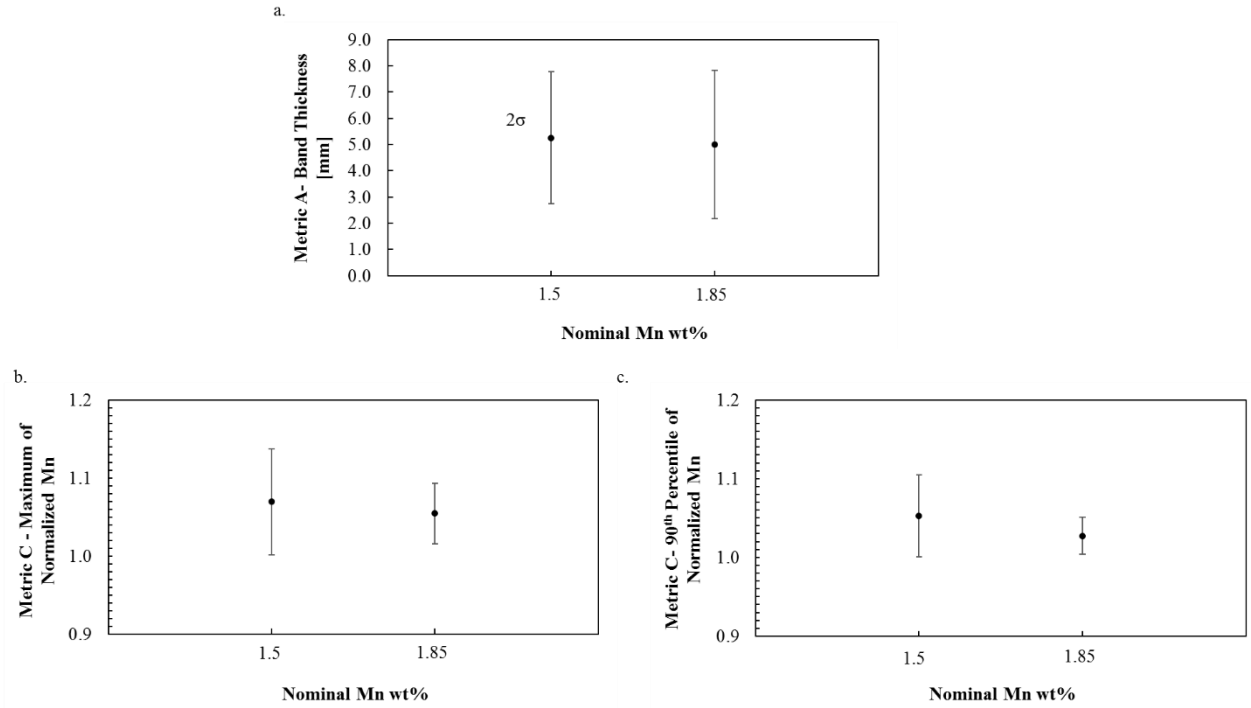

Figure 36: Metrics A and C as a function of 1.5 and 1.85 Mn wt%

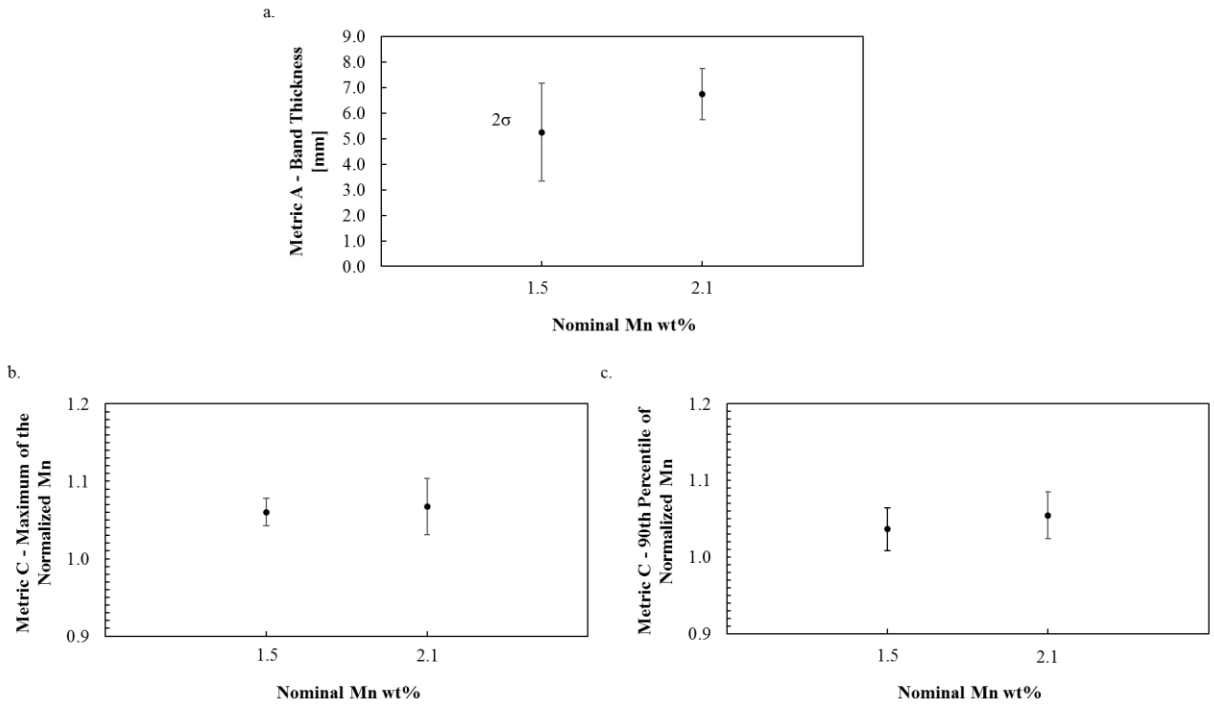

Figure 37: Metrics A and C as a function of 1.5 and 2.1 Mn wt%

The results reveal that a nominal Mn composition of 2.1 wt% has a smaller variation in band thickness than a 1.5 wt% nominal composition. On the other hand, the band thickness and two sigma standard deviations for 1.85 Mn wt% were found to be more consistent with the lower composition. Similarly, Metric C reveals that the maximum and 90th percentiles of all three nominal compositions are consistent.

The p-values, shown in Table 8, reveal that the results from Metrics A and C are statistically insignificant as the nominal composition varies.

Table 8: P values for statistical tests (1.5 vs 1.85 vs 2.1 Mn wt%)

Test Type	Casting Conditions	Nominal Mn Composition [wt%]	Metric	p - value
Mann - Whitney	Vc - Medium ΔT - Low	1.5 vs 1.85	A – Band Thickness	0.332
			C – Maximum	0.614
			C – 90th Percentile	0.807
	Vc - High ΔT - High	1.5 vs 2.1	A – Band Thickness	0.074
			C – Maximum	0.282
			C – 90th Percentile	0.193

A comparison between samples containing 1.5, 1.85 and 2.1 nominal Mn wt% composition, using Method 2 and Metric A (band thickness) and B (average of normalized Mn) is shown in Figure 38 and Figure 39. The remaining factors can be found in Appendix D. Both metrics appear to be unresponsive to changes in macro segregation as the nominal Mn composition varied. No distinct pattern emerged as the experimental data of samples from each nominal Mn composition was filtered and assessed.

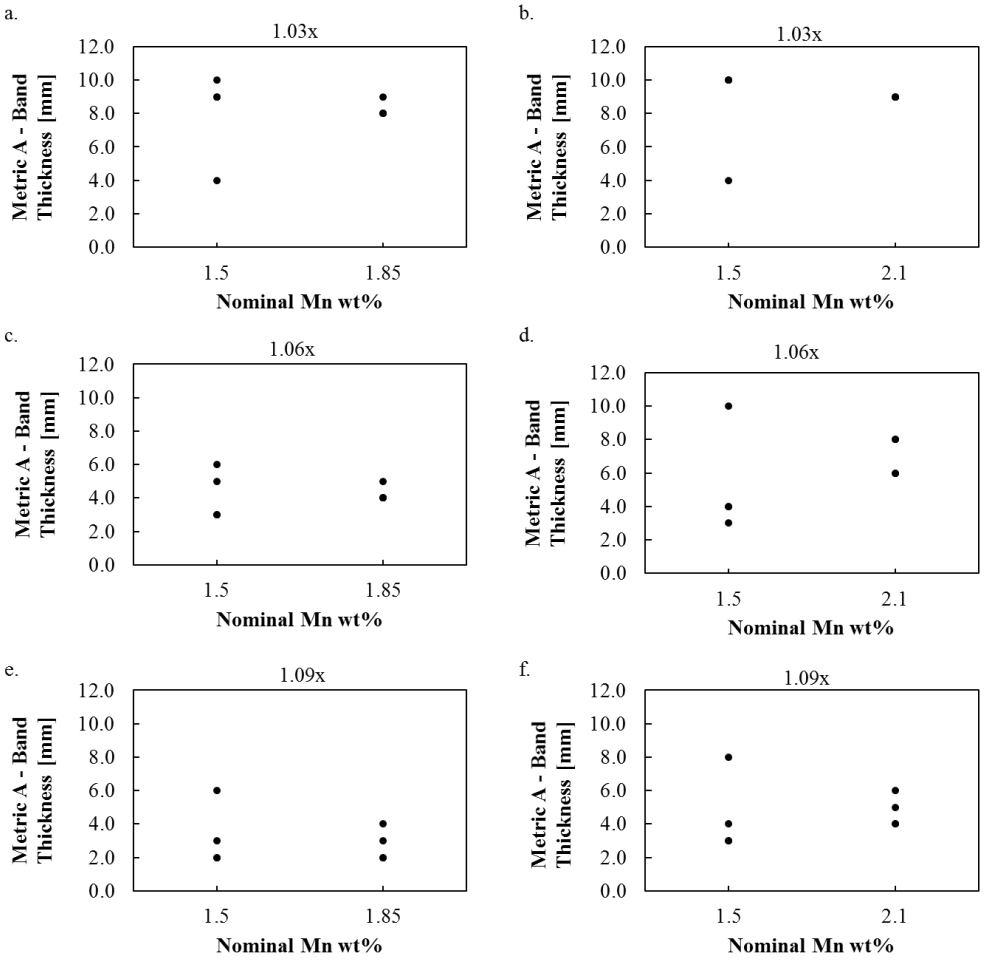

Figure 38: Metric A as a function of nominal composition of 1.5, 1.85 and 2.1 Mn wt% using a 3 value system

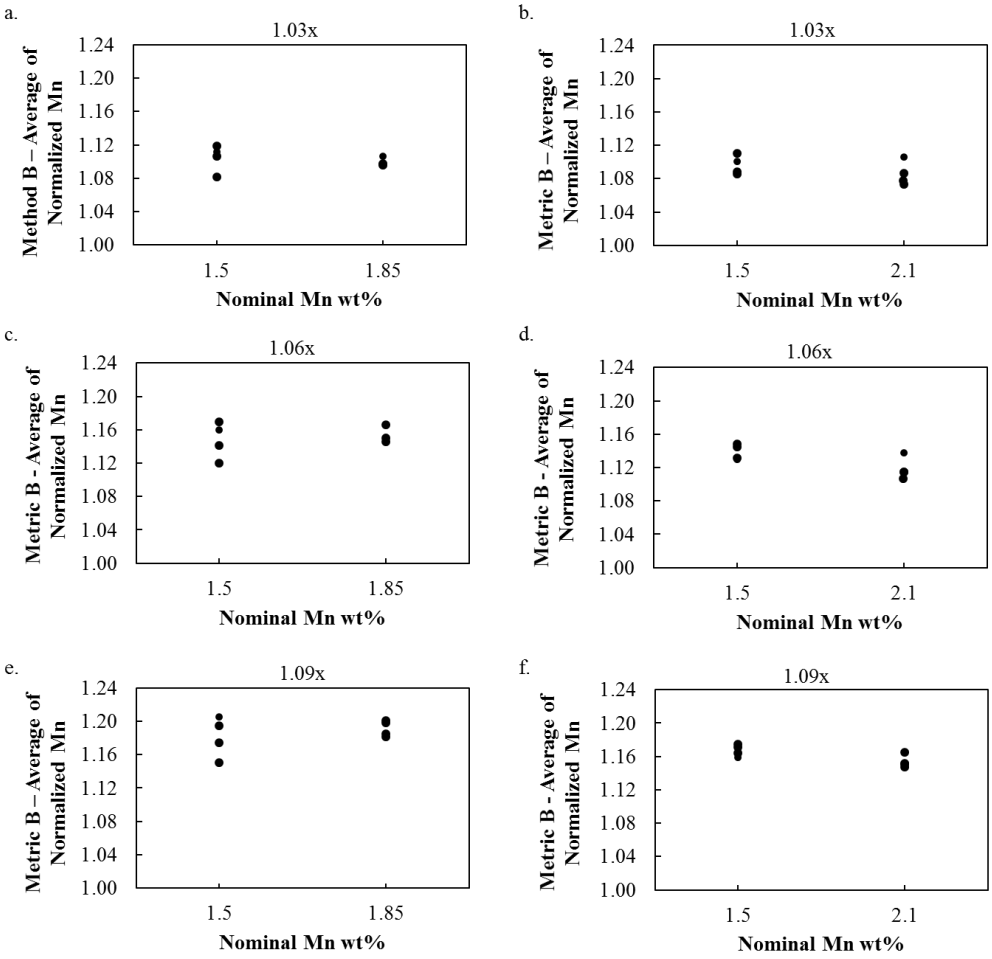

Figure 39: Metric B as a function of nominal composition of 1.5, 1.85 and 2.1 Mn wt% using factors 1.03x,1.06x, 1.09x and a 3 value system

A comparison was done using Metric D (area %) as well and is shown in Figure 40. The remaining factors can be found in Appendix D. Metric D seems to be indifferent to the change in nominal Mn composition as well.

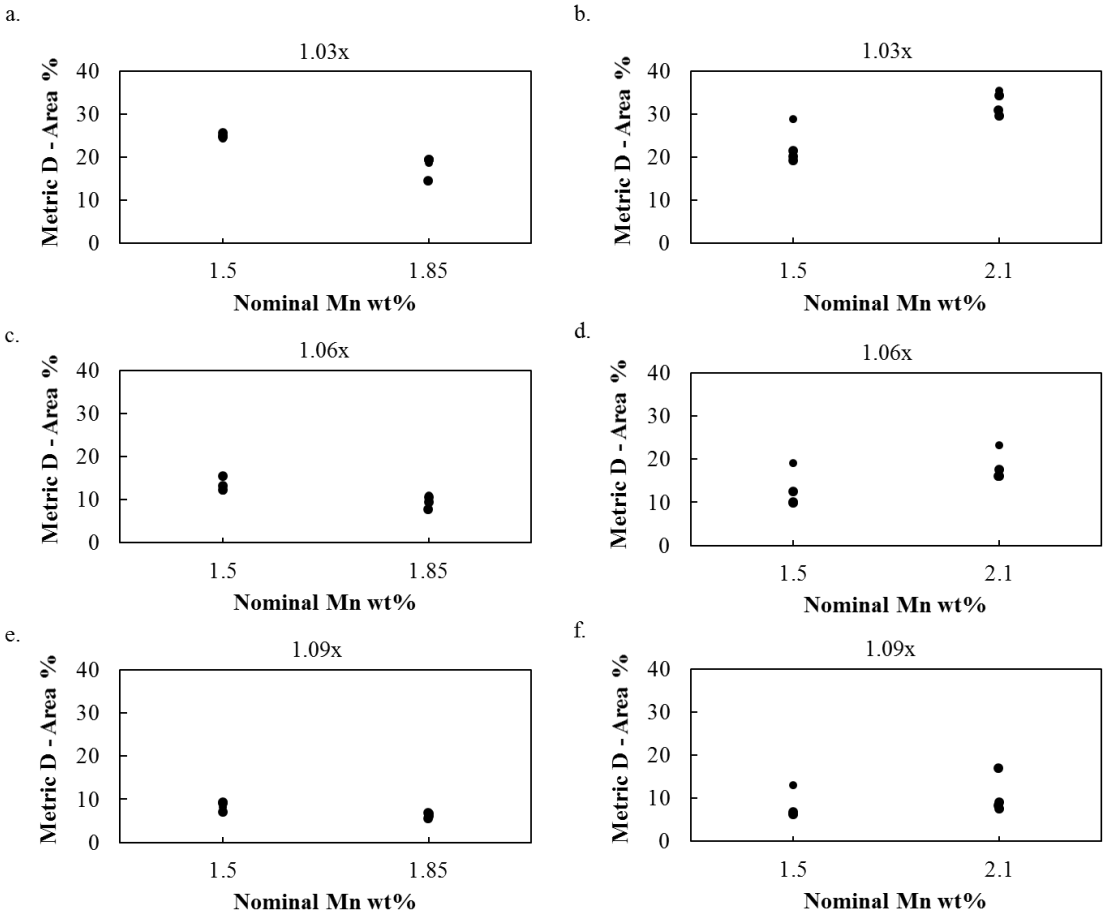

Figure 40: Metric D as a function of nominal composition of 1.5, 1.85 and 2.1 Mn wt% using factors 1.03x, 1.06x, 1.09x

4.3 Far Field

4.3.1 Metric Overview

The far field was also investigated for traces of macro segregation. As mentioned before, martensite bands appear in the far field as well, and more specifically, at the quarter thickness. One of the simplest ways to examine this is by analyzing an average of the normalized Mn in a fixed area in the FF, for Samples A to D and per slab condition. Normalized Mn values, within a 60 by 40 mm fixed area, as

shown by the red box in Figure 41, were averaged and plotted as a function of the spatial orientation, casting parameters and nominal Mn compositions.

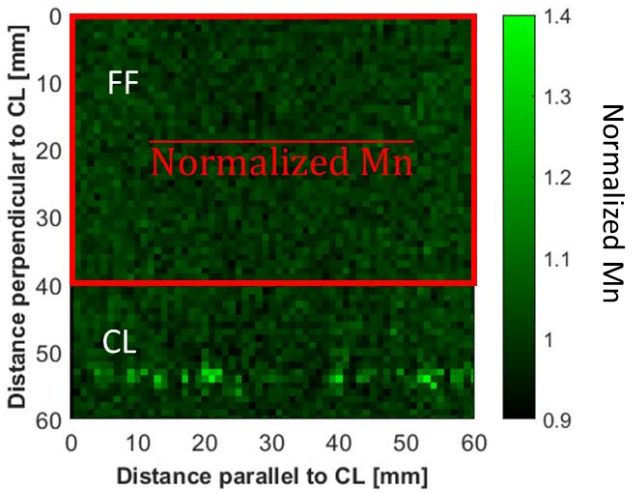

Figure 41: Fixed area used to calculate far field average

4.3.2 Effect of Spatial Orientation

Figure 42 plots the averages from Samples A to D at one casting condition. The results show that each average is close to unity and the corresponding two sigma standard deviations are relatively low and consistent in between samples. This trend is seen for all six conditions. See Appendix E.

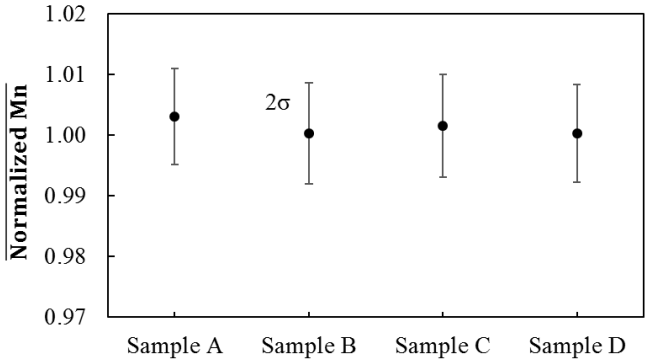

Figure 42: Far field average of the normalized Mn as a function of spatial orientation for a High Vc and High ΔT casting condition

These results indicate that regardless of the spatial orientation, the average normalized Mn, and hence the amount of macro segregation at the far field, is considerably low and similar in between samples that are 0.5 meter apart in the slab length and width direction.

4.3.3 Effect of Casting Speed

Due to the similarities in the average normalized Mn values from Samples A to D, an average of the four sample was taken to compare between casting conditions. Figure 43 plots the effect of casting speed on macro segregation in the far field.

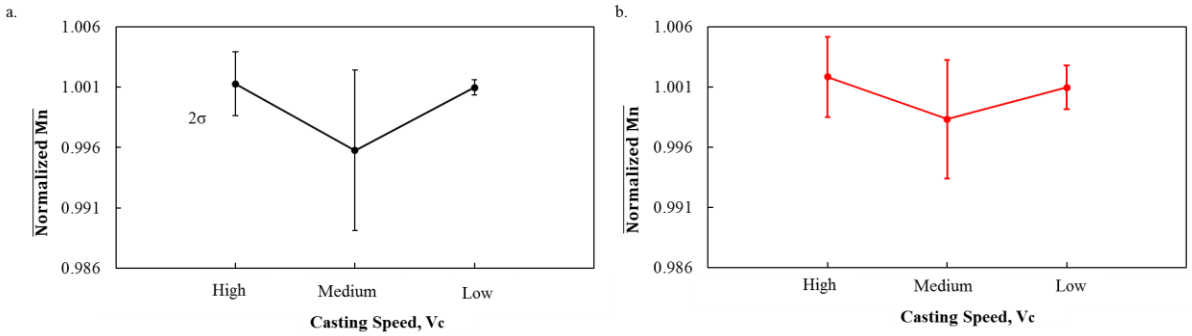

Figure 43: Effect of Vc in the far field for a. a high ΔT b. a low ΔT

The average normalized Mn in the far field remains essentially the same as the casting speed changes. At both superheats, the medium casting speed was found to have somewhat larger two sigma standard deviations. However, the scale of this deviation is insignificant. This reveals that macro segregation in the far field is largely unaffected by the tested casting speeds and applied metric.

4.3.4 Effect of Superheat

Figure 44 plots the effect of superheat on macro segregation in the far field.

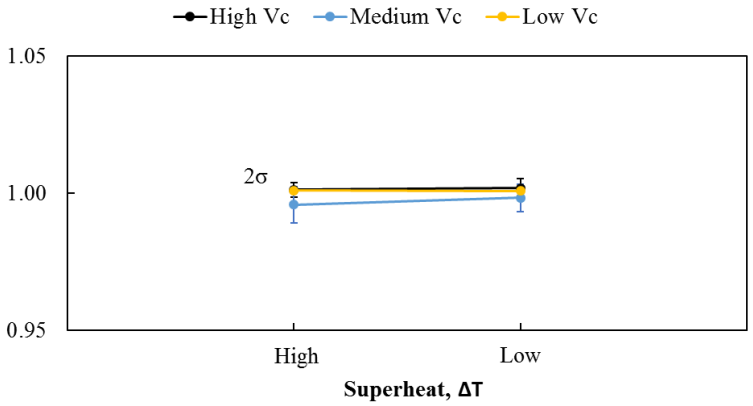

Figure 44: Effect of ΔT in the far field

Similarly, the average normalized Mn in the far field remains the same as the superheat changes. This reveals that macro segregation in the far field is largely unaffected by the tested superheat and applied metric.

4.3.5 Effect of Nominal Mn Composition

Figure 45 plots the effect of nominal Mn composition on the average normalized Mn values in the far field.

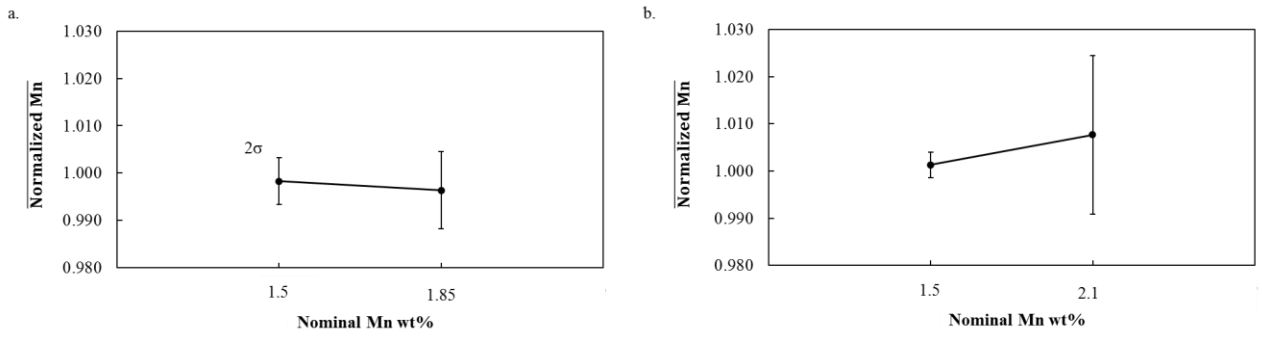

Figure 45: Effect of Nominal Mn composition in the far field

Figure 45 reveals that macro segregation in the far field in not significantly affected by a change in nominal Mn composition, at the selected casting conditions. Although results regarding the 2.1 Mn wt% samples were found to have a much larger two sigma standard deviation, the scale of it is not substantial enough to corroborate differences. Thus, this metric reveals that macro segregation in the far field is largely unaffected by the chosen nominal Mn compositions and their corresponding casting conditions.

4.4 Factors to Consider

4.4.1 Centerline

At first glance, the lack of responsiveness of Metrics A – D on the centerline, using both methods, could be due to various reasons, which includes selection of alloy, casting parameter and experimental parameters, and metric development. The DP alloy chosen for inspection has a nominal Mn composition of 1.5 wt%. This composition may be too low to create significant macro segregation differences at the centerline. However, as seen in section 4.2.6, nominal compositions of 1.85 and 2.1 Mn wt% also showed limited sensitivity to changes in macro segregation as a function of the four metrics. Thus, the nominal composition may not be the issue. However, one can argue that without analyzing a full spectrum of V_C and ΔT for slabs with nominal compositions of 1.85 and 2.1 Mn wt%, it is premature to suggest that alloy selection did not play a role in the results.

With regards to the experimental parameters, the spatial resolution and dwell time can strongly influence the quality of the experimental data obtained, and hence, affect the subsequent application of the metrics. It is well known that a longer dwell time will improve data quality while a finer spatial resolution will increase the amount of data obtained. In five out of twenty-four scans, it was evident that a finer resolution scan was required for more details at the centerline. An example of supplementary scanning with a finer spatial resolution is shown Figure 46.

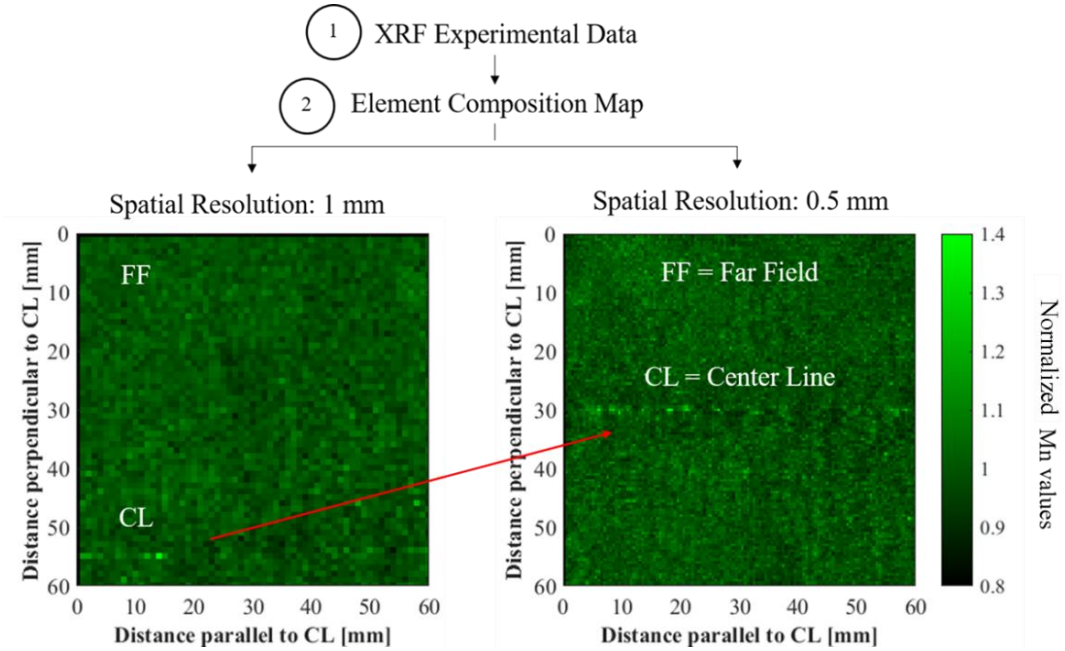

Figure 46: Comparison between 1 mm and 0.5 mm spatial resolutions

A comparison of the two frequency distributions is shown in Figure 47.

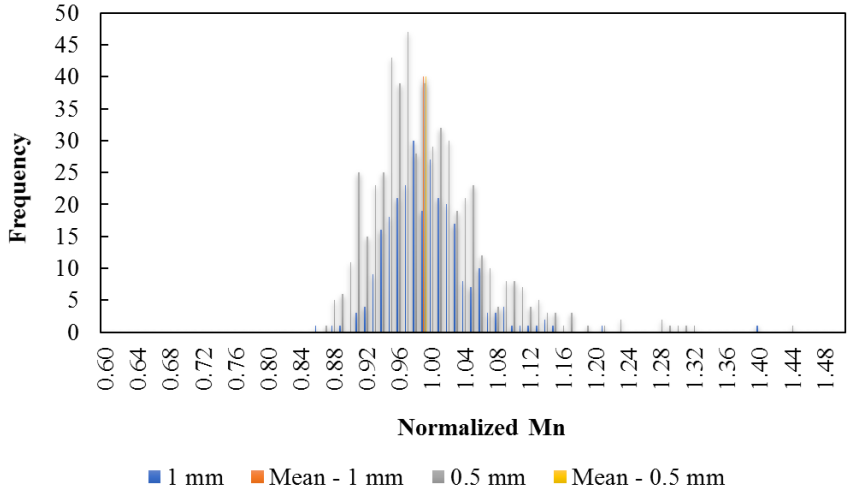

Figure 47: An overlap of centerline frequency distributions of 1 and 0.5 mm spatial resolution scans of Sample A with High Vc and high ΔT casting condition

However, a comparison between results from Method 1 and Metrics A and C for both spatial resolutions reveal that the band thickness, maximum and 90th percentiles do not differ drastically from one resolution to another. See Figure 48.

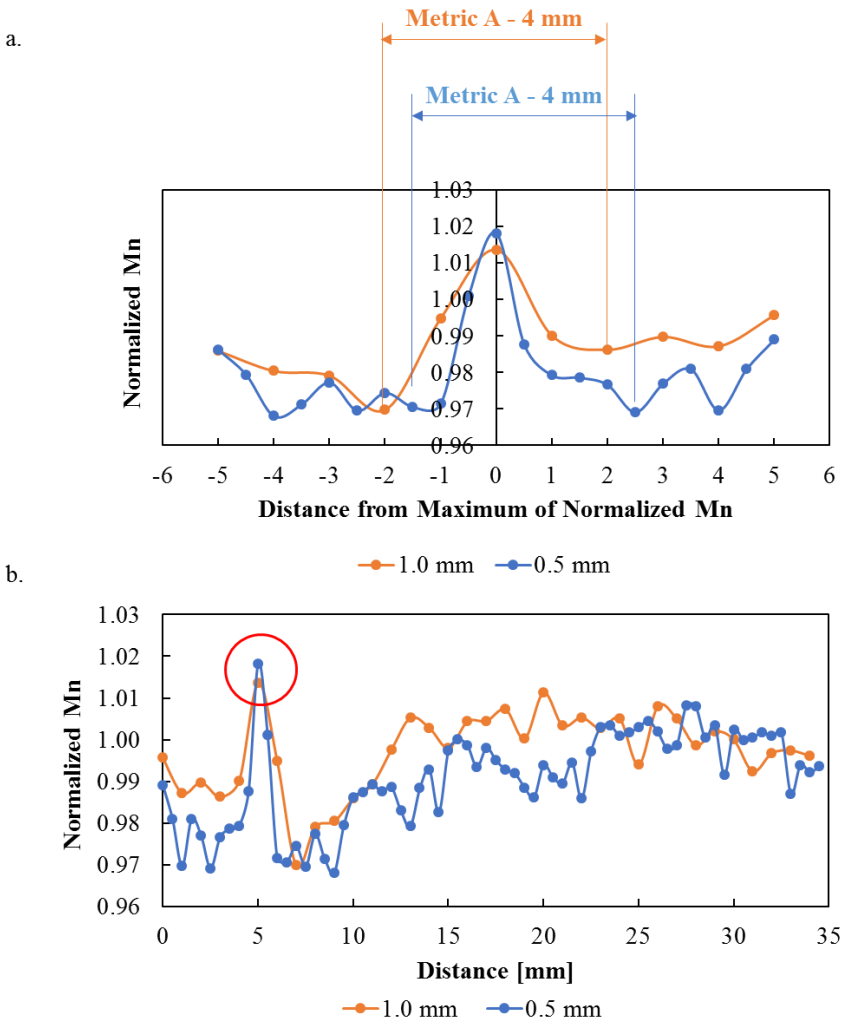

Figure 48: Comparison of a. Metric A b. Metric C for Sample A with High V_c and High ΔT casting condition

From Figure 48, it is evident that Metric A (band thickness) remains the same, while the maximum shows a negligible increase of 1% from a 1 mm to 0.5 mm spatial resolution.

Furthermore, a quantitative analysis using Method 2 and Metrics A, B and D revealed that the band thickness, average of normalized Mn and area percent also do not change radically. See Figure 49.

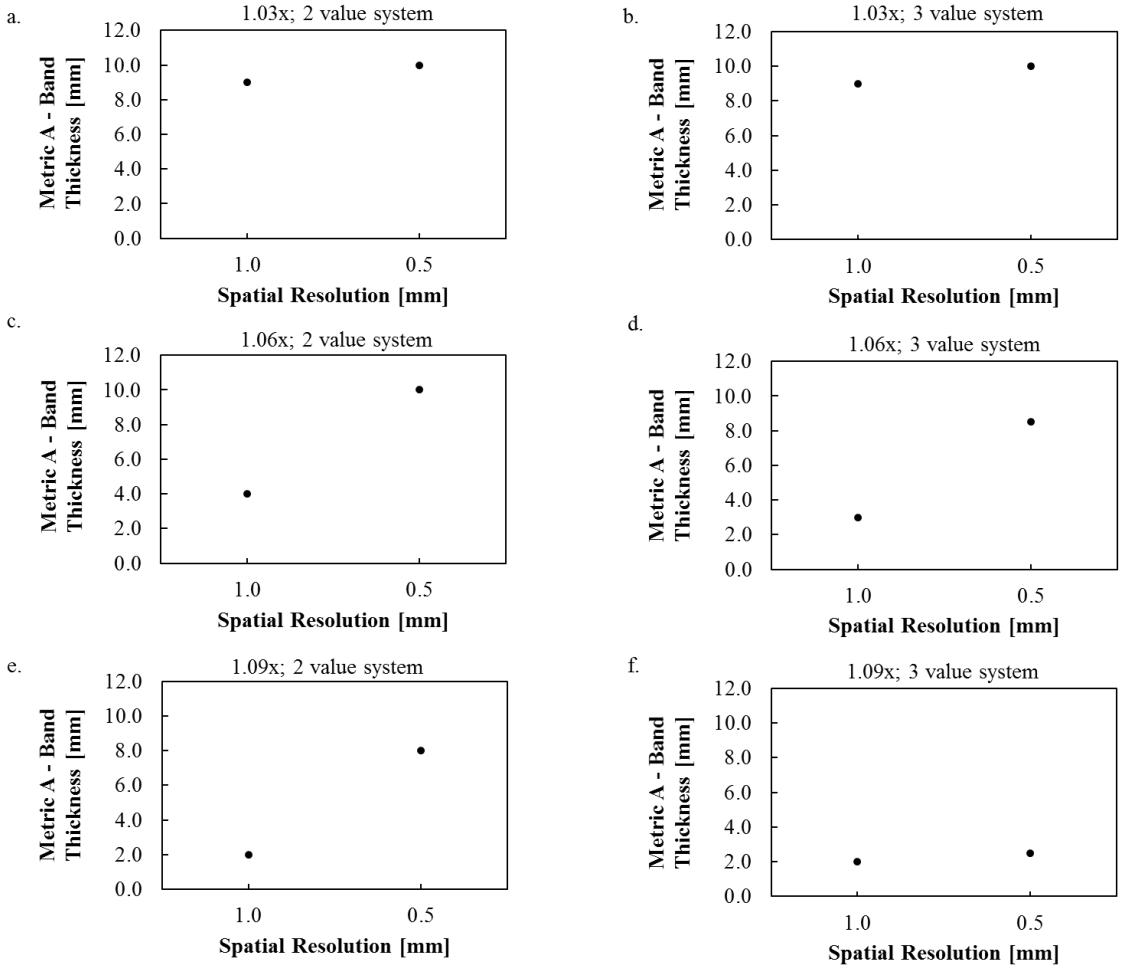

Figure 49: Metric A on 1 mm and 0.5 mm spatial resolution scans

From Figure 49, Figure 50 and Figure 51, it is evident that Metric A (band thickness), B (average of normalized Mn) and D (area percent) continues to be similar in between the two datasets. Refer to Appendix F for all the factors and value system results. Metric D reveals slightly larger area percentages for the finer resolution scans at all factors and value systems. This is expected because a 0.5 mm scan generates twice as much data as the 1 mm scans, hence leading to larger results regarding Metric D. Hence, experimental parameters such as spatial resolution may not have had a significant effect on the insensitivity of the metrics to the changes in segregation.

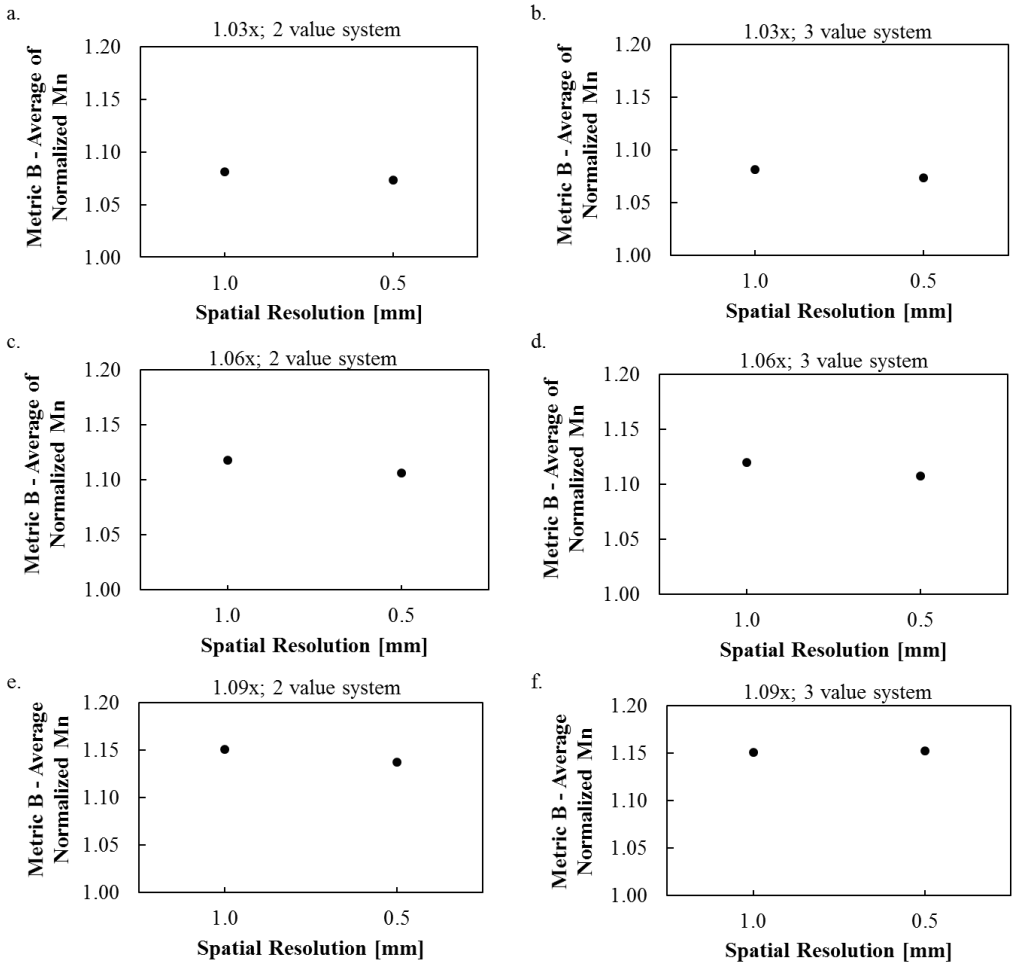

Figure 50: Metric B on 1 mm and 0.5 mm spatial resolution scans

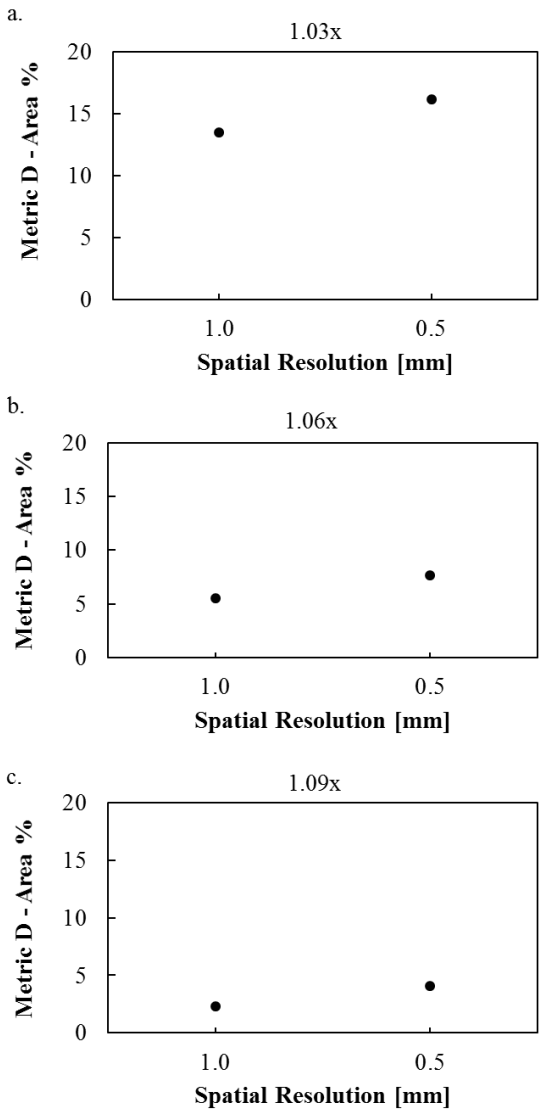

Figure 51: Metric D on 1 mm and 0.5 mm spatial resolution scans

To diversify the metrics explored, four different metrics, using two separate methods, were developed. However, the metrics and methods yielded unresponsive results. Yet, there are several advantages and disadvantages of using Methods 1 and 2. Method 1 focuses on consolidating the experimental data by identifying an arithmetic mean. The arithmetic mean is a common measure of central tendency. One of the advantages of using the arithmetic mean, and thus, Method 1, is that any metric using this method can be easily calculated. Moreover, fluctuations in arithmetic means are minimal for repeated samples from the same population i.e. slab condition. Averages are a convenient means of

summarizing large amounts of data in to singular values and highlight variability around this value from within the original dataset. Thus, the segregation profiles, and corresponding Metrics A and C, can be used for comparison purposes in a simplistic manner. However, there are some limitations associated with using this measurement. Firstly, this measurement is effective for normally distributed datasets. Skewness, such as the one seen in the centerline frequency distribution in Figure 28, renders the arithmetic mean less effective. Additionally, using a mean to summarize a large amount of data into a single value can also wash out any sensitivities in the dataset, and hence lead to a lack of results.

Furthermore, the arithmetic average is extremely sensitive to extreme or dispersed values. Metrics A and C both take an average of four samples per slab condition. For instance, one slab condition may report a larger range of band thicknesses, which may contain outliers. An average of this dataset would grossly amplify this larger range and lead to skewed results, even with the initial screening via the element composition maps.

On the other hand, Method 2 does not use an arithmetic average, and instead allows for a wide range of factors and value system that can be used to filter and assess the dataset. This customizable aspect of Method 2 could be a benefit, as it provides freedom to investigators, whether they be academic researchers or casting engineers, to select according to their purposes. However, an abundance of choice is not necessarily the most advantageous. Within the range of factors, 1.03 may be too small to filter out less segregated areas at the centerline, while 1.1 or 1.2 may be too large and results in over screening. See Figure 52.

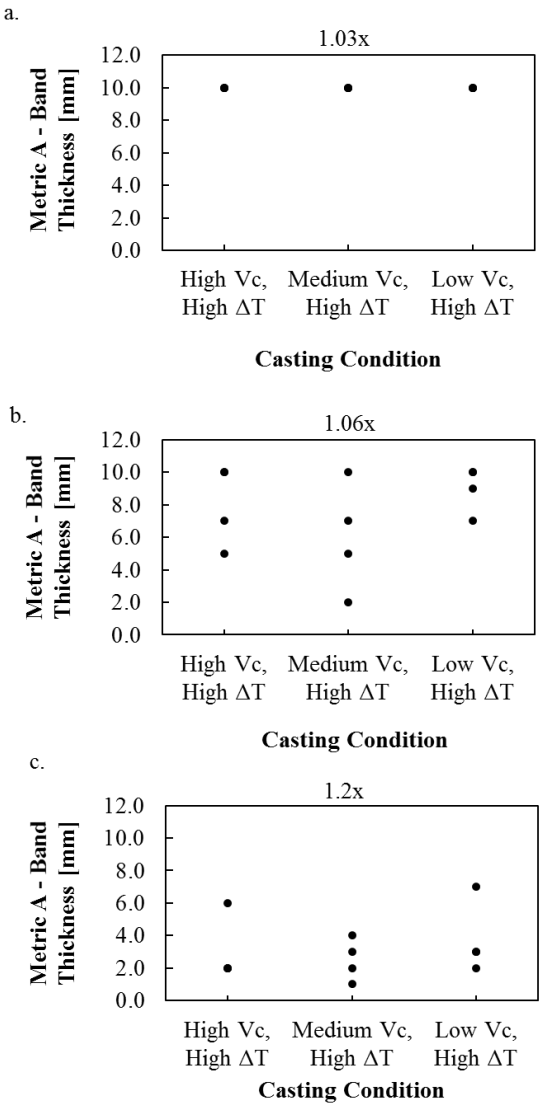

Figure 52: Metric A using 4 value system and 1.03x, 1.06x and 1.2x factors

Similarly, the 1 value system may too flexible, and thus making it more difficult to detect the start and end of centerline segregation areas, and the 4 value system may be too stringent, resulting in an incorrect assessment. See Figure 53.

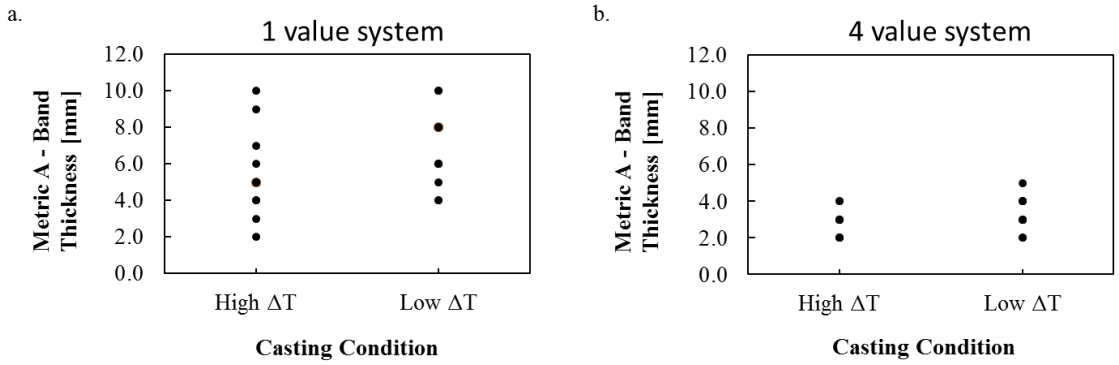

Figure 53: Metric A using 1 vs 4 value system using a 1.09x factor

Thus, a larger, more customizable range of choices is beneficial, but also allows more room for errors in judgements.

In addition to alloy selection, experimental parameters and metric development, the outcome of the results are also due to the chosen casting conditions. It is possible that, from a quantitative point of view, the selected Vc and ΔT were within a range of condition that do not produce a large enough difference in macro segregation. Although the Vc and ΔT were categorized using three and two levels respectively, these conditions do not differ from one another by large degrees. See Table 4. The chosen casting parameters fall within ranges that have been previously studied, albeit the alloy within this study had a nominal composition of 1.9 Mn wt% [36]. However, it is crucial to note the qualitative nature in which the centerline segregation was judged within the study. To develop new quantitative metrics with the aim of effectively assess centerline macro segregation, perhaps extreme casting conditions needs to be analyzed initially. Afterwards, once the relationship between casting parameters and the degree of segregation is more clearly enumerated, the metrics can be fitted to more practical industrial conditions.

Regardless, whether individually or in combination, several reasons for the lack of sensitivity of the developed metrics have been acknowledged.

4.4.2 Far Field

Although micro segregation was not investigated in this thesis, it is important to recognize that martensite bands are influenced by both macro and micro segregation. Using the experimental data, one potential way of investigating this is by focusing on the segregation profiles. These profiles spatially graph the Mn variation in the far field and the centerline, as shown in Figure 54.

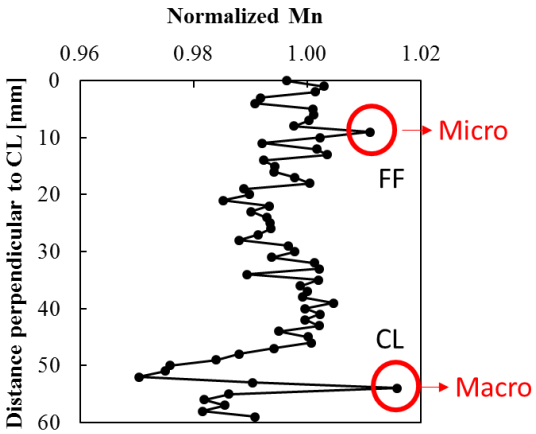

Figure 54: Segregation profile for medium casting speed and high superheat condition

Typically, the largest peak is found at the centerline and it corresponds to macro segregation. However, the plot also reveals smaller, yet prominent peaks within the far field. These peaks could potentially be related to micro segregation. Further analysis on the interval in between these peaks and their amplitudes could potentially be correlated to the thickness of the bands or the distance in between them. Thus, the experimental data also has prospect of characterizing both macro and micro segregation in the as-cast structure, prior to the formation of martensite bands.

Chapter 5: Conclusions and Recommendations

Mn macro segregation in the far field and centerline of the as-cast surface of DP 600 was examined as a function of slab spatial orientation, casting parameters and nominal Mn compositions. The experimental technique used, MXRF, was a departure from predominantly qualitative practices. Major conclusions are as follows:

1. The MXRF technique was used to successfully reveal and quantify macro segregation at the centerline and far field.
2. A dwell time of 3000 ms and spatial resolution of 1 mm were found to be suitable experimental parameters to reveal and detect Mn macro segregation in the as-cast structure.
3. The normalized experimental data provided numerous means to analyze centerline Mn distributions, leading to the development of two distinct methods. Method 1, which represented the datasets using a measurement of central tendency, the arithmetic average, was more predisposed to diminish sensitivities, yet, provided a more simplistic approach. On the other hand, Method 2 provided robustness and customization.
4. Using these two methods, four different metrics were created and their responsiveness to the change in centerline macro segregation as a function of spatial orientation, casting parameters and nominal compositions, were investigated. It was found that all metrics were insensitive to the variation in centerline macro segregation. Various factors, starting from alloy selection to metric development may have contributed to the overall insensitivity. In hopes of acquiring more severe macro segregation and the subsequent development of efficient metrics, it is recommended to choose more extreme casting conditions.
5. Far field macro segregation investigations revealed that as a function of spatial orientation, casting parameters and nominal compositions, Mn distribution was homogenous. From the analysis, segments of micro segregation were primitively identified. It is suggested that these regions could potentially lead to the formation of martensite bands and thus, more detailed analysis is advised.
6. Overall, the techniques developed and results obtained in this thesis opens a gateway that will lead to a shift from existing qualitative practices to more quantitative and standardized approaches of assessing Mn macro segregation in the as-cast structure of AHSS.

References

[1] C. Scott, S. Allain, M. Faral and N. Guelton, "The development of a new Fe-Mn-C austenitic steel for automotive applications," *Revue de Métallurgie–International Journal of Metallurgy,* vol. 103, no. 6, pp. 293-302, 2006.

[2] A. Grajcar, "Segregation behaviour of third generation advanced high-strength Mn-Al steels," *Archives of Foundry Engineering,* vol. 12, no. 2, pp. 123-128, 2012.

[3] A. Grajcar, R. Kuziak and W. Zalecki, "Third generation of AHSS with increased fraction of retained austenite for the automotive industry," *Archives of Civil and Mechanical Engineering,* vol. 12, p. 334–341, 2012.

[4] D. K. Matlock, J. G. Speer, E. De Moor and P. J. Gibbs, "Recent Developments in Advanced High Strength Sheet Steels for Automotive Applications: An Overview," *Jestech,* vol. 1, pp. 1-12, 2012.

[5] D. K. Matlock and J. G. Speer, "Processing Opportunities for New Advanced High-Strength Sheet Steels," *Materials and Manufacturing Processes,,* vol. 25, pp. 7-13, 2010.

[6] W. Bleck, D. Raabe and H. Dong, "High Manganese Steels 2014," in *International High Manganese Steel Conference*, Weinheim, 2015.

[7] G. Krauss, "Solidification, Segregation, and Banding in Carbon," *Metallurgical and Materials Transactions B,* vol. 34B, no. 6, pp. 781-792, 2003.

[8] M. Thompson, M. Ferry and P. Manohar, "Simulation of Hot-band Microstructure of C–Mn Steels during," *The Iron and Steel Institute of Japan International,* vol. 41, no. 8, pp. 891-899, 2001.

[9] L. Shi, Z.-s. Yong-chang Liu, Y. Xu Yang, C. Zhang and H.-j. Li, "Effect of acicular ferrite on banded structures in low-carbon microalloyed," *International Journal of Minerals, Metallurgy and Materials,* vol. 21, no. 12, pp. 1167-1174, 2014.

[10] S. Thompson and H. P.R., "Factors influencing ferrite/pearlite banding and origin of large pearlite nodules in a hypoeutectoid plate steel," *Materials Science and Technology,* vol. 8, pp. 777-784, 1992.

[11] L. Li, H. Ding, L.-x. Du, J.-l. Wen, H.-m. Song and P.-j. Zhang, "Influence of Mn Content and Hot Deformation on Transformation Behavior of C-Mn Steels," *Journal of Iron and Steel Research International,* vol. 15, no. 2, pp. 51-55, 2008.

[12] S. K. Sarna, "STEELS FOR AUTOMOTIVE APPLICATIONS," Ispat Digest, 21 November 2015. [Online]. Available: http://ispatguru.com/steels-for-automotive-applications/. [Accessed 05 September 2017].

[13] "Automotive Steel Definitions," World Auto Steel Association, [Online]. Available: http://www.worldautosteel.org/steel-basics/automotive-steel-definitions/. [Accessed 9 September 2017].

[14] D. J. Schaeffler, "Introduction to advanced high-strength steels - Part I," Stamping Journal, 9 August 2005. [Online]. Available: http://www.thefabricator.com/article/metalsmaterials/introduction-to-advanced-high-strength-steels---part-i. [Accessed 05 September 2017].

[15] R. Kuziak, K. R. Kawalla and S. Waengler, "Advanced high strength steels for automotive industry," *Archives of Civil and Mechanical Engineering,* vol. 8, no. 2, pp. 103-117, 2008.

[16] L. A. Dobrzanski, A. Grajcar and W. Borek, "Microstructure evolution of high-manganese steel during the thermomechanical processing," *Archives of Materials Science and Engineering*, vol. 37, no. 2, pp. 69-76, 2009.

[17] B. C. De Cooman, K.-g. Chin and J. Kim, "High Mn TWIP Steels for Automotive Applications," in *New Trends and Developments in Automotive System Engineering*, Intechopen, 2011.

[18] B. Mintz and J. M. Arrowsmith, "Hot-ductility behaviour of C-Mn-Nb-Al steels and its relationship to crack propagation during straightening of continuously cast strand," *Metals Technology,* pp. 24-32, 1979.

[19] B. G. Thomas, "Continuous Casting of Steel," in *Modeling for Casting and Solidification Processing*, New York, CRC Press, 2001, pp. 499-540.

[20] S. Seetharaman, Treatise on Process Metallurgy, Volume 3: Industrial Processes, Oxford: Elsevier Ltd, 2013.

[21] B. Kozak and J. Dzierzawski, "Continuous Casting of Steel: Basic Principles," American Iron and Steel Institute, [Online]. Available: http://www.steel.org/making-steel/how-its-made/processes/processes-info/continuous-casting-of-steel---basic-principles.aspx. [Accessed 5 September 2017].

[22] "Secondary steel making," TATA Corus Education, [Online]. Available: http://resources.schoolscience.co.uk/Corus/14-16/steel/msch5pg1.html. [Accessed 5 September 2017].

[23] D. Kopeliovich, "Solidification," SubsTech, 1 June 2012. [Online]. Available: http://www.substech.com/dokuwiki/doku.php?id=solidification. [Accessed 5 September 2017].

[24] M. C. Flemings, Solidification Processing, New York: McGraw-Hill, 1974.

[25] T. F. Bower, H. D. Brody and M. C. Flemings, "Measurements of solute redistribution in dendritic solidification," *Transaction of the Metallurgical Society of AIME,* vol. 236, pp. 624-633, 1966.

[26] S. Choudhary and S. Ganguly, "Morphology and Segregation in Continuously Cast High Carbon," *The Iron and Steel Institute of Japan International* , vol. 47, no. 12, p. 1759–1766, 2007.

[27] J. J. Moore, "Review of Axial Segregation in Continuously Cast Steel," in *Continuous Casting*, vol. 2, Chelsea, Iron and Steel Society of AIME, 1984, pp. 185-192.

[28] X. Huang, B. Thomas and F. Najjar, "Modeling Superheat Removal during Continuous Casting of Steel Slabs," *Metallurgical Materials Transactions B,* vol. 23B, no. 6, pp. 339-356, 1992.

[29] K. Ayata, H. Mori, K. Taniguchi and H. Matsuda, "Low Superheat Teeming with Electromagnetic Stirring," *The Iron and Steel Institute of Japan International*, vol. 35, no. 6, pp. 680-685, 1995).

[30] J. E. Lait and J. K. Brimacombe, "Solidification During Continuous Casting of Steel," in *Continuous Casting*, vol. 2, Chelsea, Iron and Steel Society of AIME, 1984, pp. 171-182.

[31] V. V. G. F, Metallography: Principles and Practice, ASM International, 1984.

[32] t. Pikkarainen, V. Vuorenmaa, I. Rentola, M. Leinonen and D. Porter, "Effect of superheat on macrostructure and macrosegregation in continuous cast low-alloy steel slabs," *Materials Science and Engineering,* vol. 117, pp. 1-7, 2016.

[33] E. J. Pickering and M. Holland, "Detection of macrosegregation in a large metallic specimen using XRF," *Ironmaking and Steelmaking,* vol. 41, no. 7, pp. 493-499, 2014 .

[34] E. J. Pickering, C. Chesman, S. Al-Bermani, M. Holland, P. Davies and J. Talamantas-Silvia, "A Comprehensive Case Study of Macrosegregation in a Steel Ingot," *Metallurgical and Materials Transactions B,* vol. 46B, pp. 1860-1874, 2015.

[35] S. E. Offerman, N. H. Van Dijk, M. T. Rekveldt, J. Sietsma and S. Van der Zwaag, "Ferrite/pearlite band formation in hot rolled medium carbon steel," *Materials Science and Technology*, vol. 18, no. 3, pp. 297-303, 2001.

[36] S. Alibeigi, J. Sengupta and E. Biro, "Quantification of martensitic banded microsrtucture in dual phase steels and its application at ArcelorMittal Dofasco's No. 1 continuous caster," in *The METEC and 2nd European Steel Technology and Application Days*, Dusseldorf, 2015.

[37] G. Avramovic-Cingara, Y. Ososlov, M. Jain and D. S. Wilkinson, "Effect of martensite distribution on damage behaviour in DP600 dual phase steels," *Materials Science and Engineering A*, vol. 516, no. 1-2, p. 7–16, 2009.

[38] F. D'Errico, "Failures Induced by Abnormal Banding in Steels," *Journal of Failure Analysis and Prevention*, vol. 10, no. 5, p. 351–357, 2010.

[39] M. Haschke, Laboratory Micro-X-Ray Fluorescence Spectroscopy Instrumentation and Applications, Springer International Publishing, 2014.

[40] Z. W. Chen, W. M. Gibson and H. Huang, "High Definition X-Ray Fluorescence: Principles and Techniques," *X-Ray Optics and Instrumentation*, vol. 2008, pp. 1-10, 2008.

[41] W. B. Morrison, "Influence of controlled levels of centreline segregation on the toughness of structural steel," Brussels: Commission of the European Communities, Luxembourg, 1990.

Appendix A: Effect of Spatial Orientation on CL Segregation

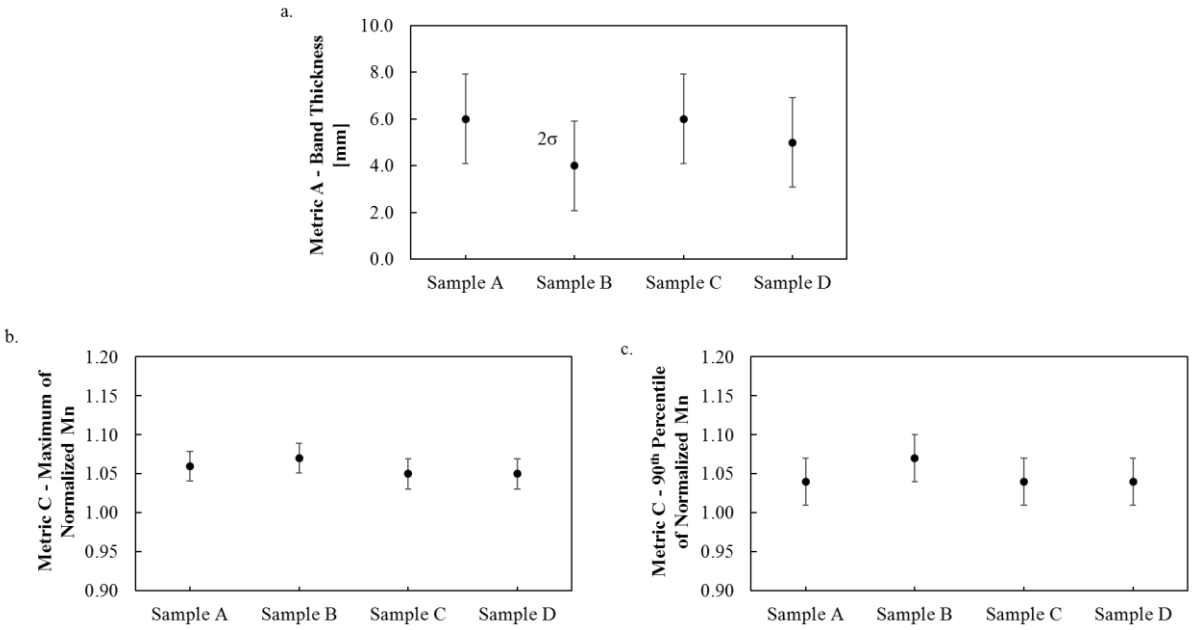

Figure 55: Method 1 and Metrics A and C as a function of spatial orientation for a High Vc and Low ΔT condition

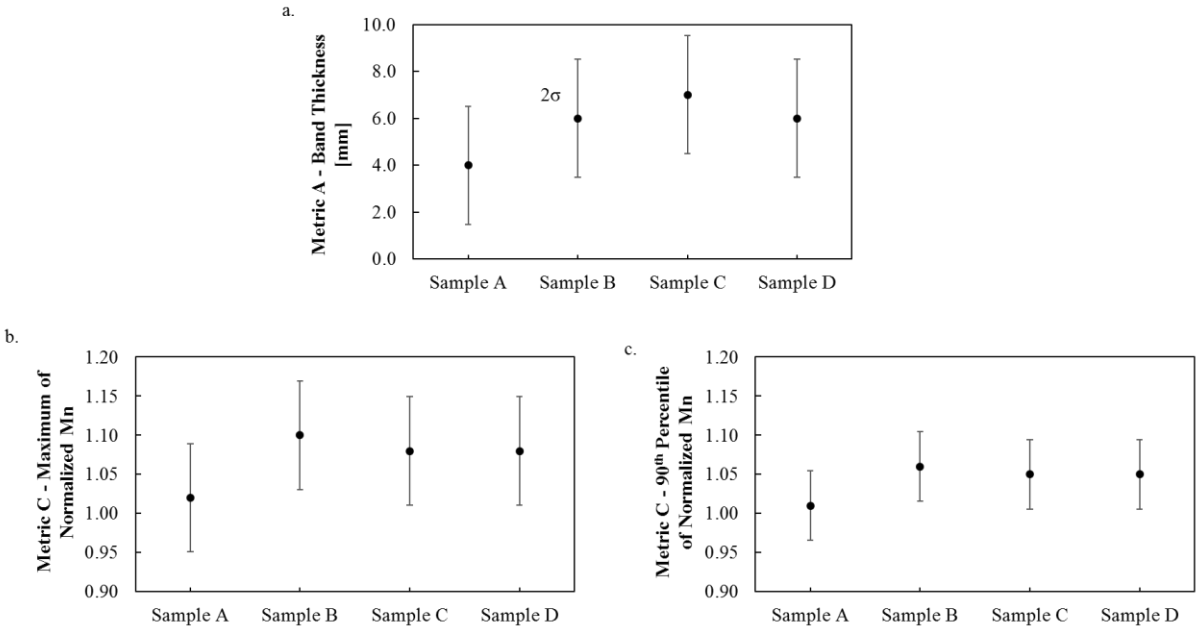

Figure 56: Method 1 and Metrics A and C as a function of spatial orientation for a Medium Vc and High ΔT condition

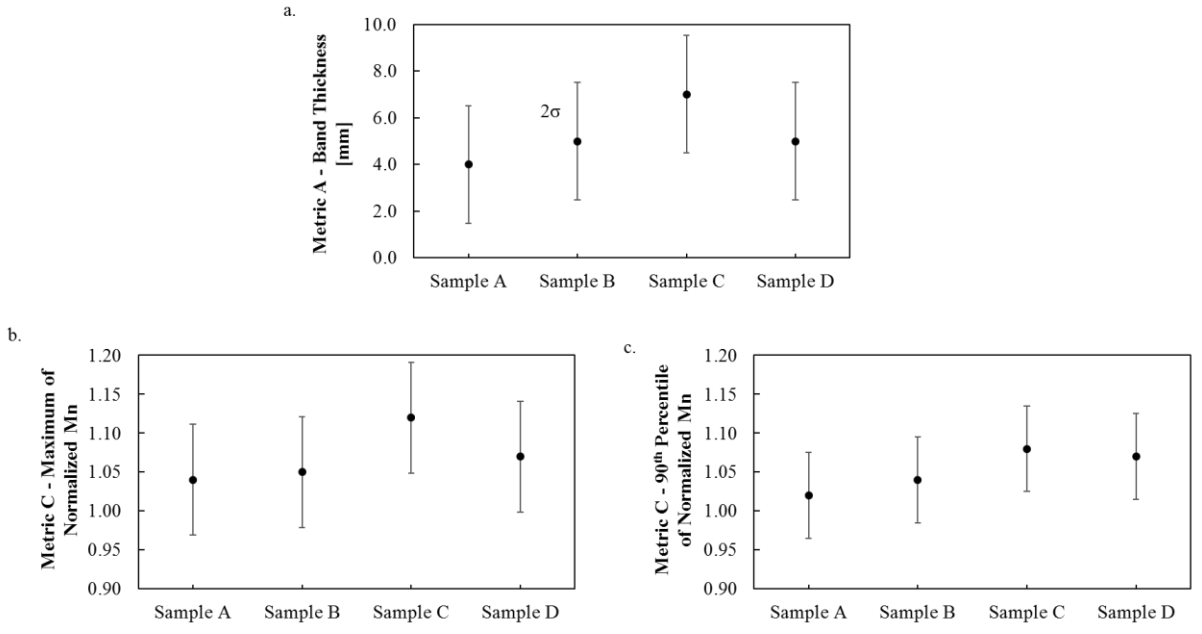

Figure 57: Method 1 and Metrics A and C as a function of spatial orientation for a Medium Vc and Low ΔT condition

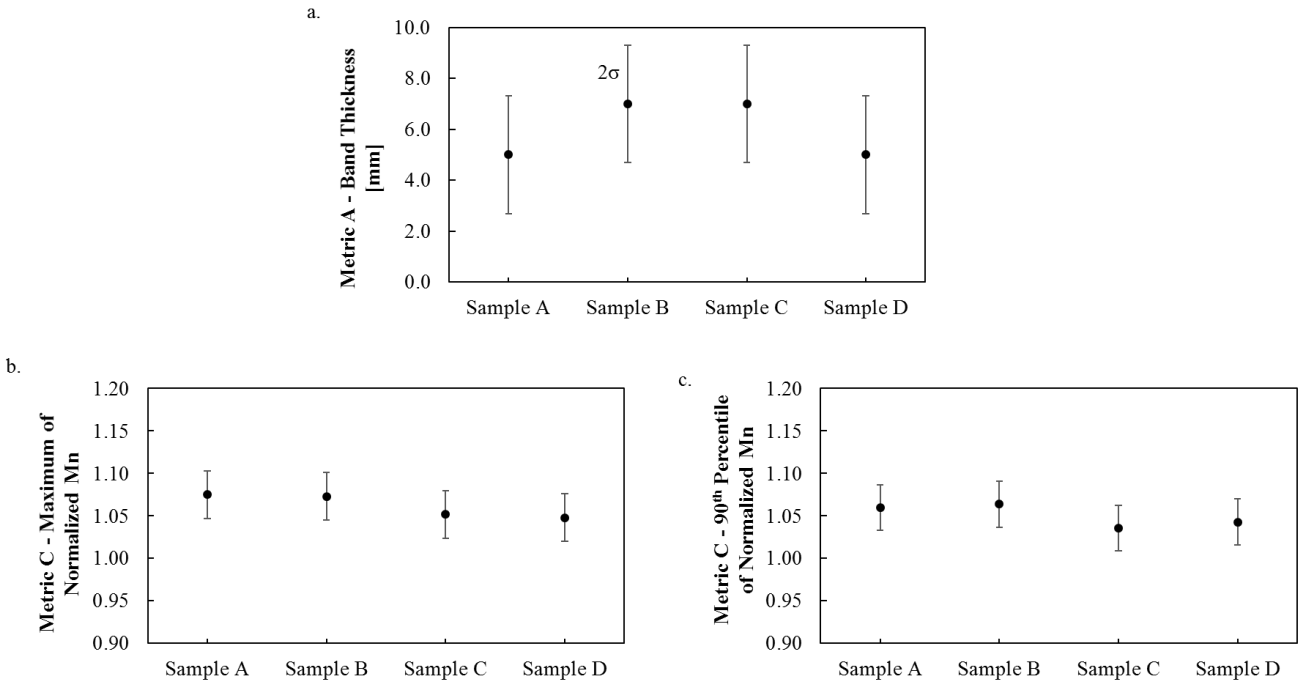

Figure 58: Method 1 and Metrics A and C as a function of spatial orientation for a Low Vc and High ΔT condition

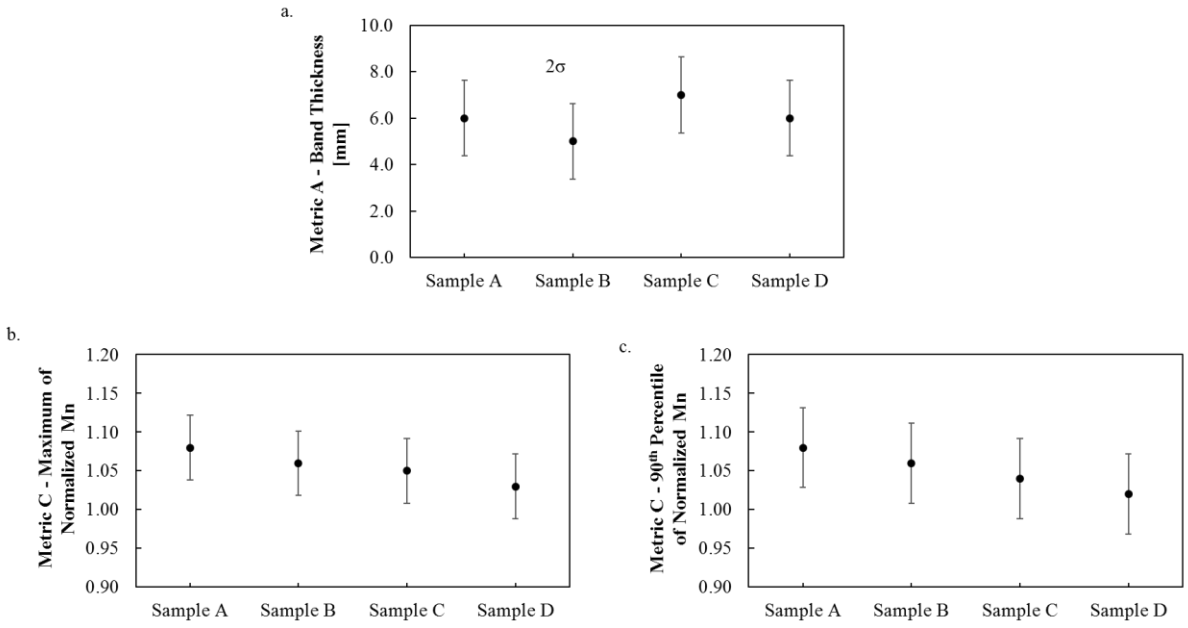

Figure 59: Method 1 and Metrics A and C as a function of spatial orientation for a Low Vc and Low ΔT condition

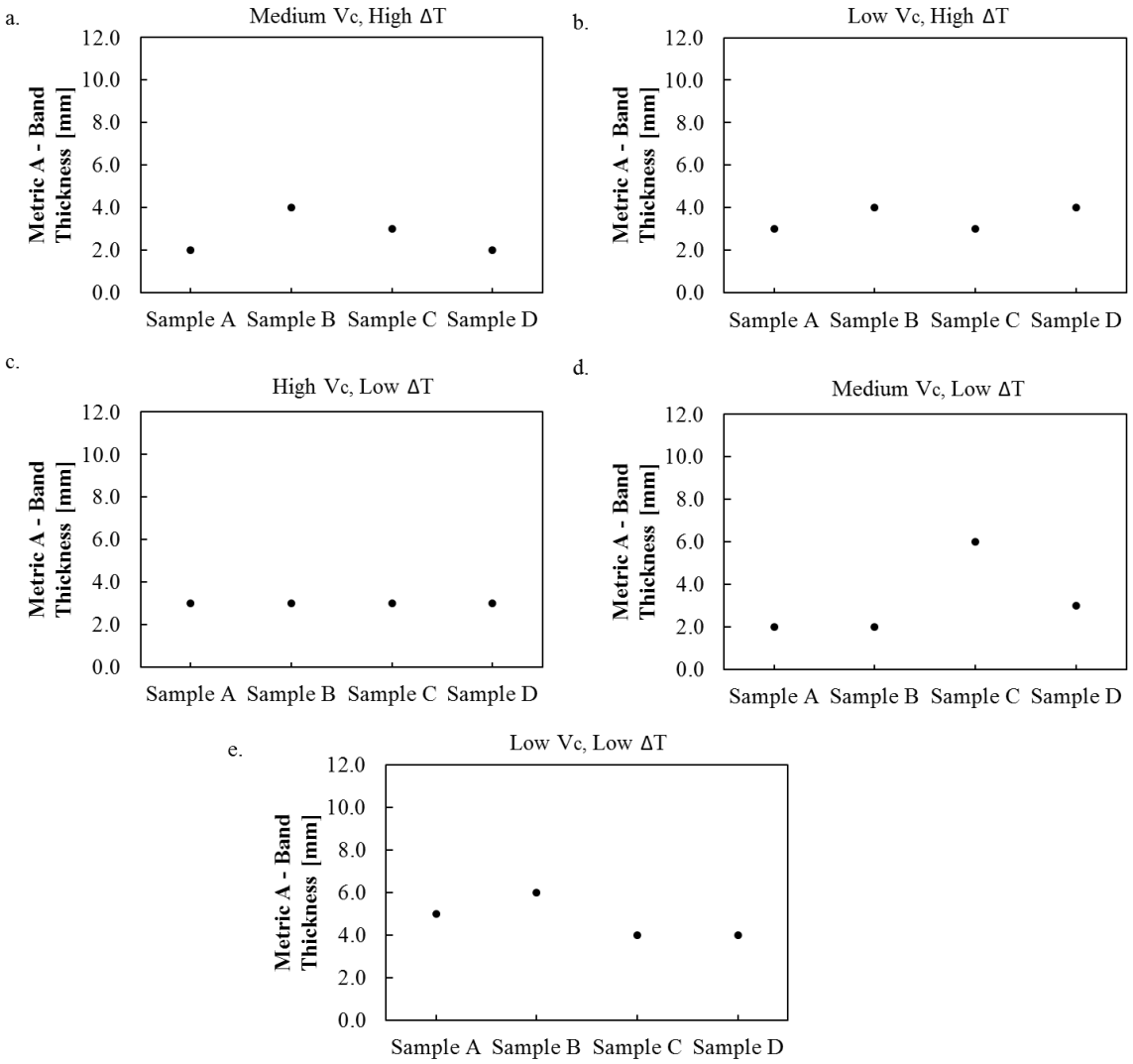

Figure 60: Method 2 and Metric A as a function of spatial orientation for five casting conditions using 1.09x and a 3 value system

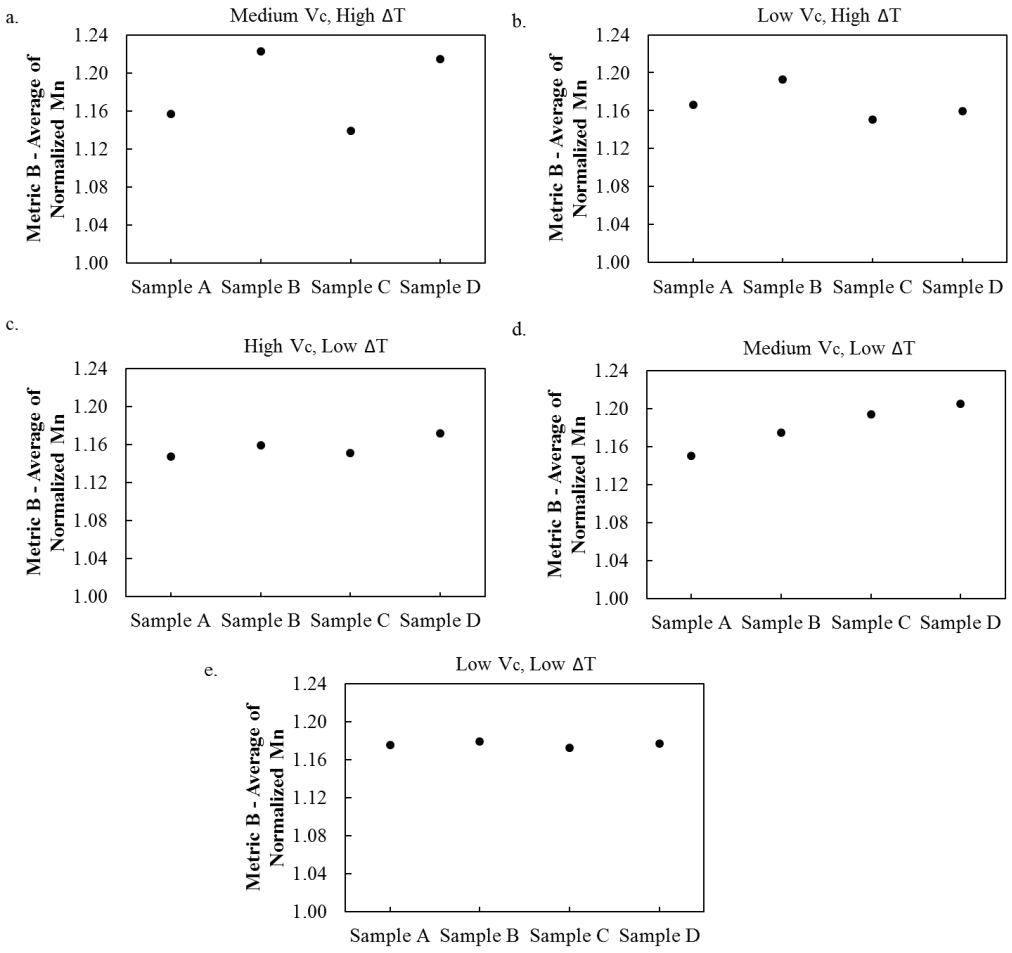

Figure 61: Metric B as a function of spatial orientation for five casting conditions using 1.09x and a 3 value system

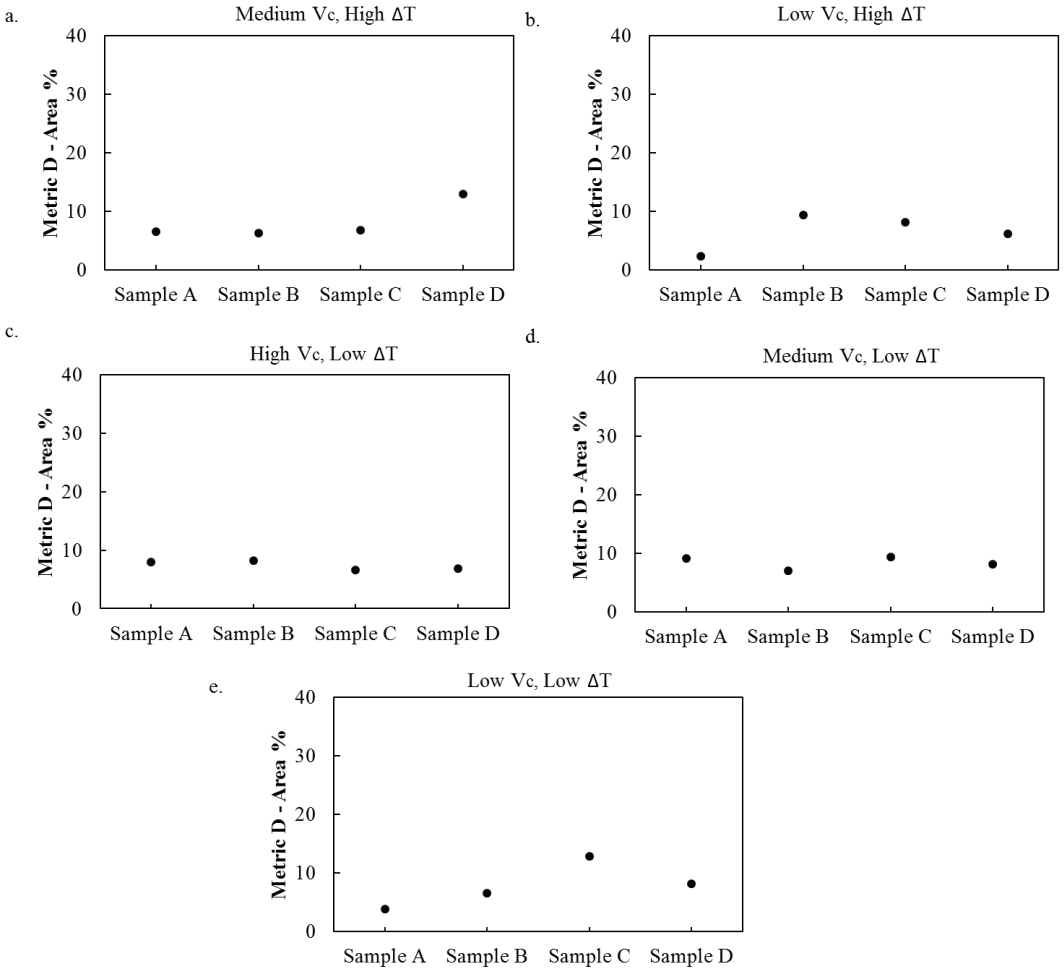

Figure 62: Metric D as a function of spatial orientation for five casting conditions using 1.09x

Appendix B: Effect of Casting Speed on CL Segregation

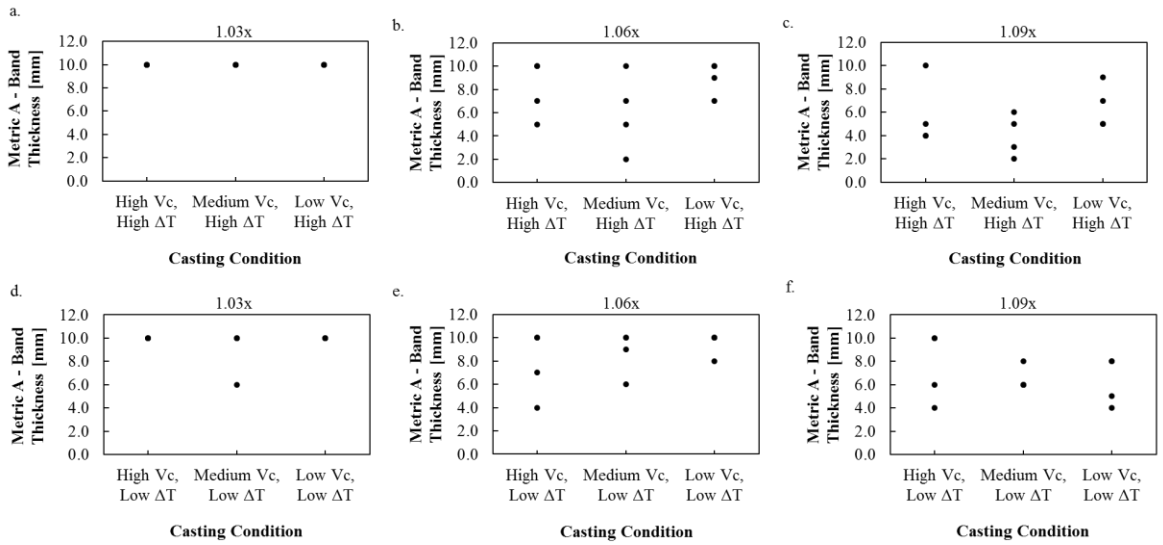

Figure 63: Method 2 and Metric A as a function of casting speed for 1.5 Mn wt% using factors 1.03x, 1.06x, 1.09x and a 1 value system

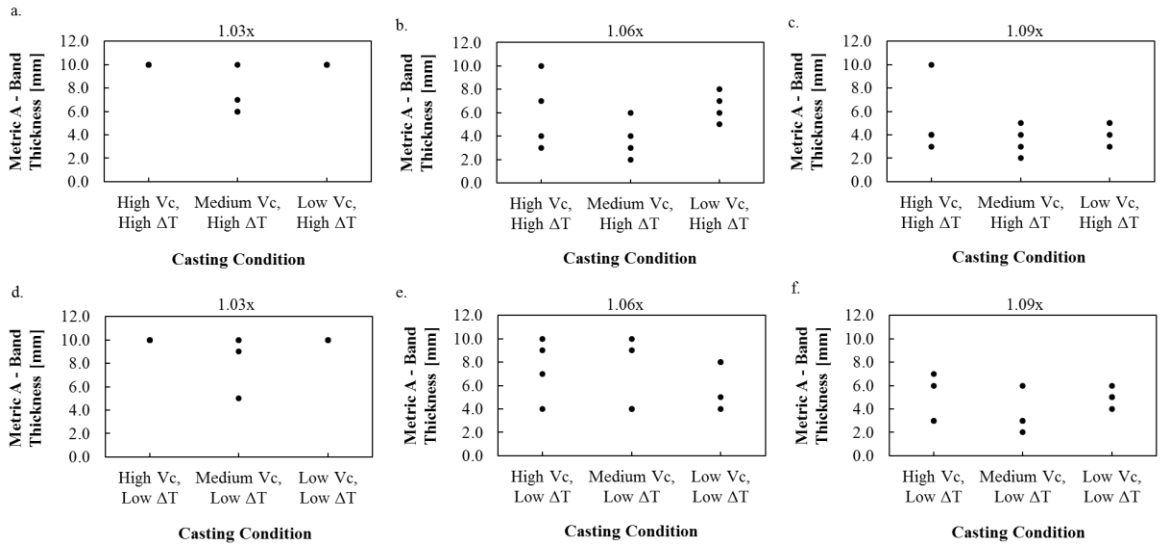

Figure 64: Method 2 and Metric A as a function of casting speed for 1.5 Mn wt% using factors 1.03x, 1.06x, 1.09x and a 2 value system

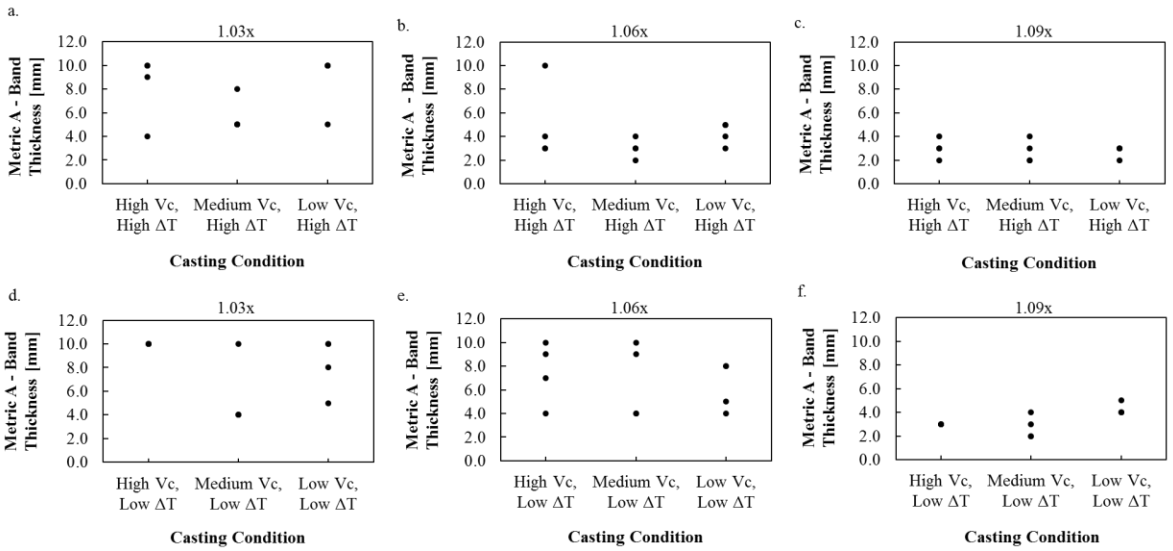

Figure 65: Method 2 and Metric A as a function of casting speed for 1.5 Mn wt% using factors 1.03x, 1.06x, 1.09x and a 4 value system

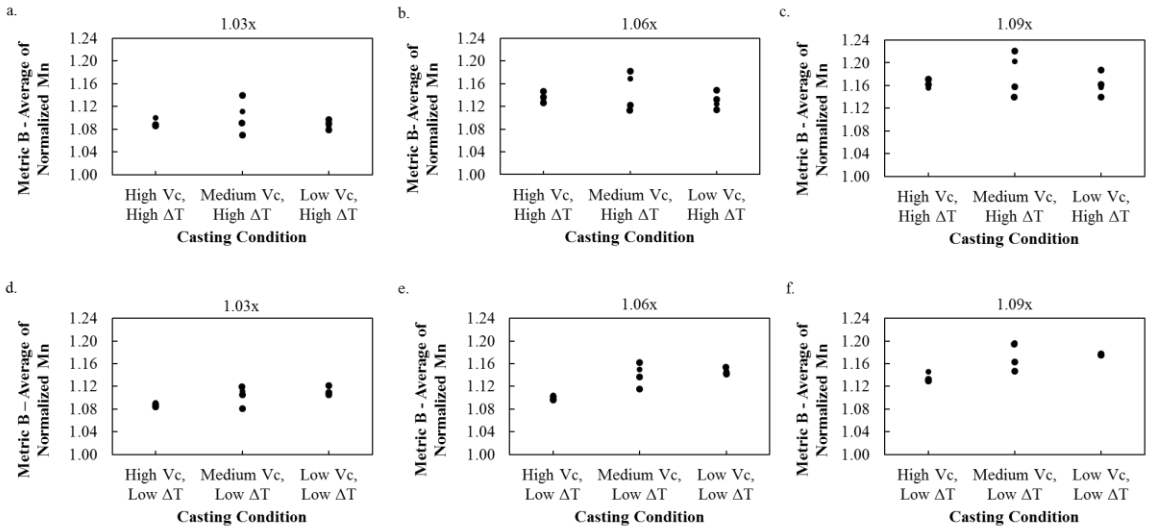

Figure 66: Metric B as a function of casting speed for 1.5 Mn wt% using factors 1.03x, 1.06x, 1.09x and a 1 value system

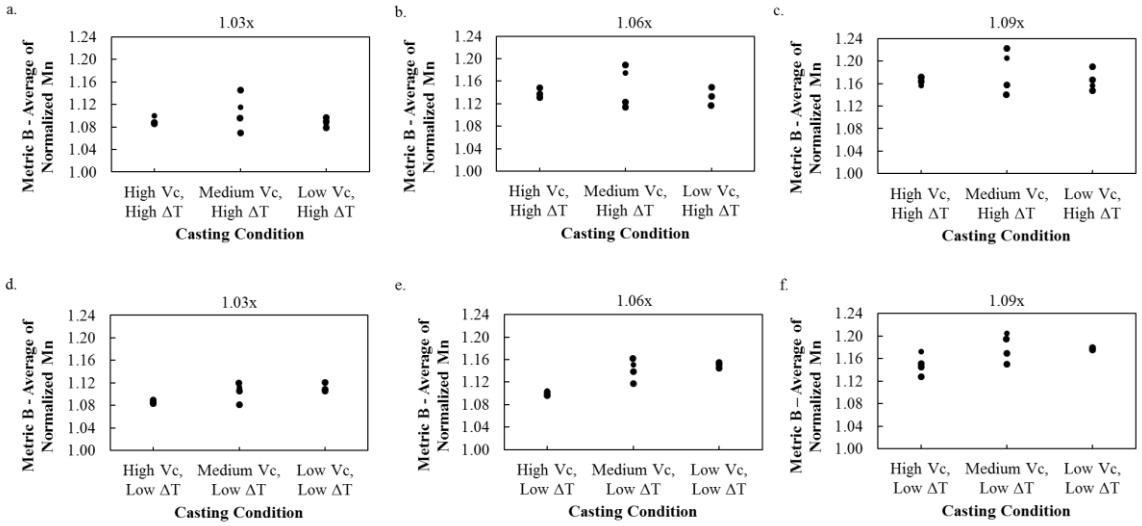

Figure 67: Metric B as a function of casting speed for 1.5 Mn wt% using factors 1.03x, 1.06x, 1.09x and a 2 value system

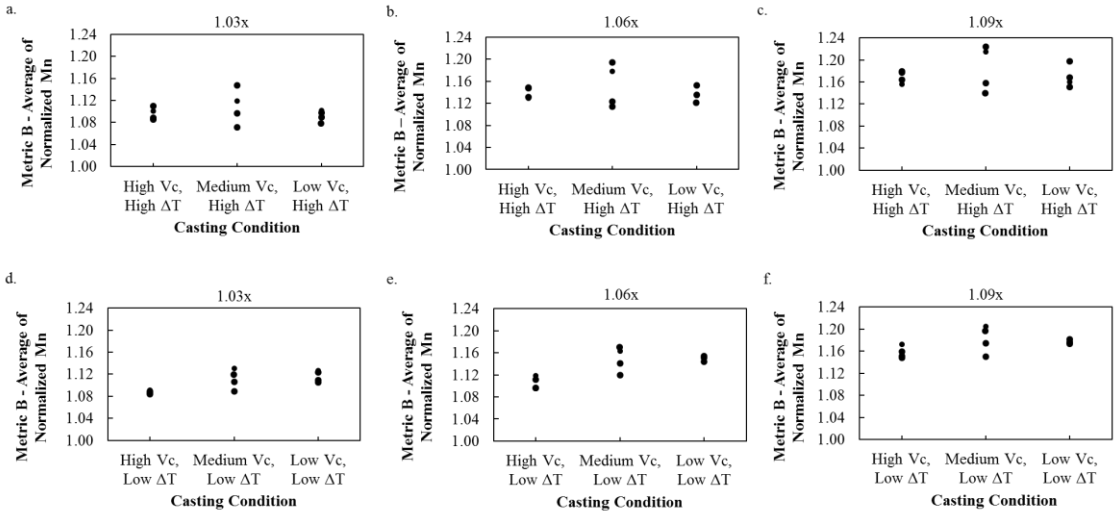

Figure 68: Metric B as a function of casting speed for 1.5 Mn wt% using factors 1.03x, 1.06x, 1.09x and a 4 value system

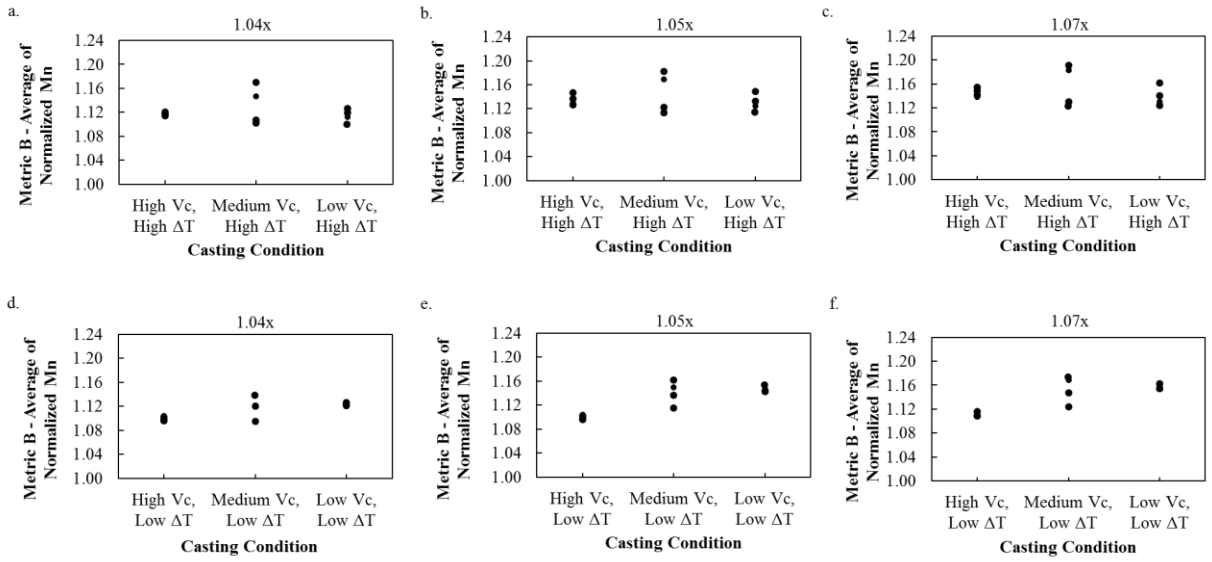

Figure 69: Metric B as a function of casting speed for 1.5 Mn wt% using factors 1.04x, 1.05x, 1.07x and a 1 value system

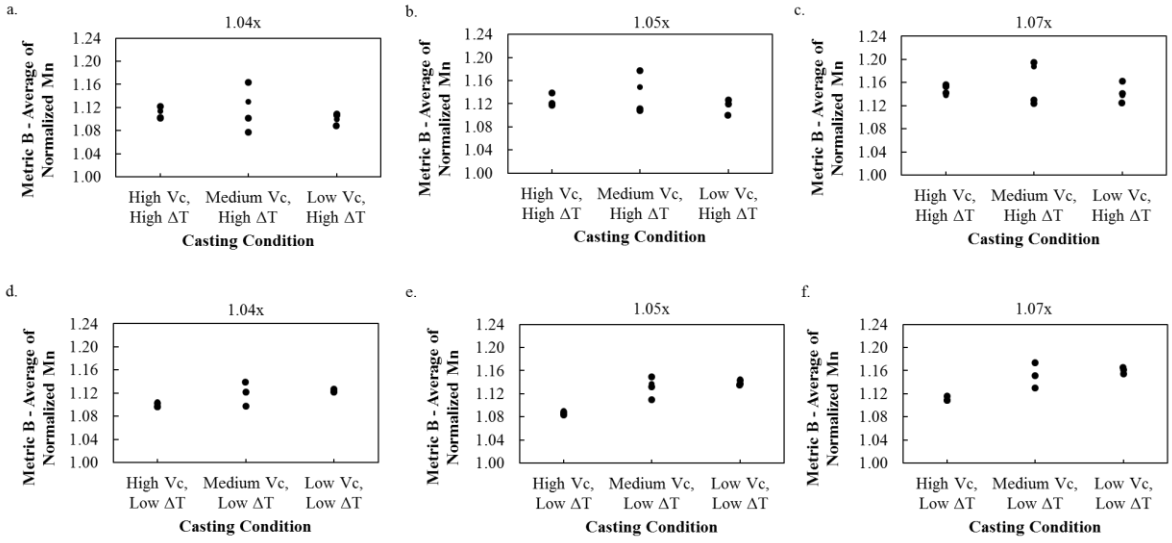

Figure 70: Metric B as a function of casting speed for 1.5 Mn wt% using factors 1.04x, 1.05x, 1.07x and a 2 value system

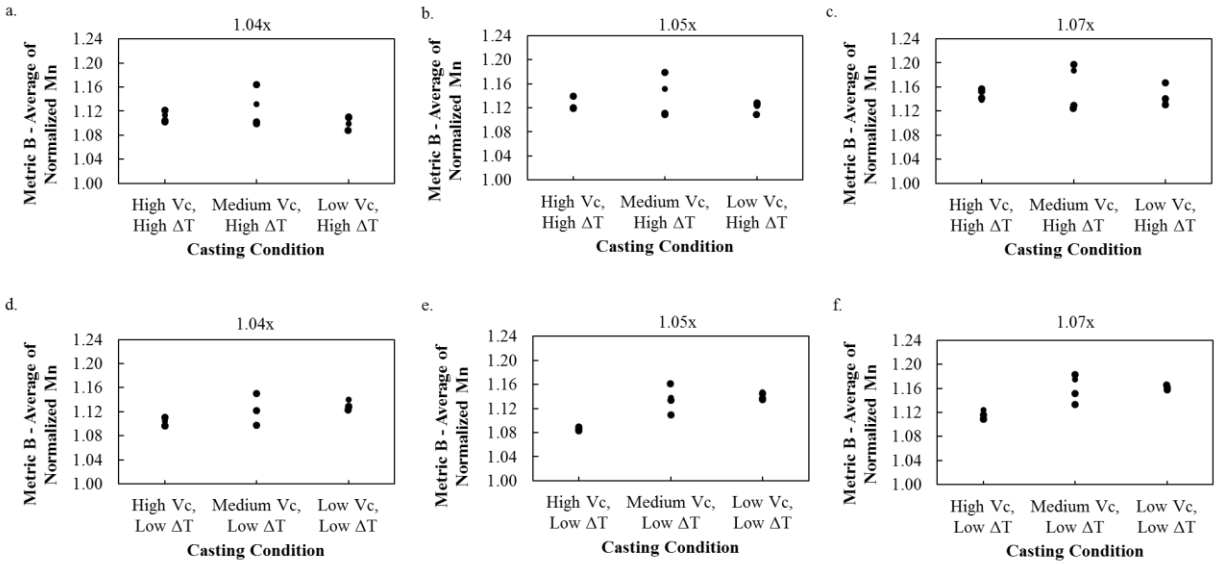

Figure 71: Metric B as a function of casting speed for 1.5 Mn wt% using factors 1.04x, 1.05x, 1.07x and a 3 value system

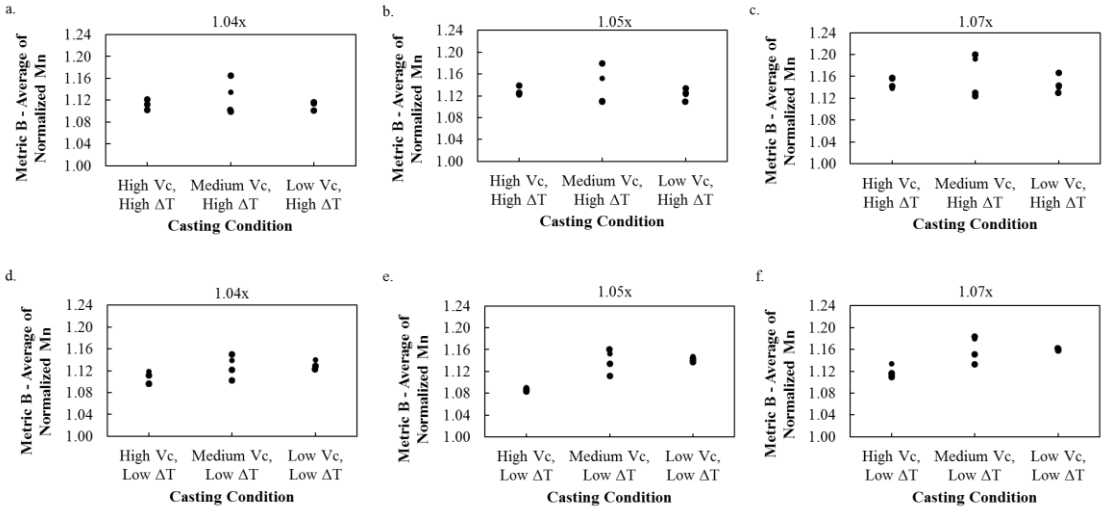

Figure 72: Metric B as a function of casting speed for 1.5 Mn wt% using factors 1.04x, 1.05x, 1.07x and a 4 value system

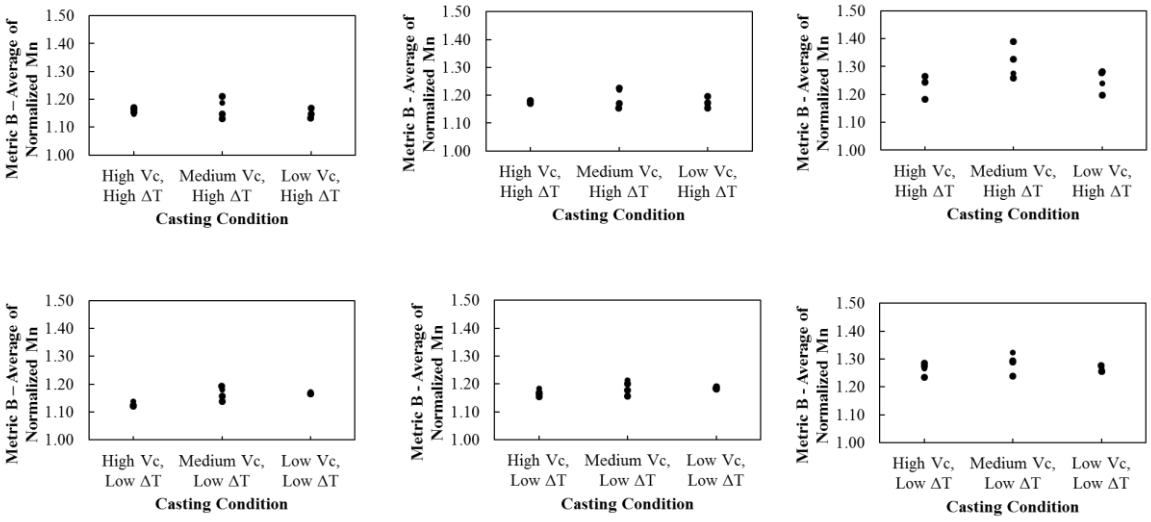

Figure 73: Metric B as a function of casting speed for 1.5 Mn wt% using factors 1.08x, 1.1x, 1.2x and a 1 value system

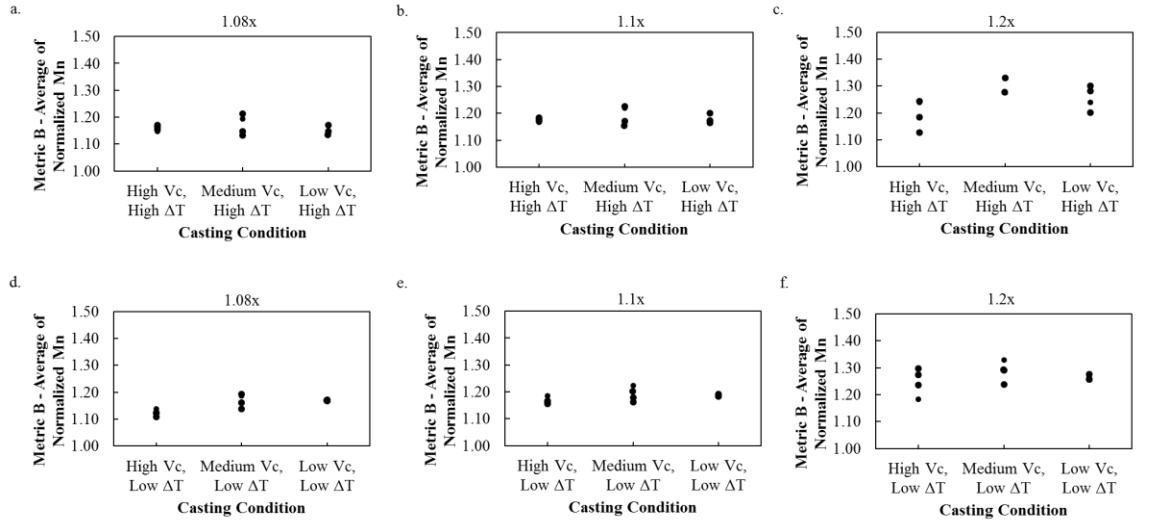

Figure 74: Metric B as a function of casting speed for 1.5 Mn wt% using factors 1.08x, 1.1x, 1.2x and a 2 value system

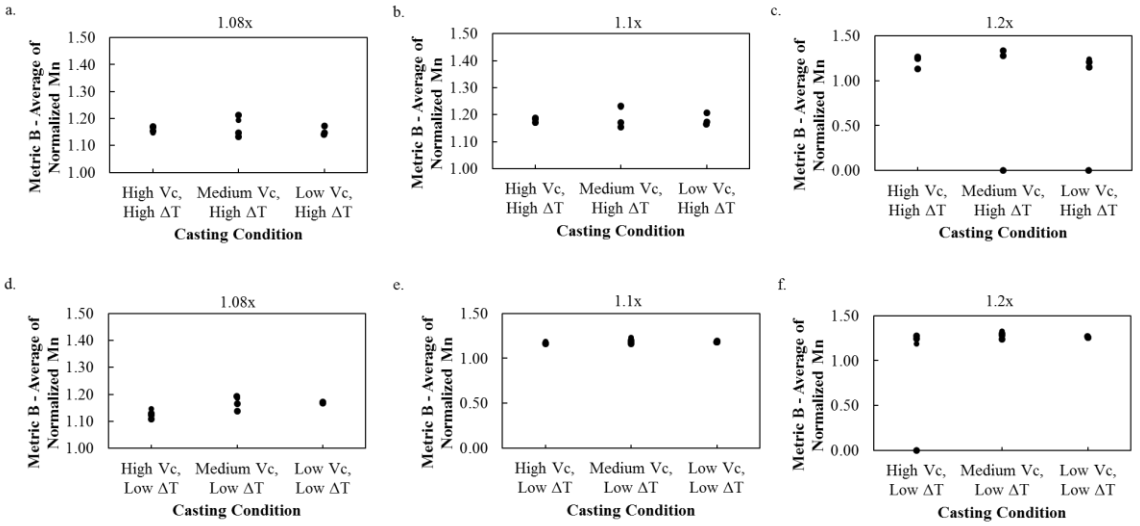

Figure 75: Metric B as a function of casting speed for 1.5 Mn wt% using factors 1.08x, 1.1x, 1.2x and a 3 value system

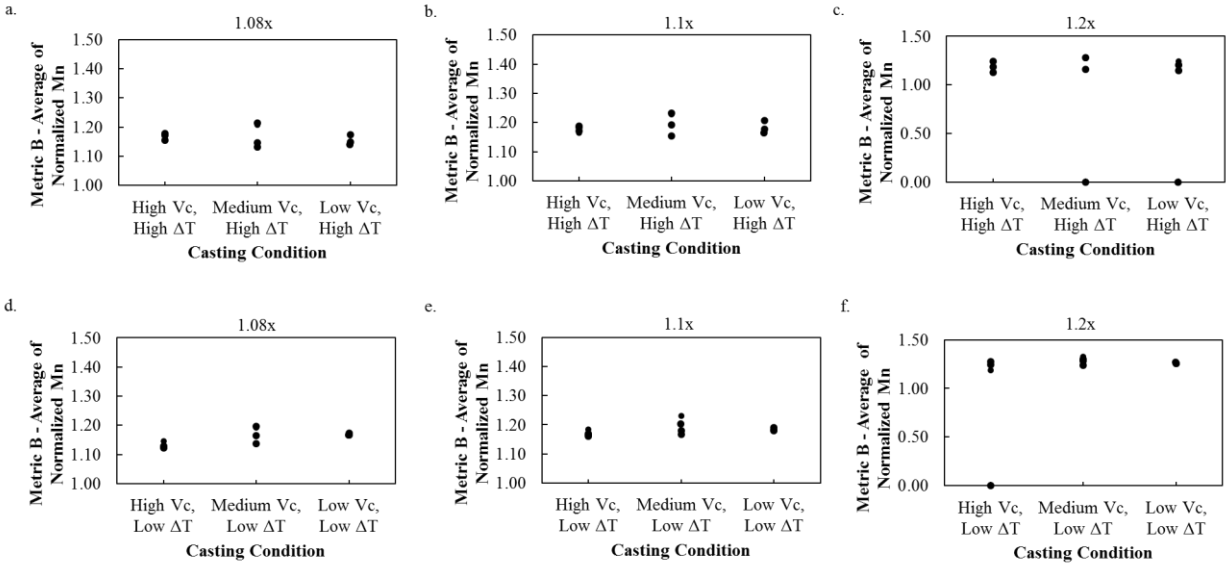

Figure 76: Metric B as a function of casting speed for 1.5 Mn wt% using factors 1.08x, 1.1x, 1.2x and a 4 value system

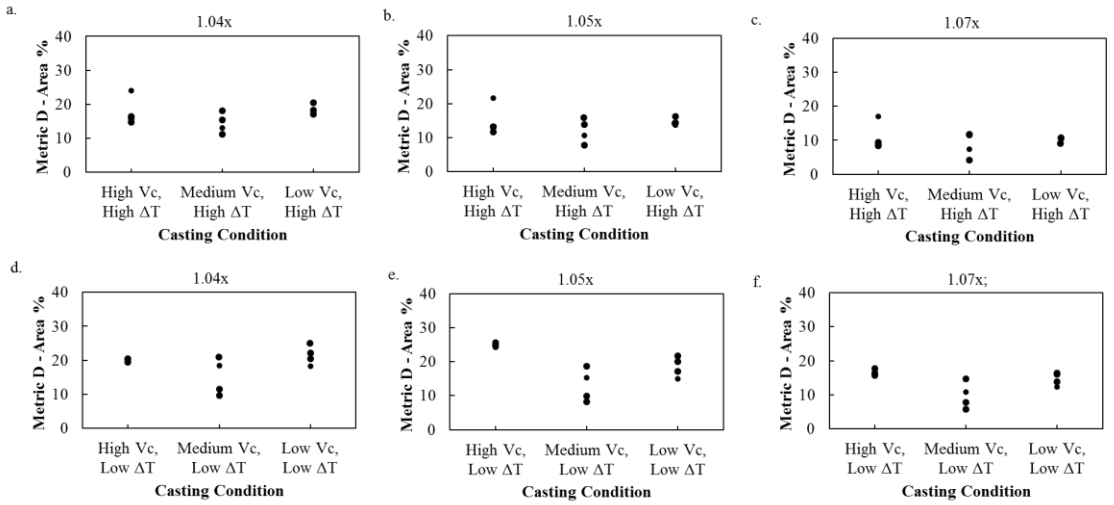

Figure 77: Metric D as a function of casting speed for 1.5 Mn wt% using factors 1.04x, 1.05x and 1.07x

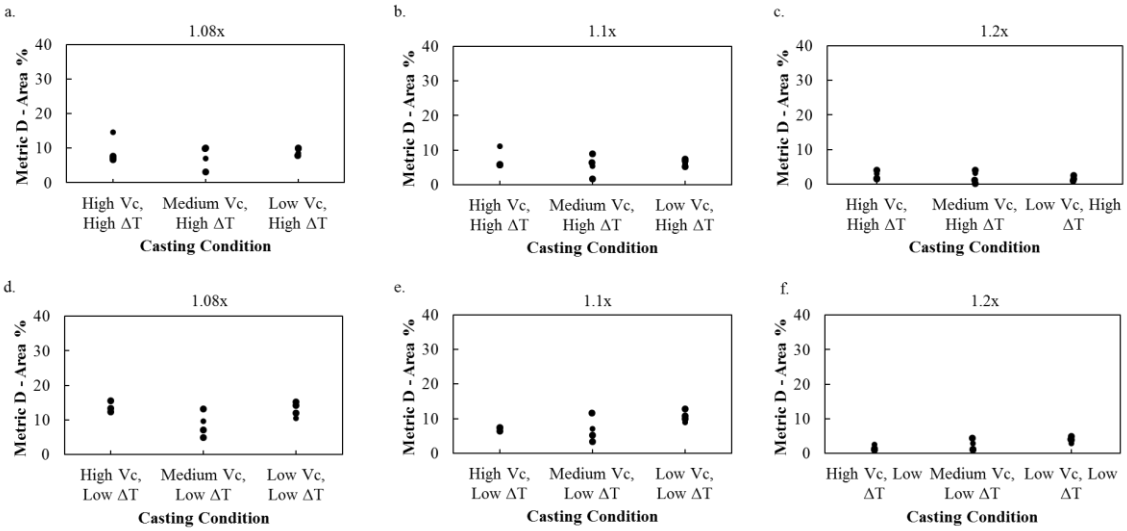

Figure 78: Metric D as a function of casting speed for 1.5 Mn wt% using factors 1.08x, 1.1x and 1.2x

Appendix C: Effect of Superheat on CL Segregation

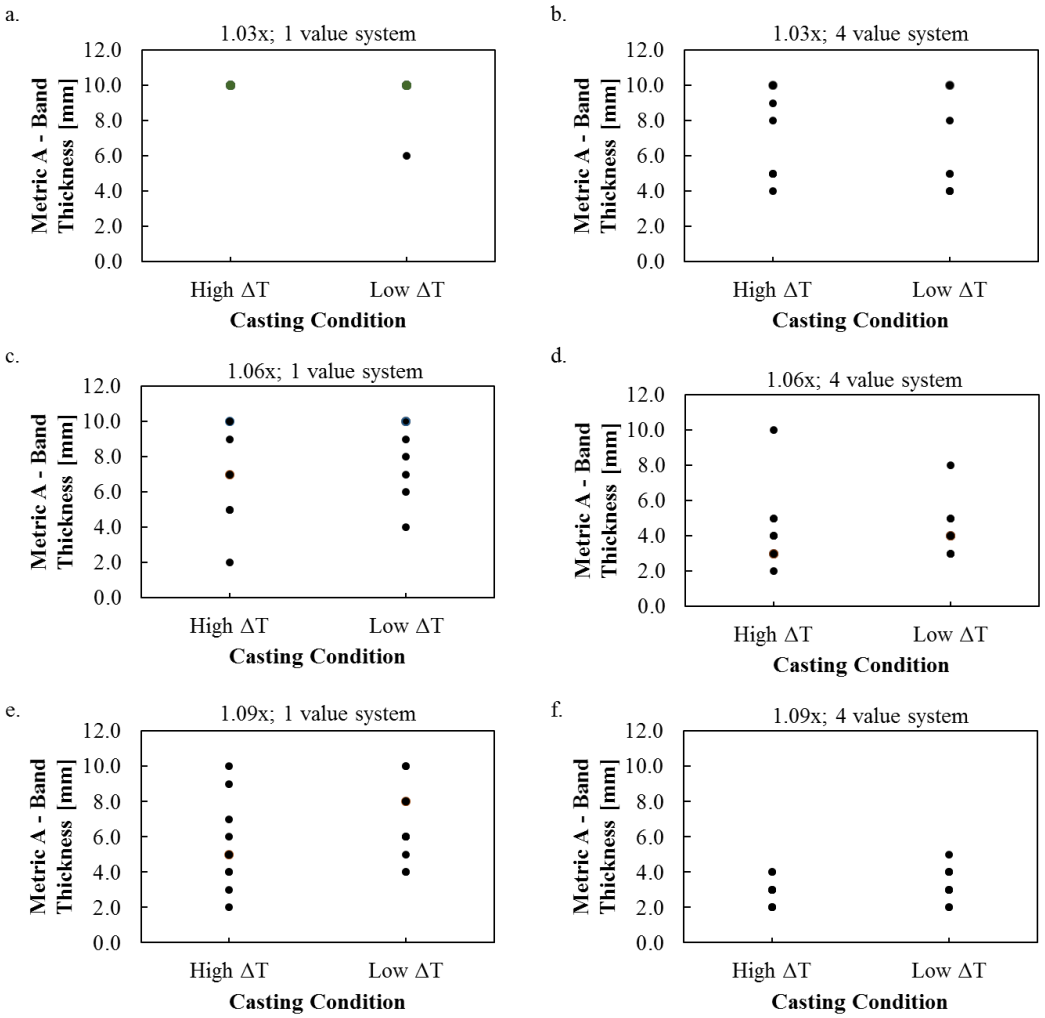

Figure 79: Method 2 and Metric A as a function of superheat for 1.5 Mn wt% using factors 1.03x, 1.06x, 1.09x and 1 and 4 value systems

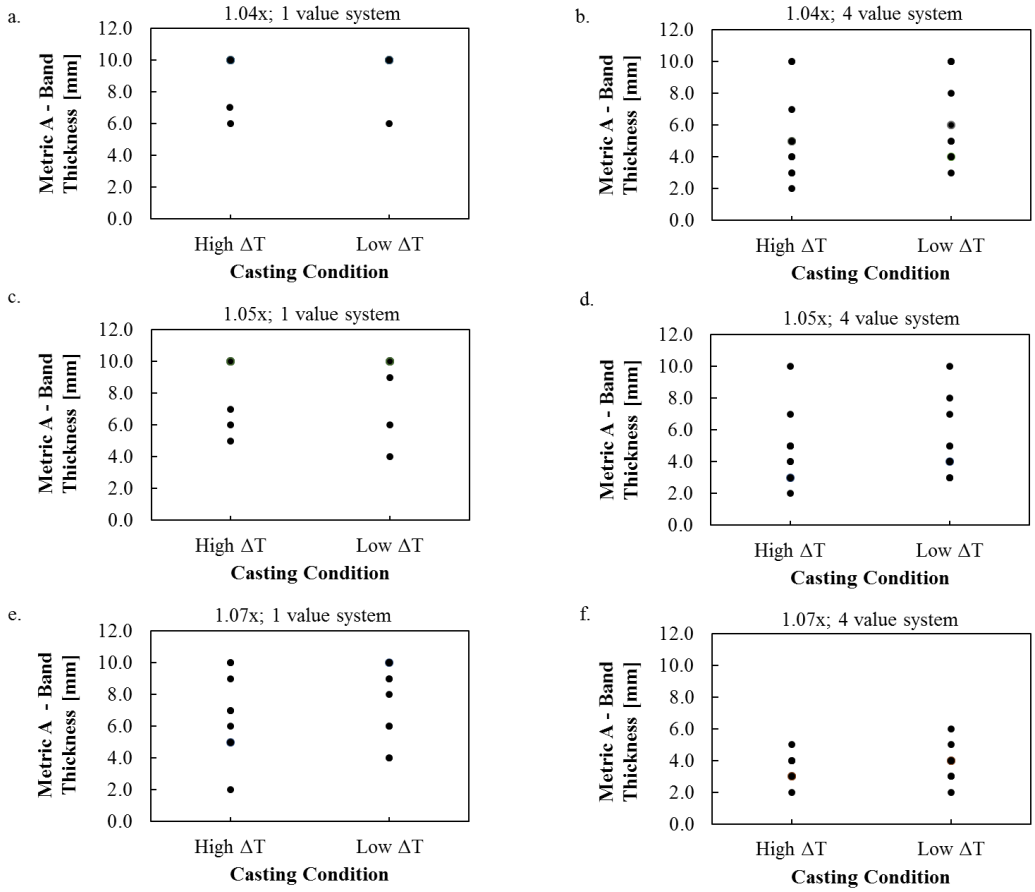

Figure 80: Method 2 and Metric A as a function of superheat for 1.5 Mn wt% using factors 1.04x, 1.05x, 1.07x and 1 and 4 value systems

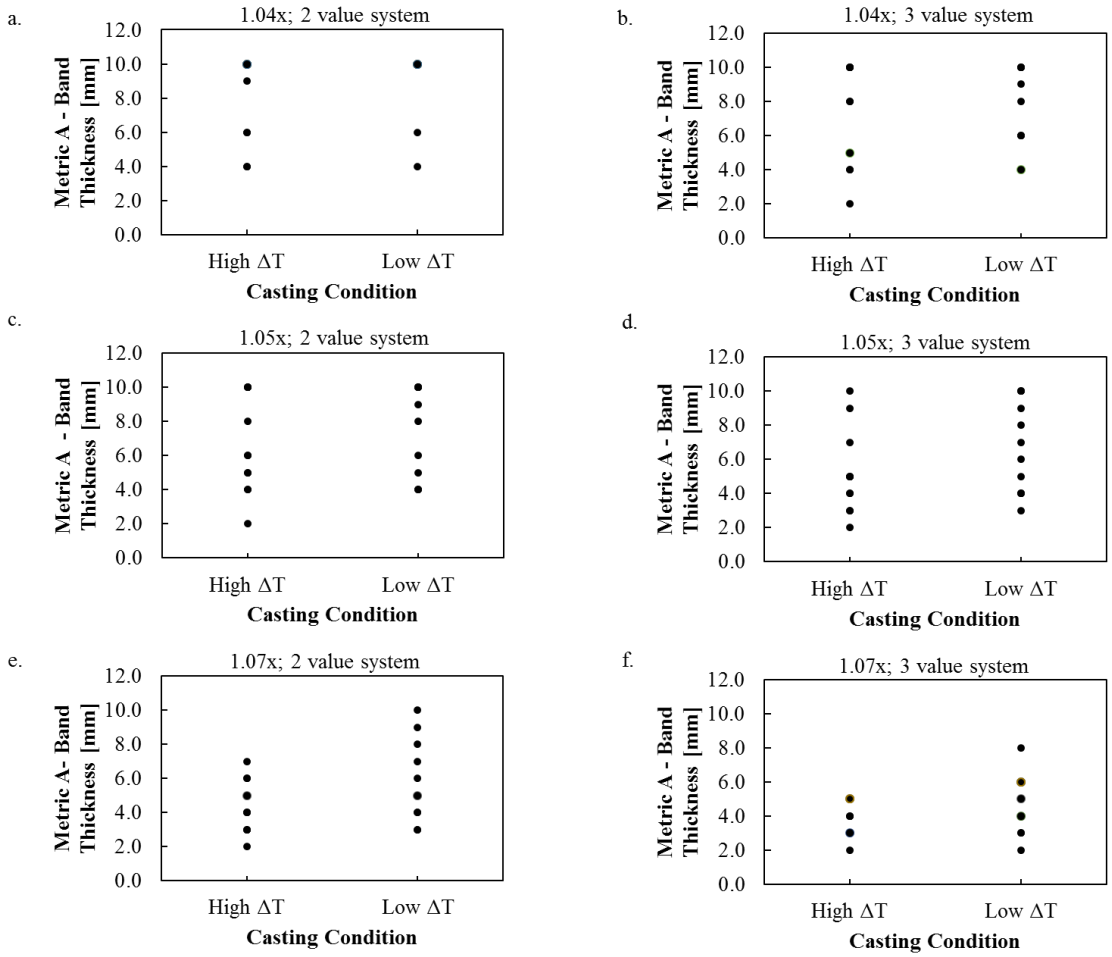

Figure 81: Method 2 and Metric A as a function of superheat for 1.5 Mn wt% using factors 1.04x, 1.05x, 1.07x and 2 and 3 value systems

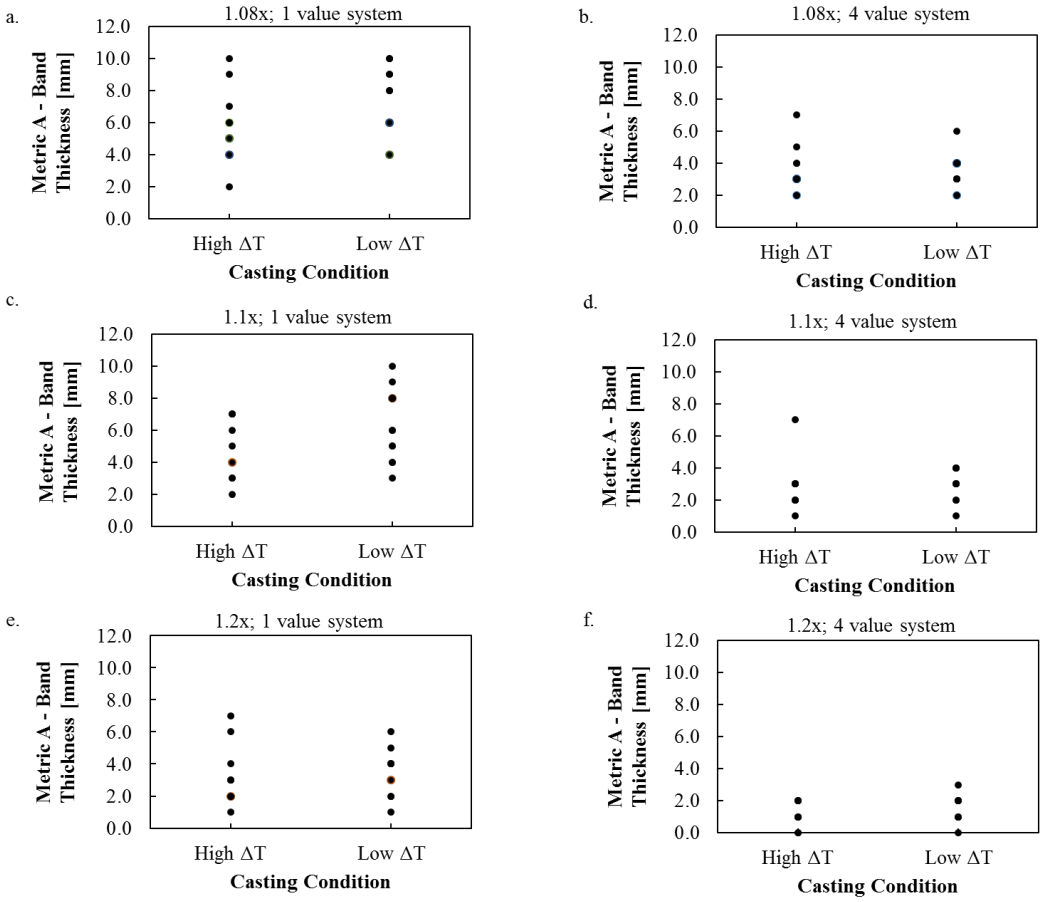

Figure 82: Method 2 and Metric A as a function of superheat for 1.5 Mn wt% using factors 1.08x, 1.1x, 1.2x and 1 and 4 value systems

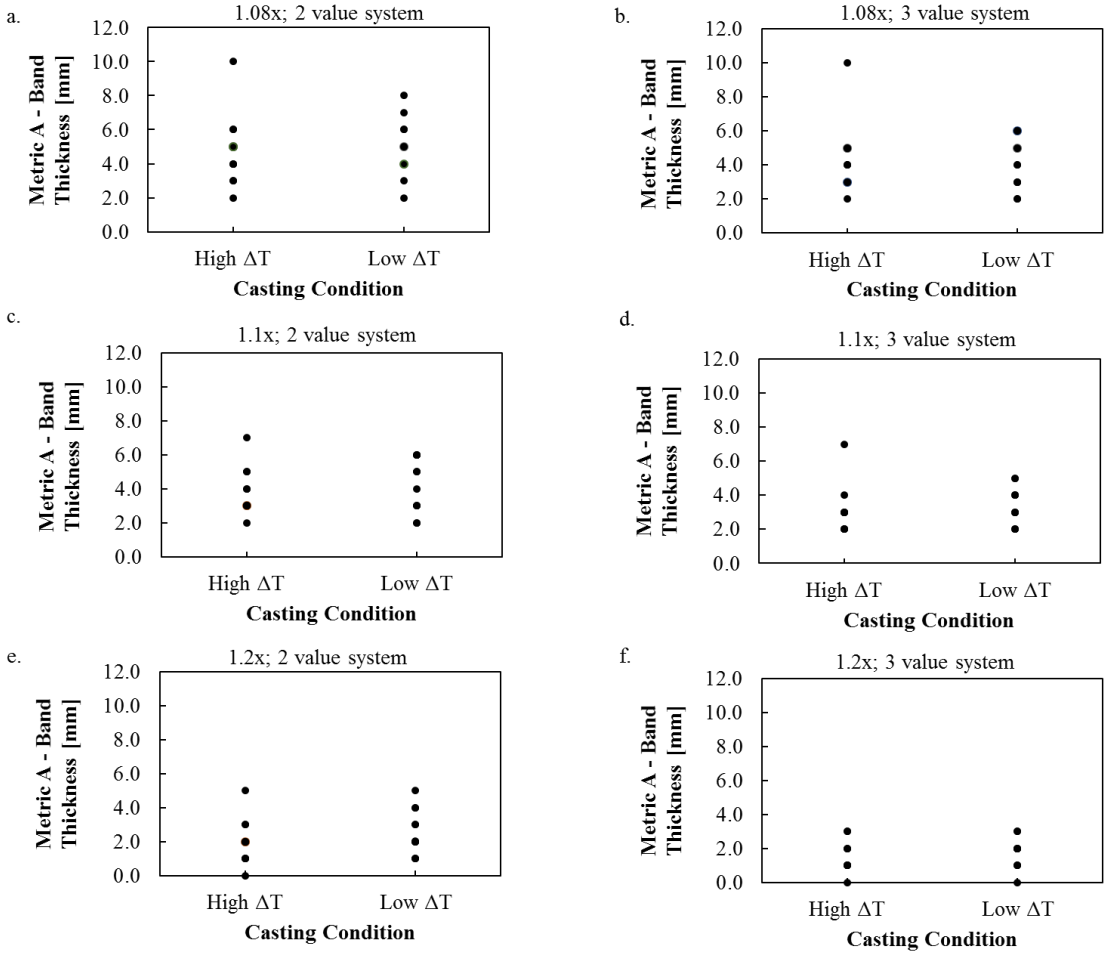

Figure 83: Method 2 and Metric A as a function of superheat for 1.5 Mn wt% using factors 1.08x, 1.1x, 1.2x and 2 and 3 value systems

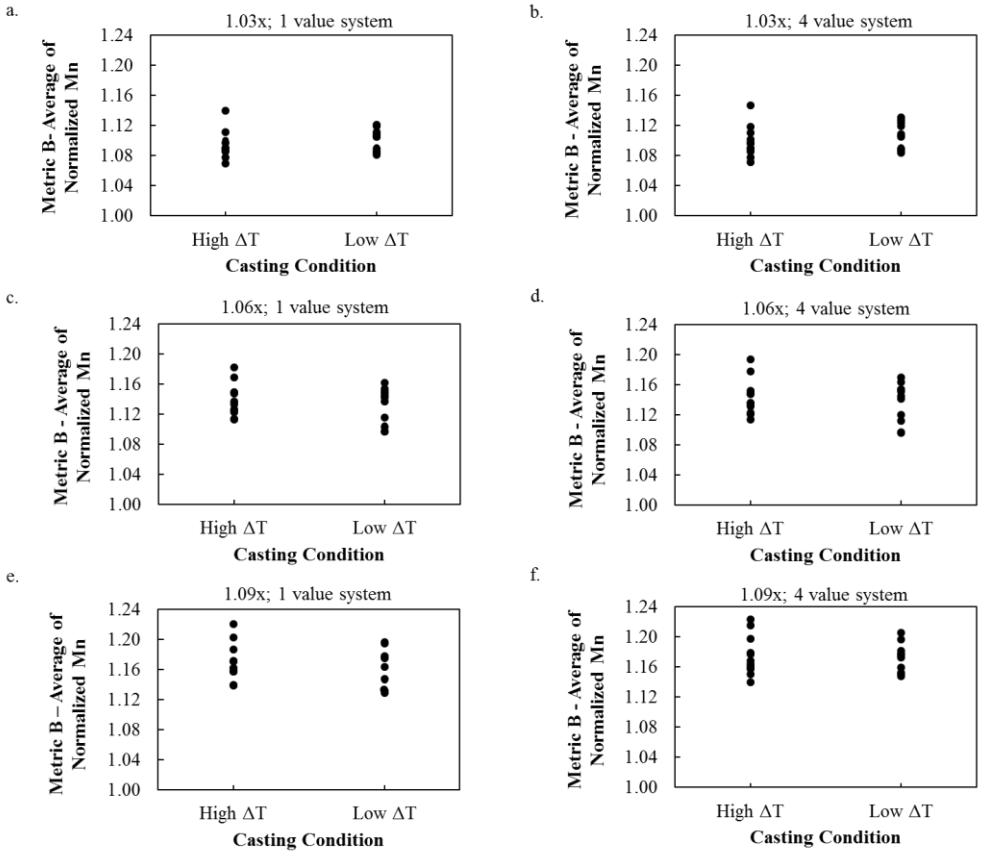

Figure 84: Metric B as a function of superheat for 1.5 Mn wt% using factors 1.03x, 1.06x, 1.09x and 1 and 4 value systems

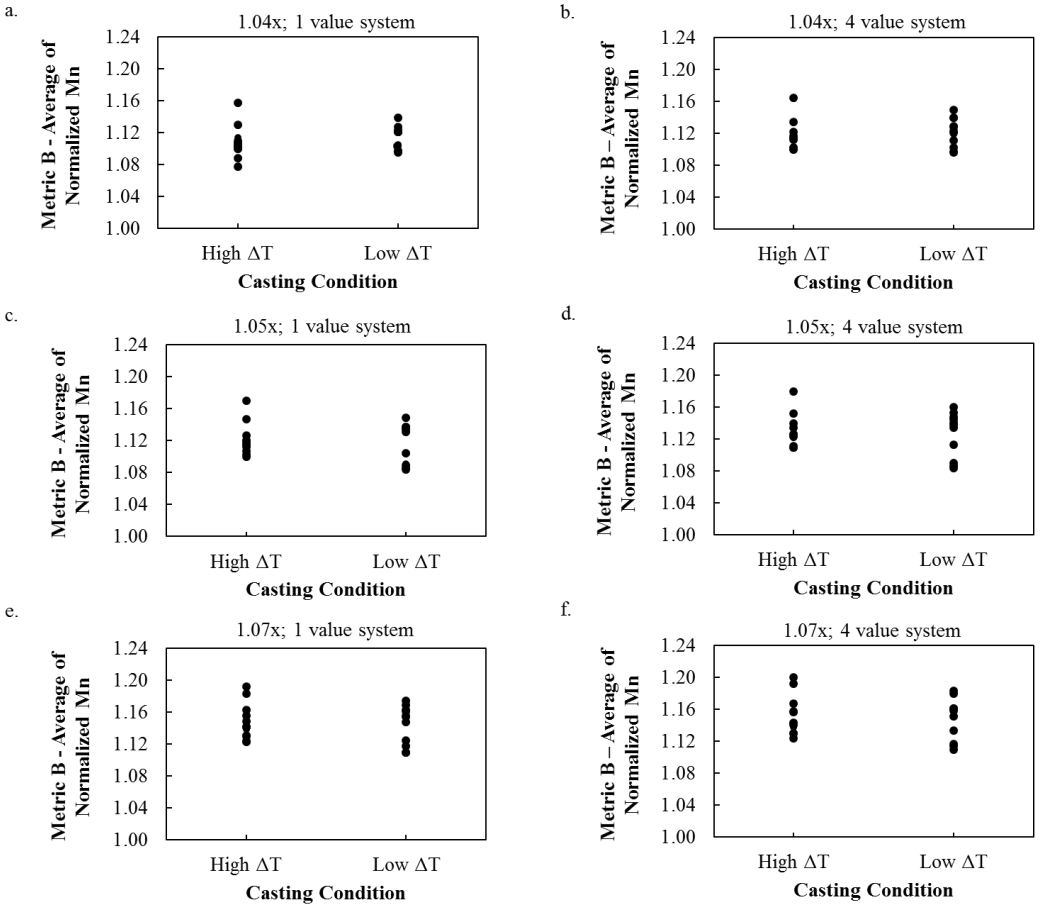

Figure 85: Metric B as a function of superheat for 1.5 Mn wt% using factors 1.04x, 1.05x, 1.07x and 1 and 4 value systems

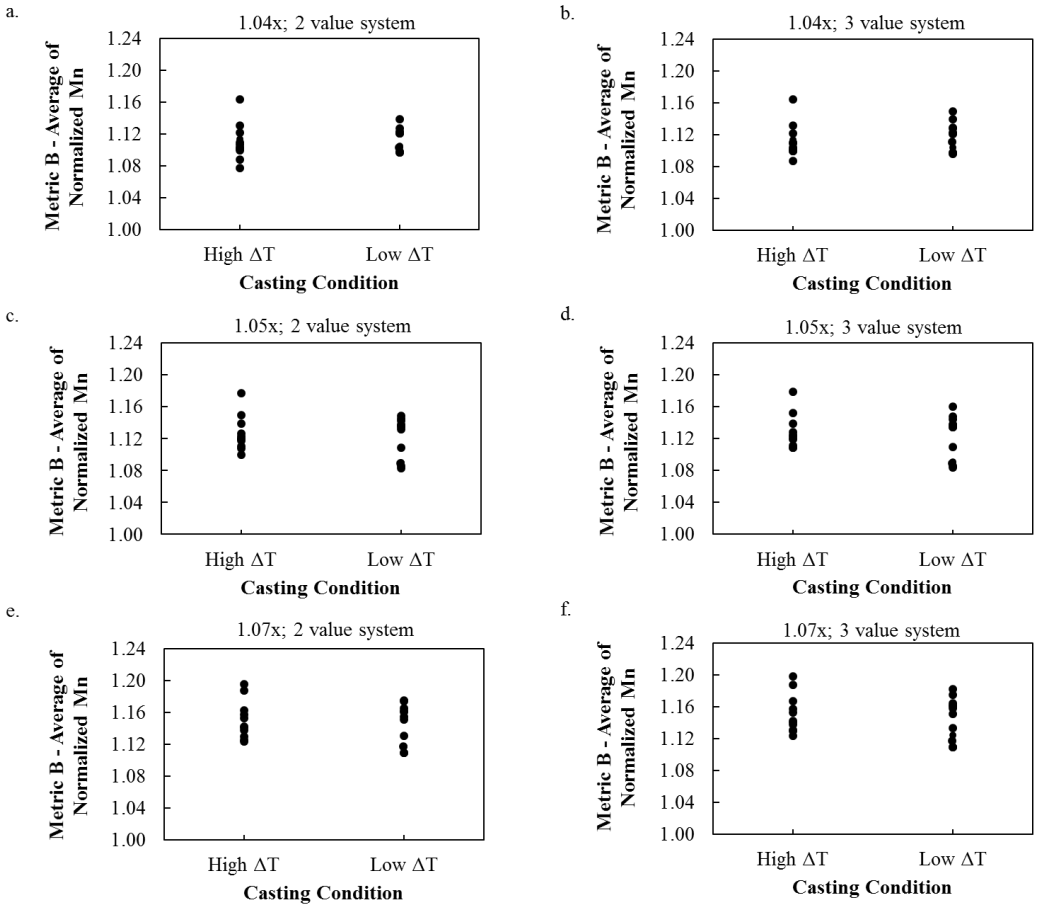

Figure 86: Metric B as a function of superheat for 1.5 Mn wt% using factors 1.04x, 1.05x, 1.07x and 2 and 3 value systems

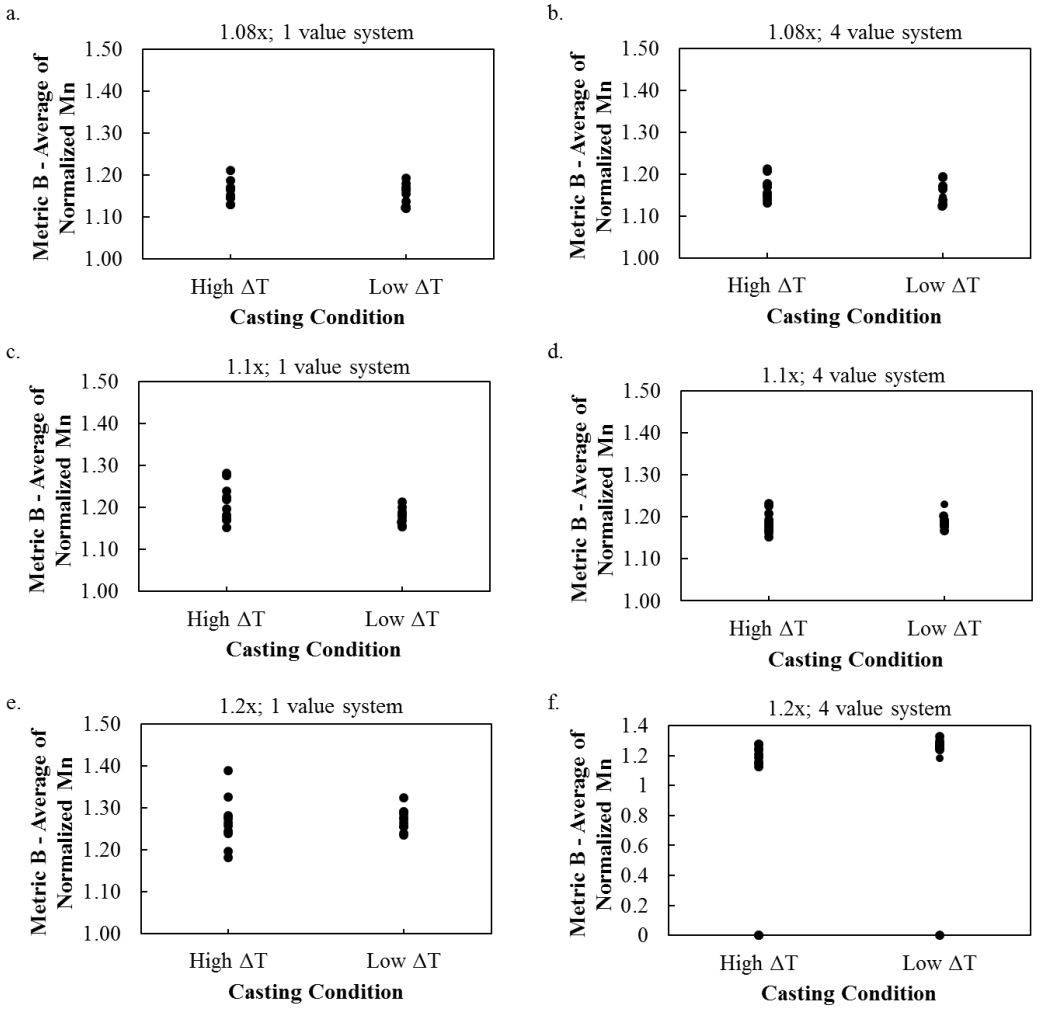

Figure 87: Metric B as a function of superheat for 1.5 Mn wt% using factors 1.08x, 1.1x, 1.2x and 1 and 4 values

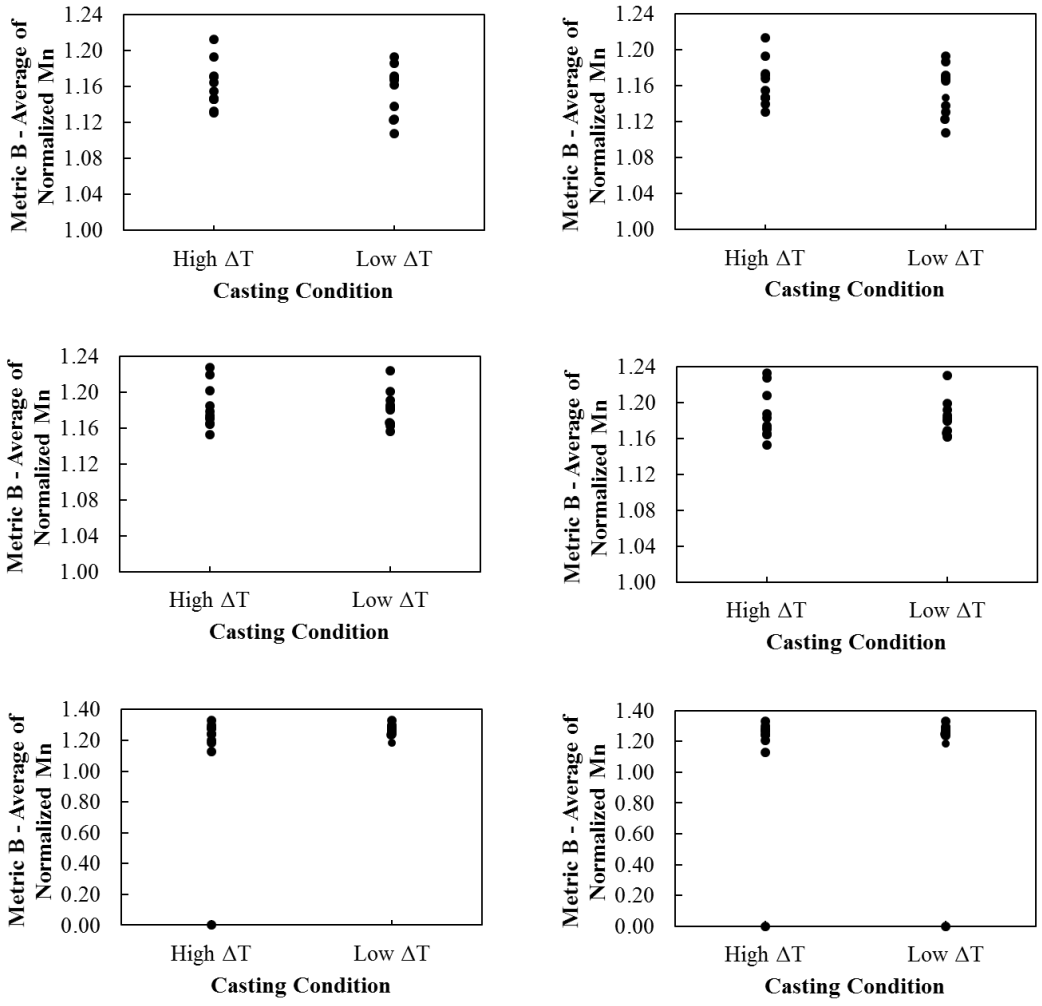

Figure 88: Metric B as a function of superheat for 1.5 Mn wt% using factors 1.08x, 1.1x, 1.2x and 2 and 3 values

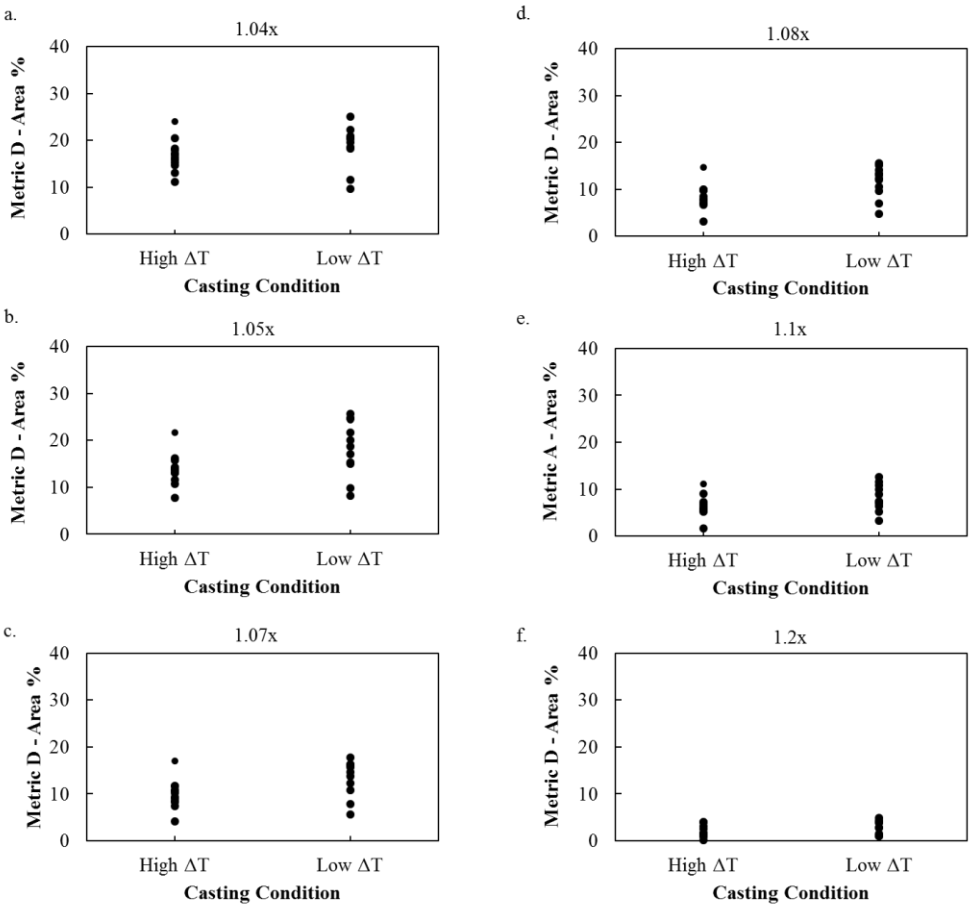

Figure 89: Metric D as a function of superheat for 1.5 Mn wt% using factors 1.04x, 1.05x, 1.07x, 1.08x, 1.1x and 1.2x

Appendix D: Effect of Nominal Mn Composition on CL Segregation

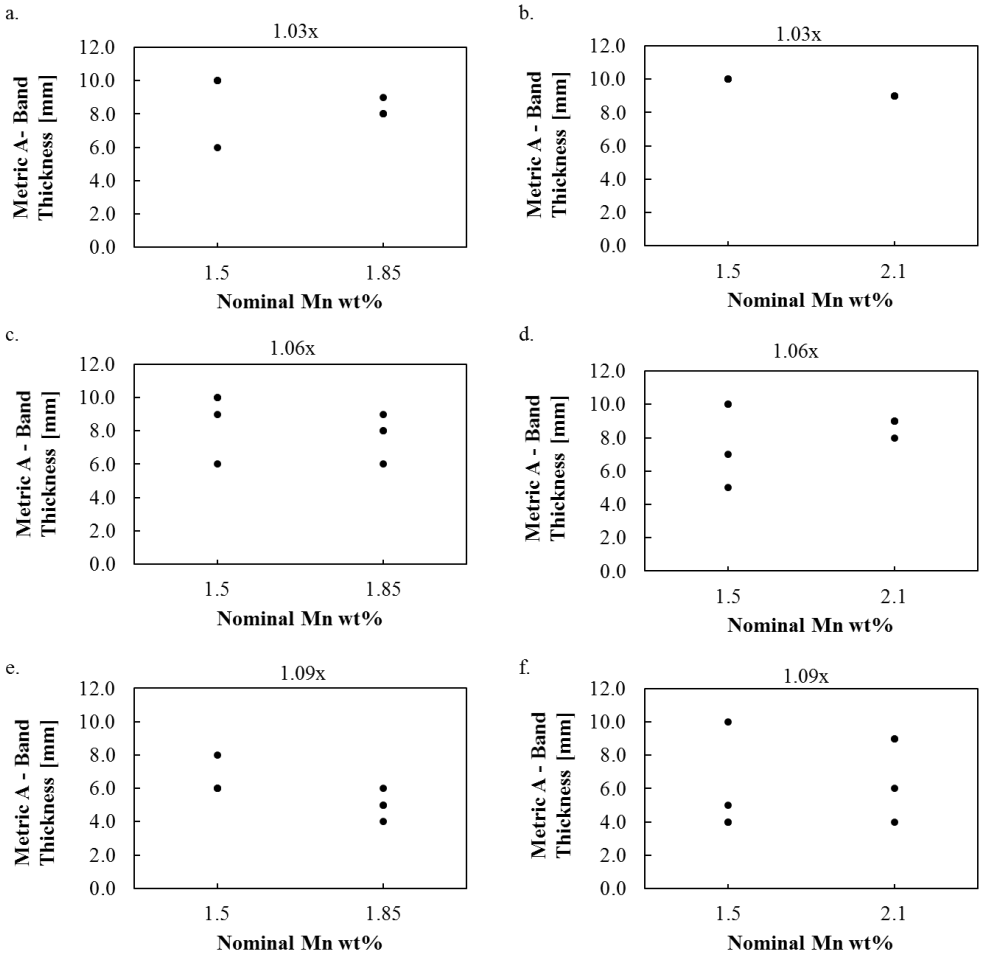

Figure 90: Metric A as a function of nominal composition of 1.5, 1.85 and 2.1 Mn wt% using factors 1.03x, 1.06x and 1.09x and a 1 value system

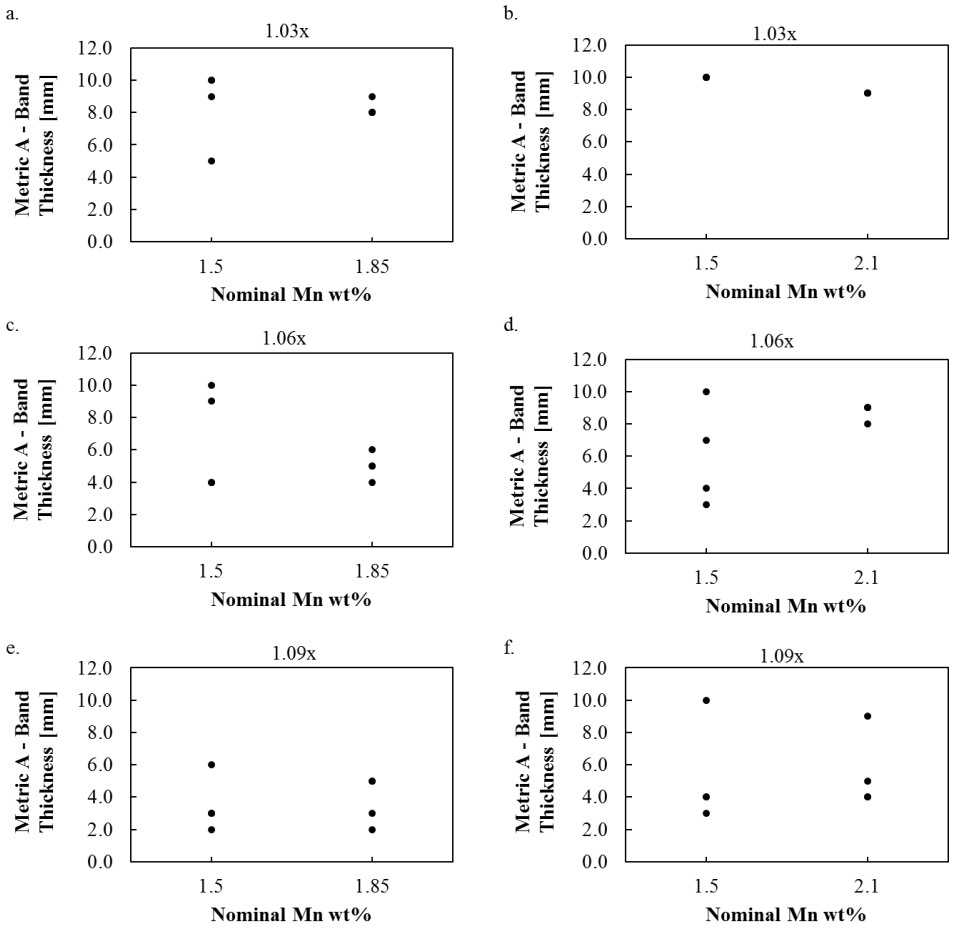

Figure 91: Metric A as a function of nominal composition of 1.5, 1.85 and 2.1 Mn wt% using factors 1.03x, 1.06x and 1.09x and a 2 value system

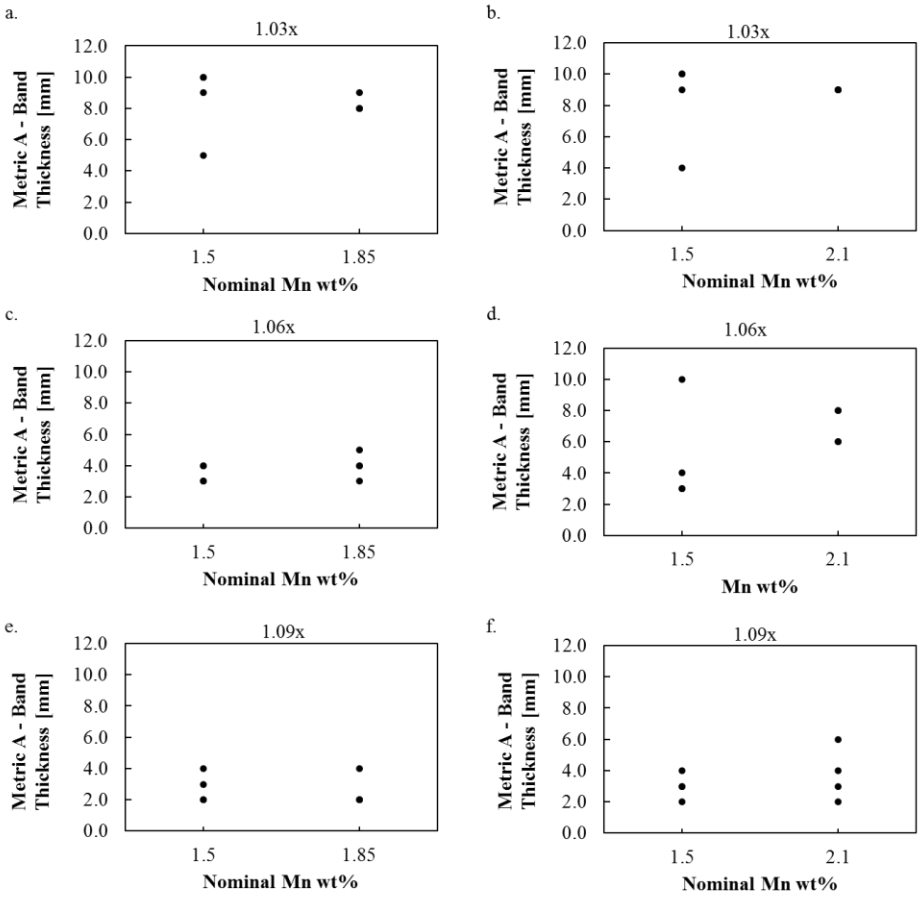

Figure 92: Metric A as a function of nominal composition of 1.5, 1.85 and 2.1 Mn wt% using factors 1.03x, 1.06x and 1.09x and a 4 value system

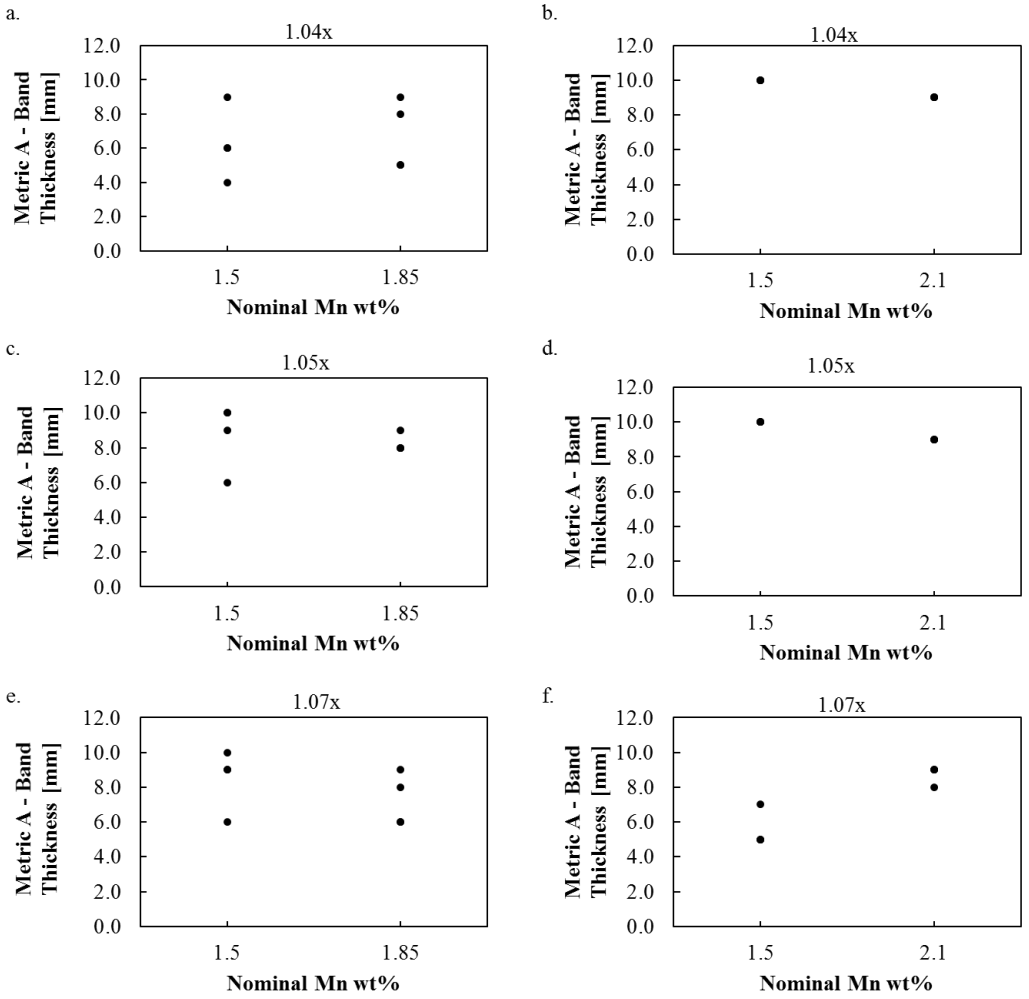

Figure 93: Metric A as a function of nominal composition of 1.5, 1.85 and 2.1 Mn wt% using factors 1.04x, 1.05x and 1.07x and a 1 value system

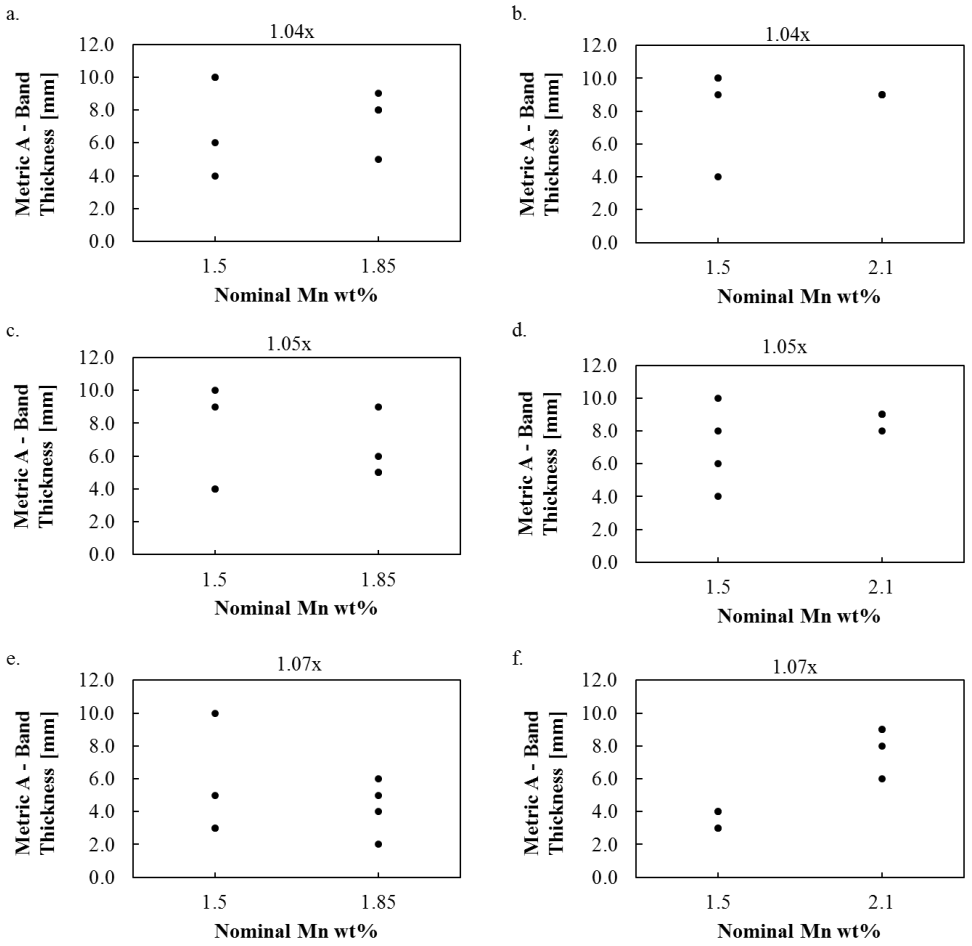

Figure 94: Metric A as a function of nominal composition of 1.5, 1.85 and 2.1 Mn wt% using factors 1.04x, 1.05x and 1.07x and a 2 value system

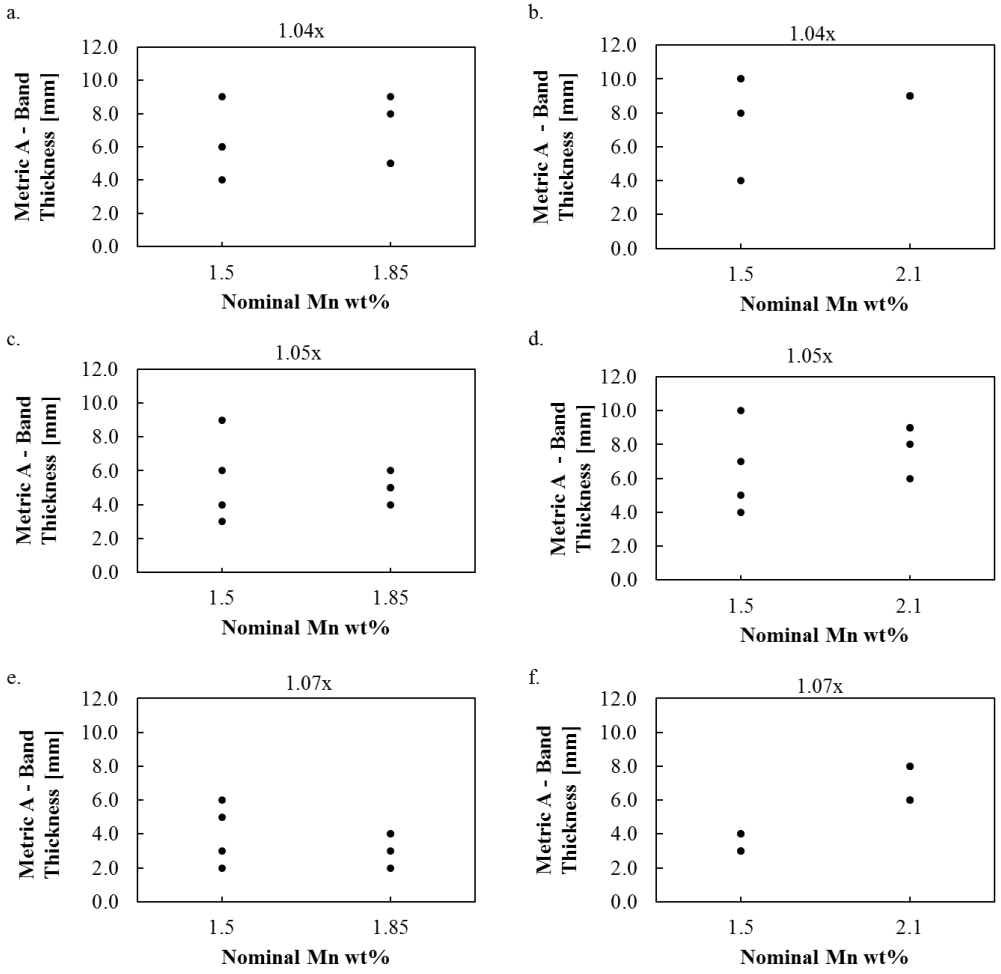

Figure 95: Metric A as a function of nominal composition of 1.5, 1.85 and 2.1 Mn wt% using factors 1.04x, 1.05x and 1.07x and a 3 value system

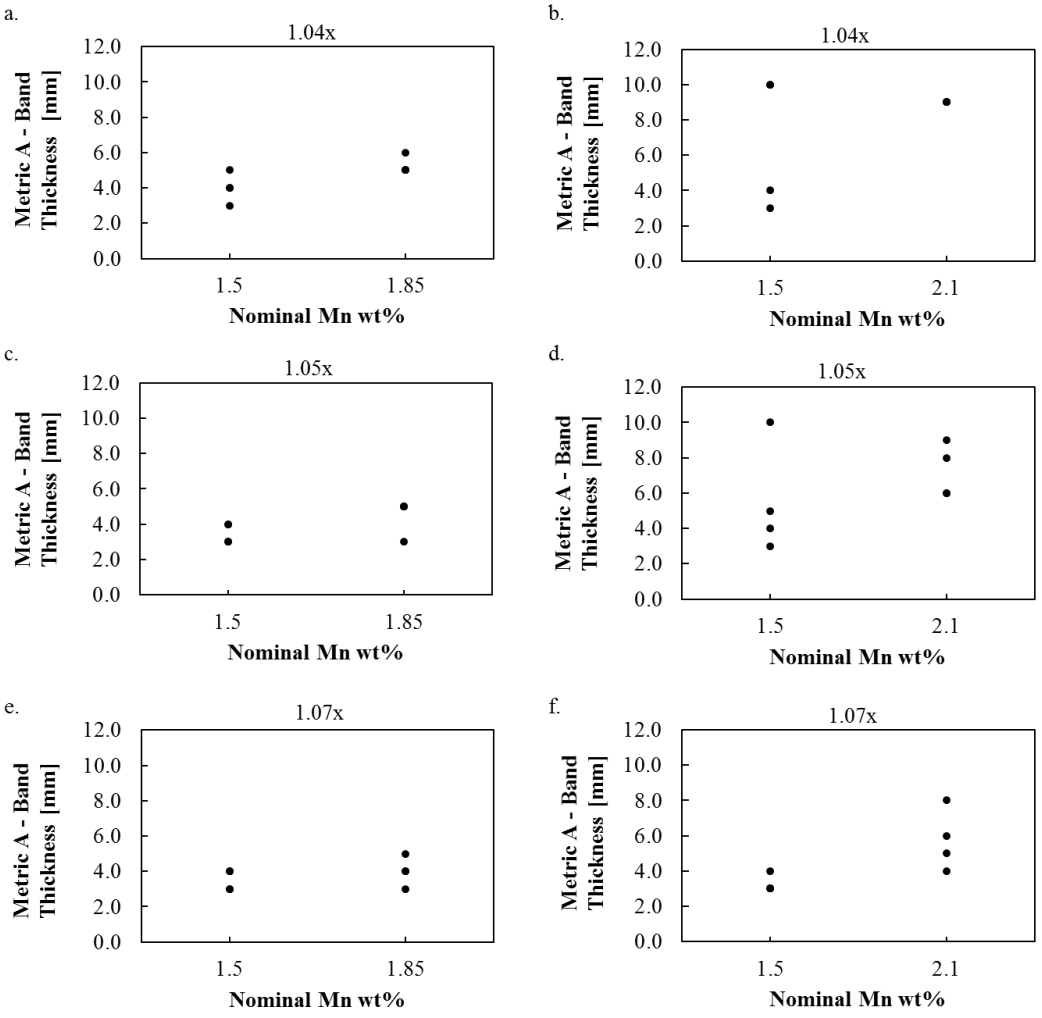

Figure 96: Metric A as a function of nominal composition of 1.5, 1.85 and 2.1 Mn wt% using factors 1.04x, 1.05x and 1.07x and a 4 value system

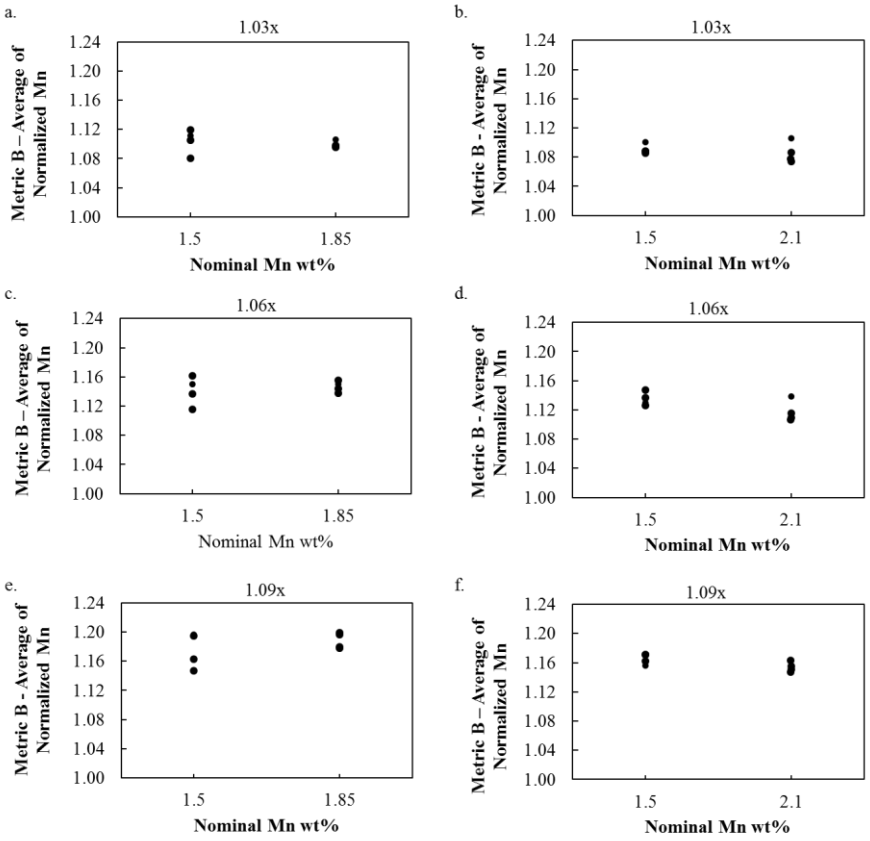

Figure 97: Metric B as a function of nominal composition of 1.5, 1.85 and 2.1 Mn wt% using factors 1.03x, 1.06x and 1.09x and a 1 value system

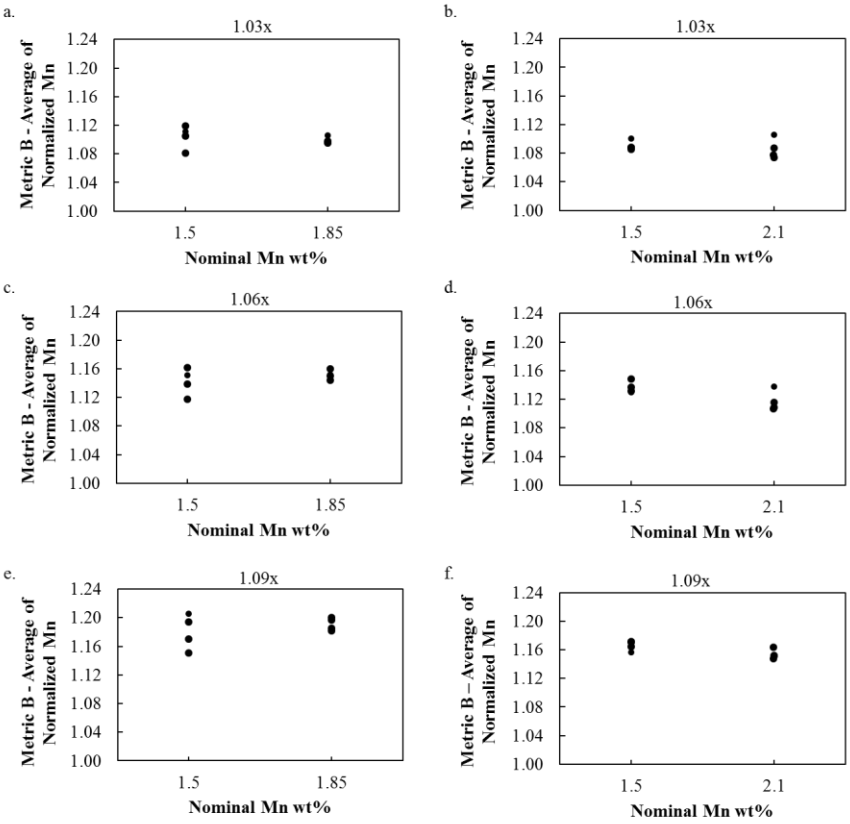

Figure 98: Metric B as a function of nominal composition of 1.5, 1.85 and 2.1 Mn wt% using factors 1.03x, 1.06x and 1.09x and a 2 value system

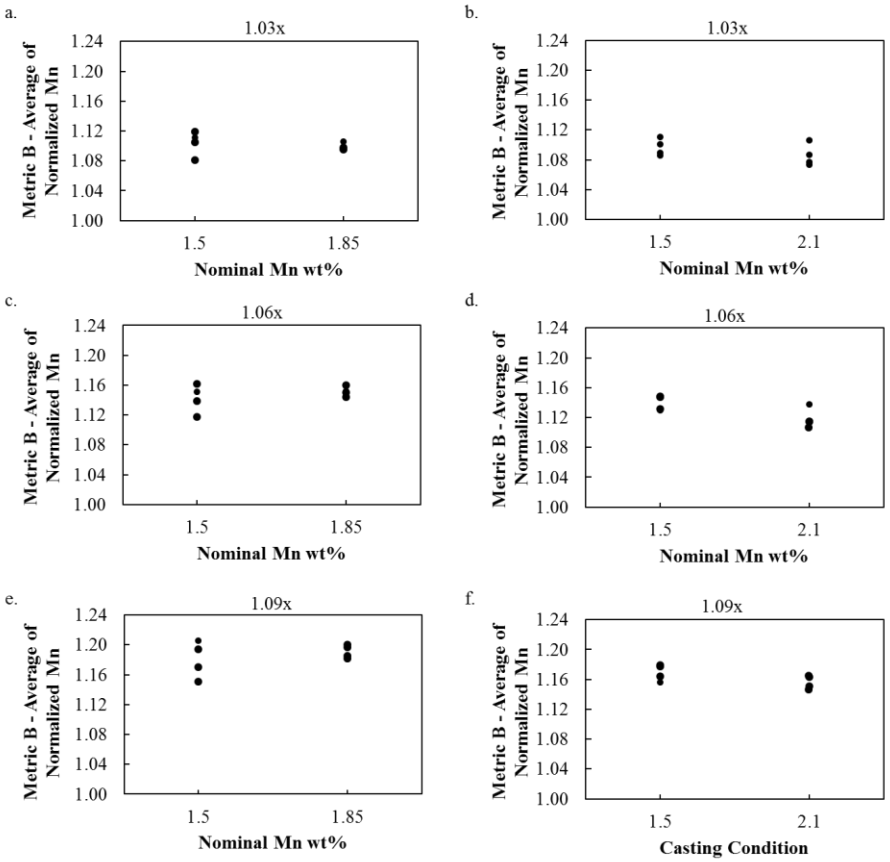

Figure 99: Metric B as a function of nominal composition of 1.5, 1.85 and 2.1 Mn wt% using factors 1.03x, 1.06x and 1.09x and a 4 value system

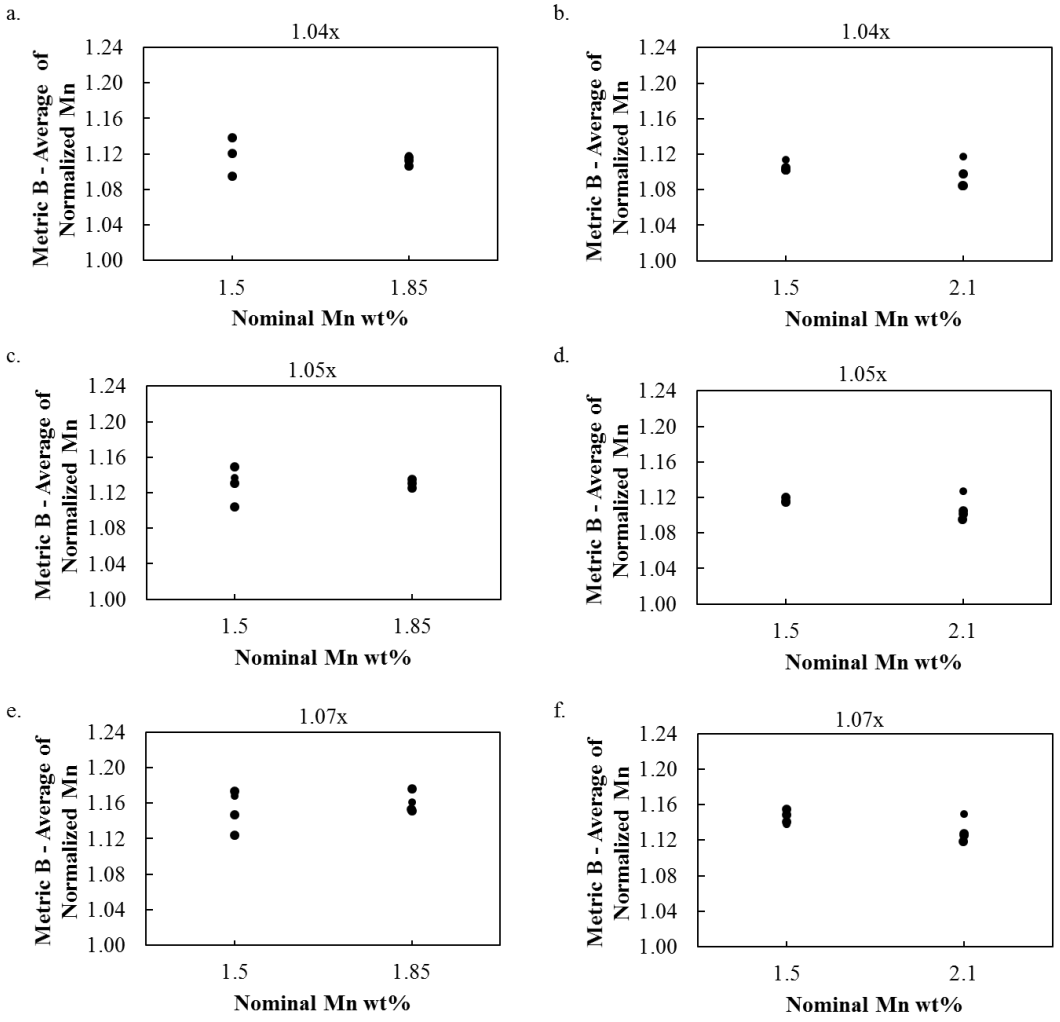

Figure 100: Metric B as a function of nominal composition of 1.5, 1.85 and 2.1 Mn wt% using factors 1.04x, 1.05x and 1.07x and a 1 value system

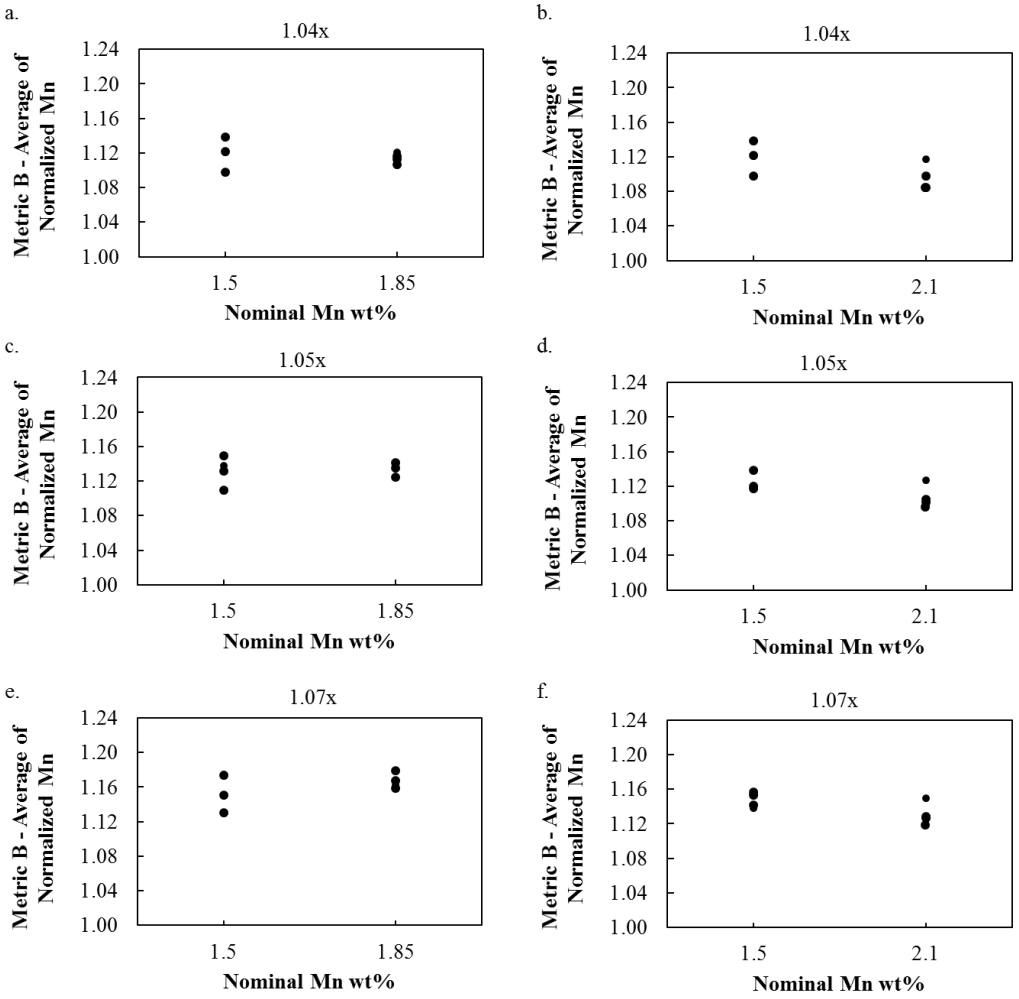

Figure 101: Metric B as a function of nominal composition of 1.5, 1.85 and 2.1 Mn wt% using factors 1.04x, 1.05x and 1.07x and a 2 value system

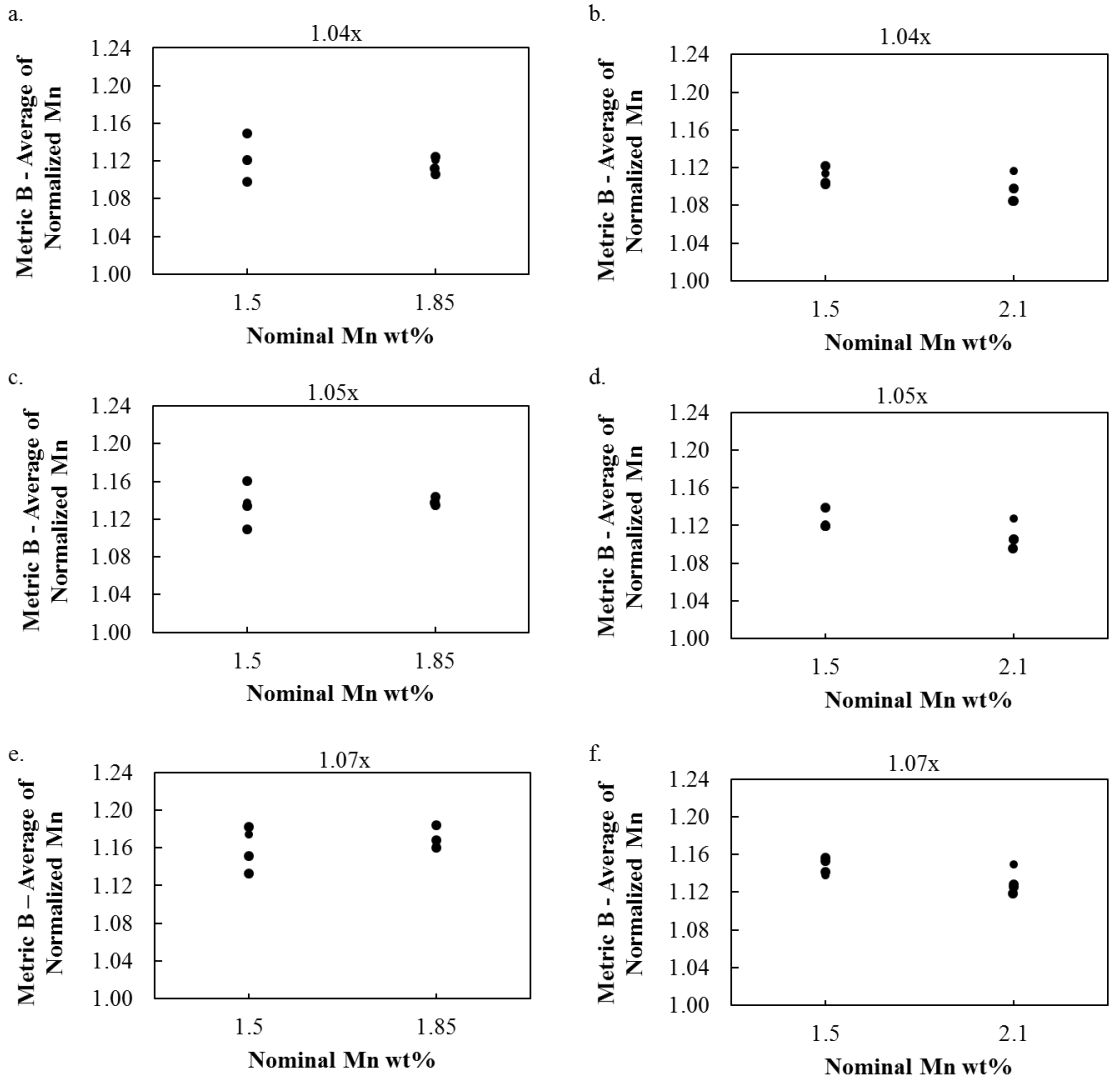

Figure 102: Metric B as a function of nominal composition of 1.5, 1.85 and 2.1 Mn wt% using factors 1.04x, 1.05x and 1.07x and a 3 value system

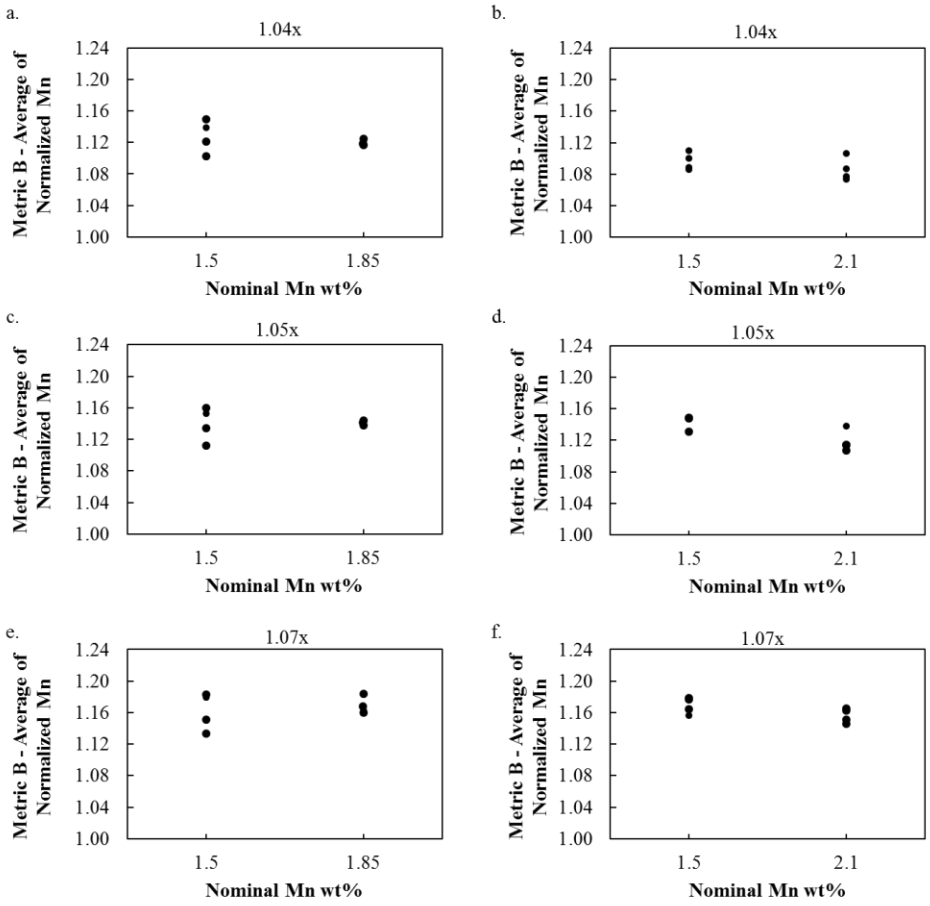

Figure 103: Metric B as a function of nominal composition of 1.5, 1.85 and 2.1 Mn wt% using factors 1.04x, 1.05x and 1.07x and a 4 value system

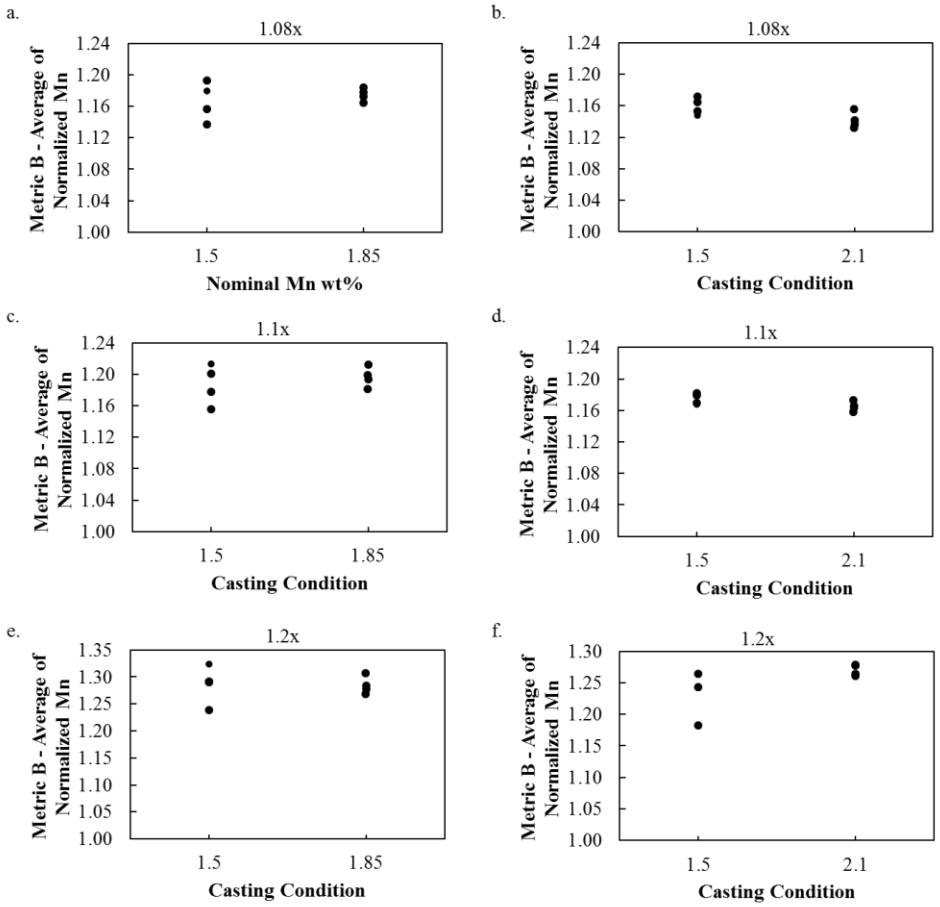

Figure 104: Metric B as a function of nominal composition of 1.5, 1.85 and 2.1 Mn wt% using factors 1.08x, 1.1x and 1.2x and a 1 value system

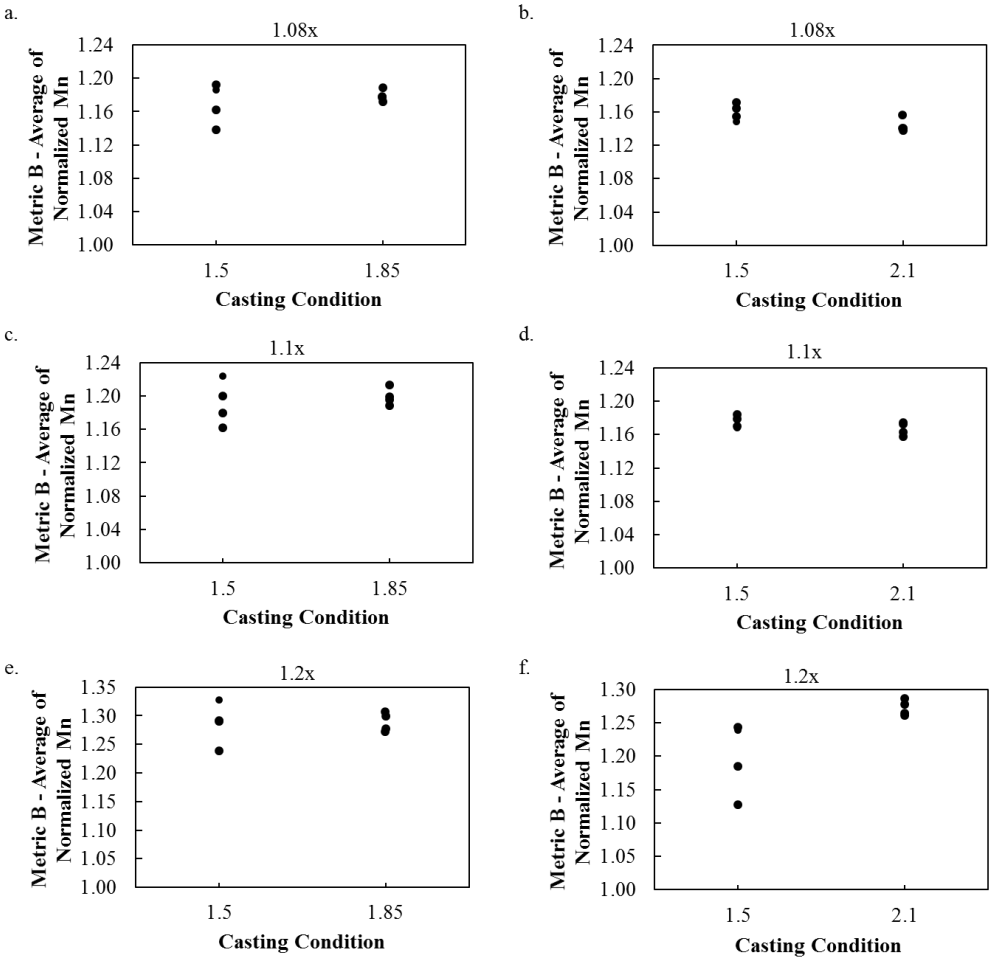

Figure 105: Metric B as a function of nominal composition of 1.5, 1.85 and 2.1 Mn wt% using factors 1.08x, 1.1x and 1.2x and a 2 value system

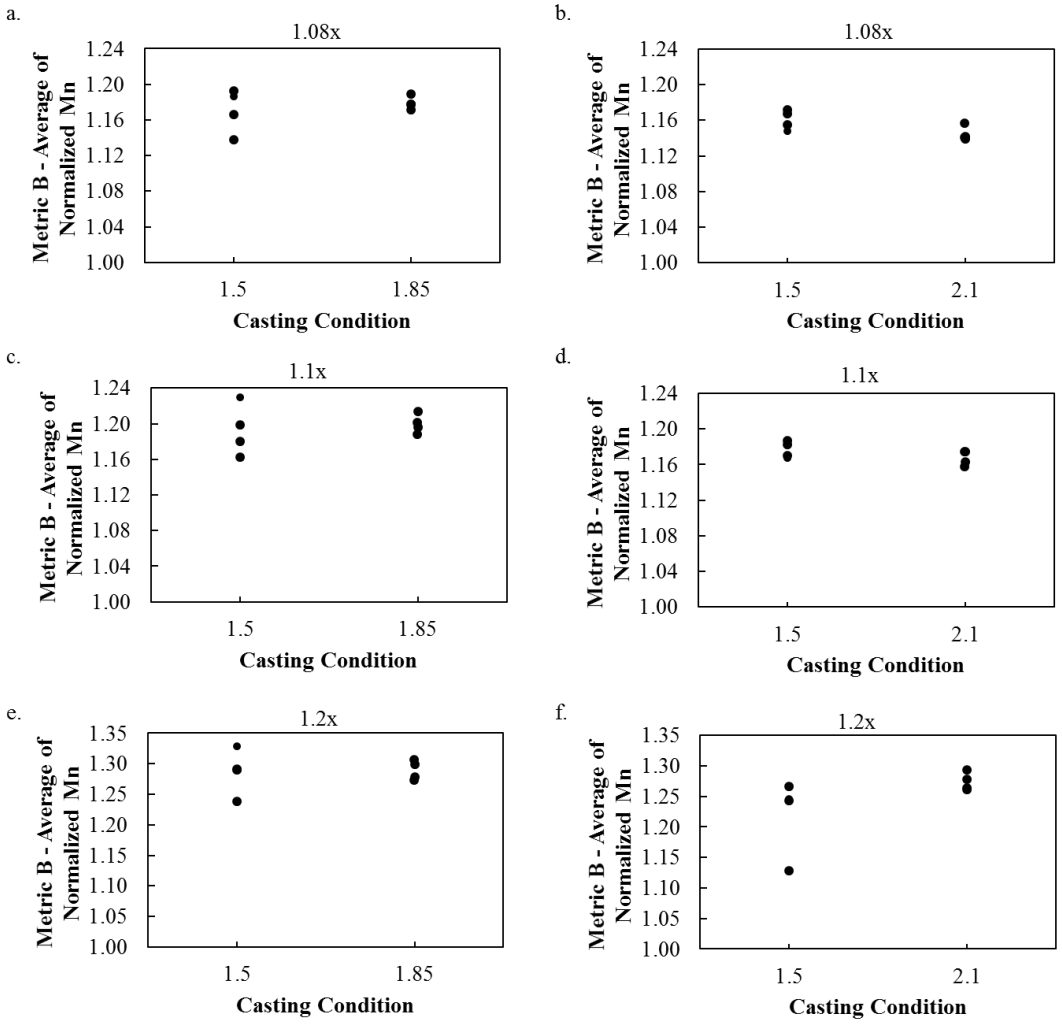

Figure 106: Metric B as a function of nominal composition of 1.5, 1.85 and 2.1 Mn wt% using factors 1.08x, 1.1x and 1.2x and a 3 value system

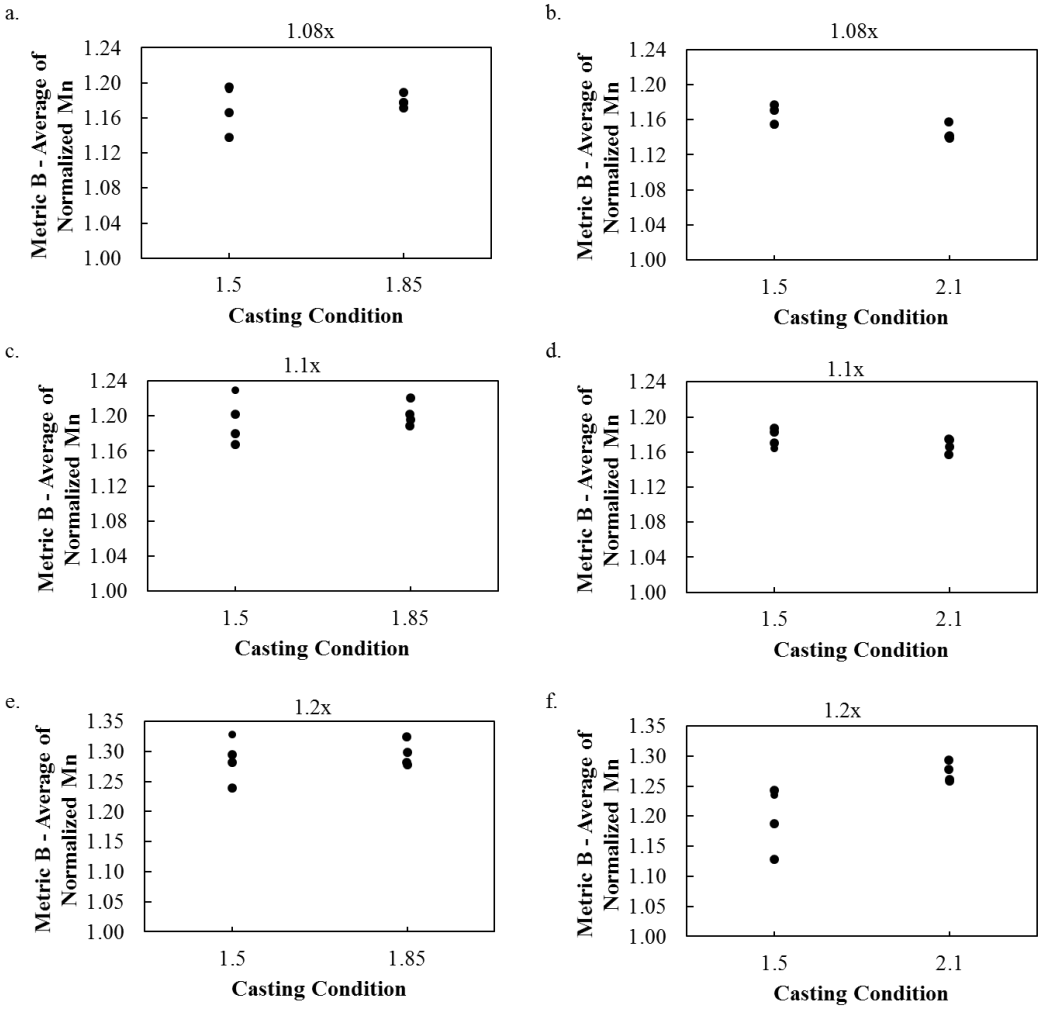

Figure 107: Metric B as a function of nominal composition of 1.5, 1.85 and 2.1 Mn wt% using factors 1.08x, 1.1x and 1.2x and a 4 value system

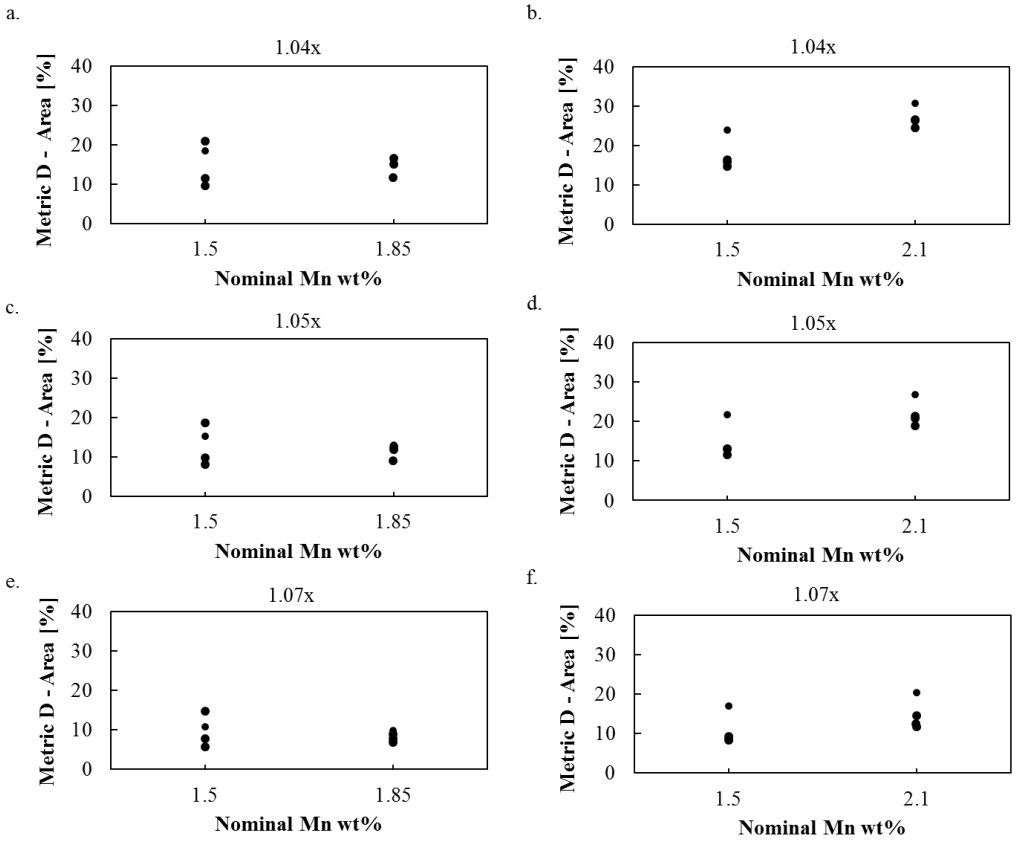

Figure 108: Metric D as a function of nominal composition of 1.5, 1.85 and 2.1 Mn wt% using factors 1.04x, 1.05x, 1.07x

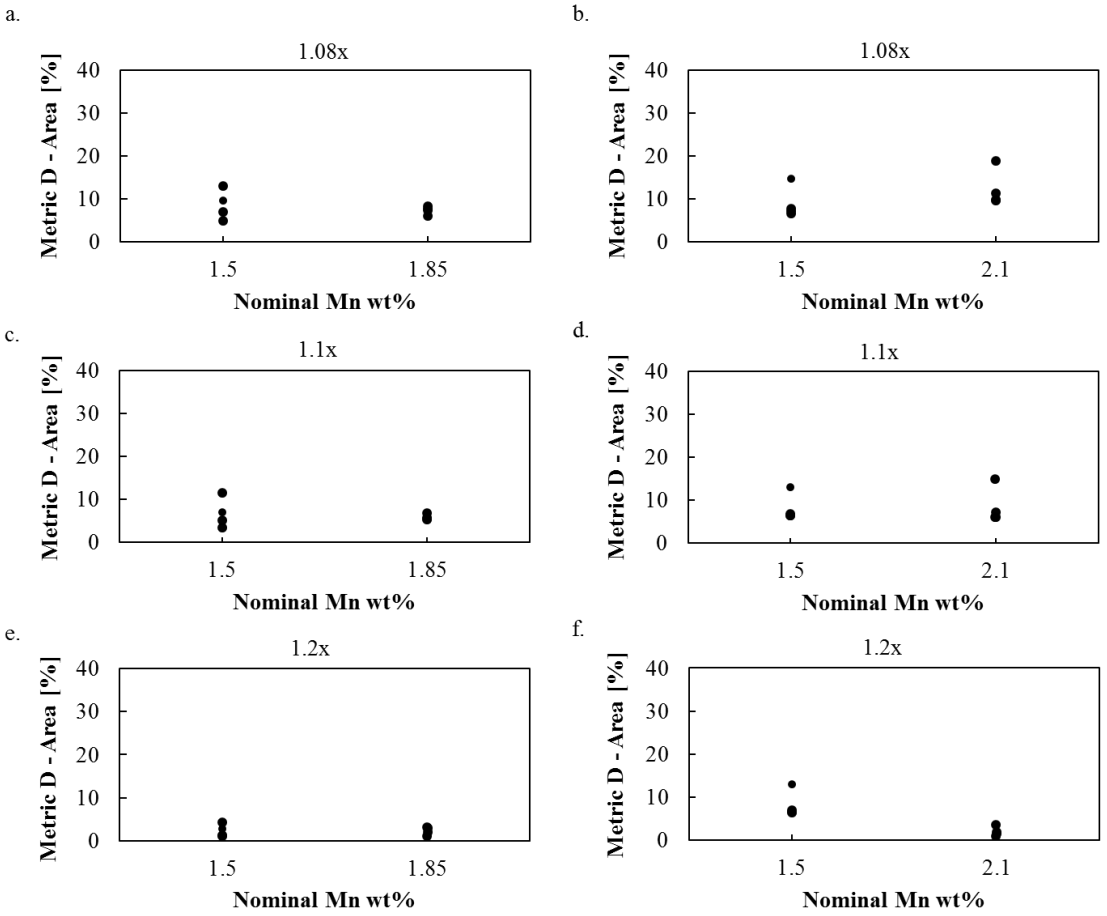

Figure 109: Metric D as a function of nominal composition of 1.5, 1.85 and 2.1 Mn wt% using factors 1.08x, 1.1x, 1.2x

Appendix E: Effect of Spatial Orientation on FF Segregation

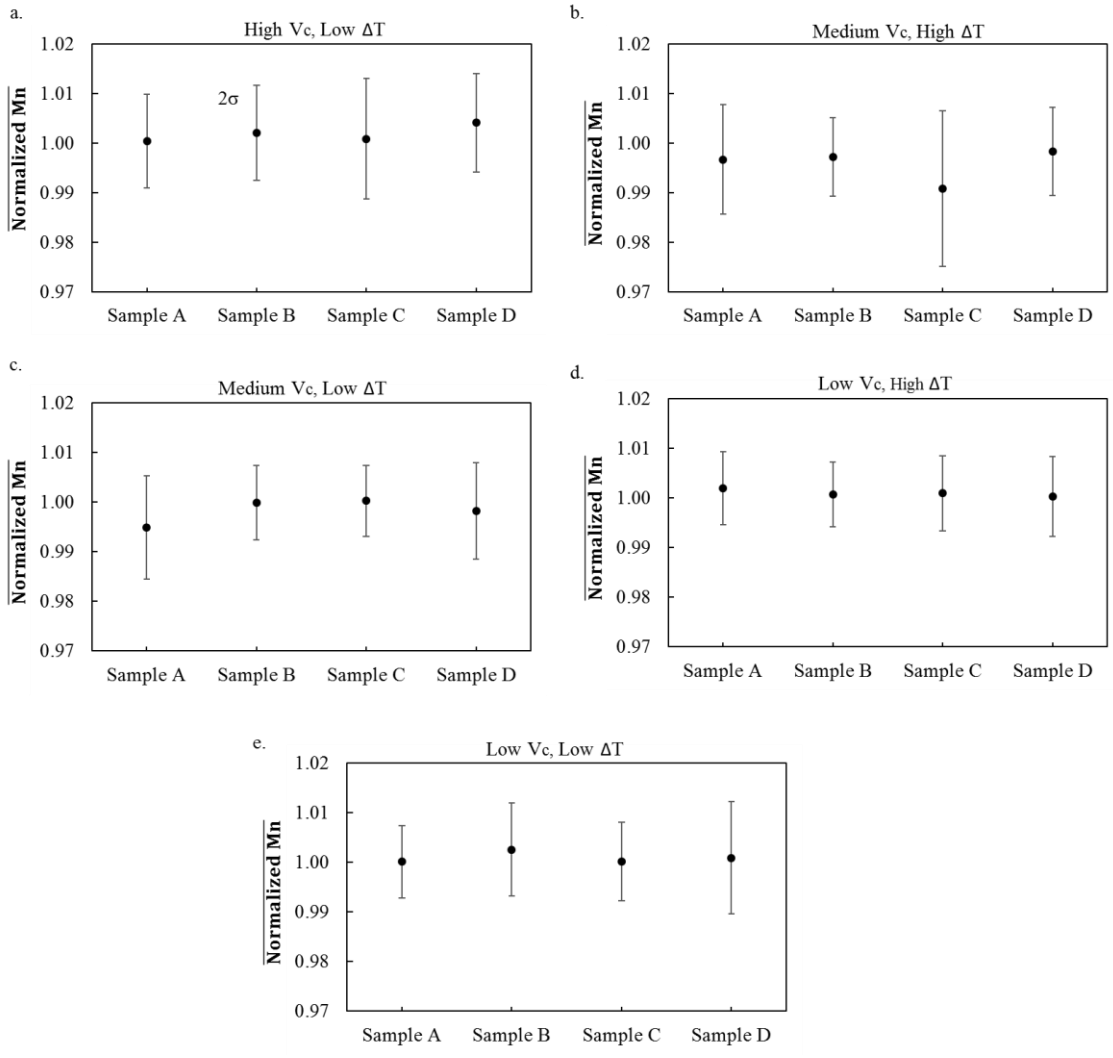

Figure 110: Far field average of the normalized Mn as a function of spatial orientation for 1.5 Mn wt%

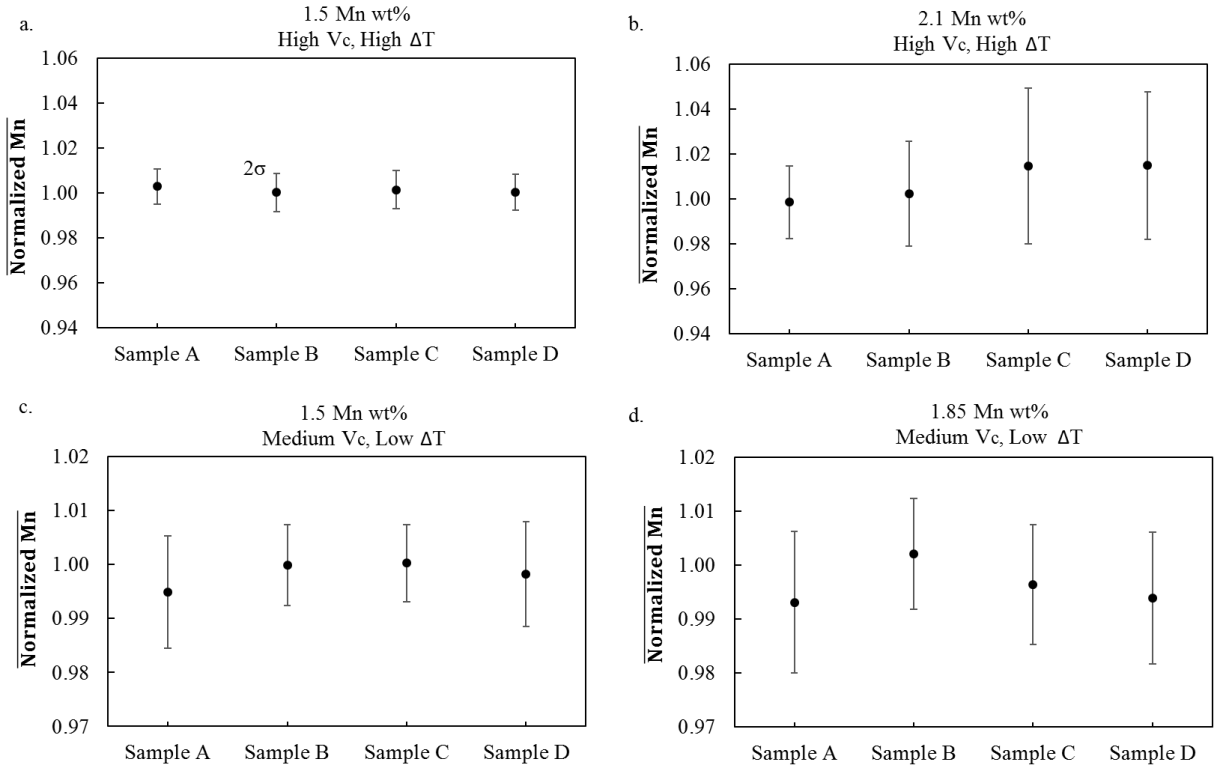

Figure 111: A comparison of the far field average as a function of spatial orientation for 1.5, 1.85 and 2.1 Mn wt%

Appendix F: Extended Factors to Consider

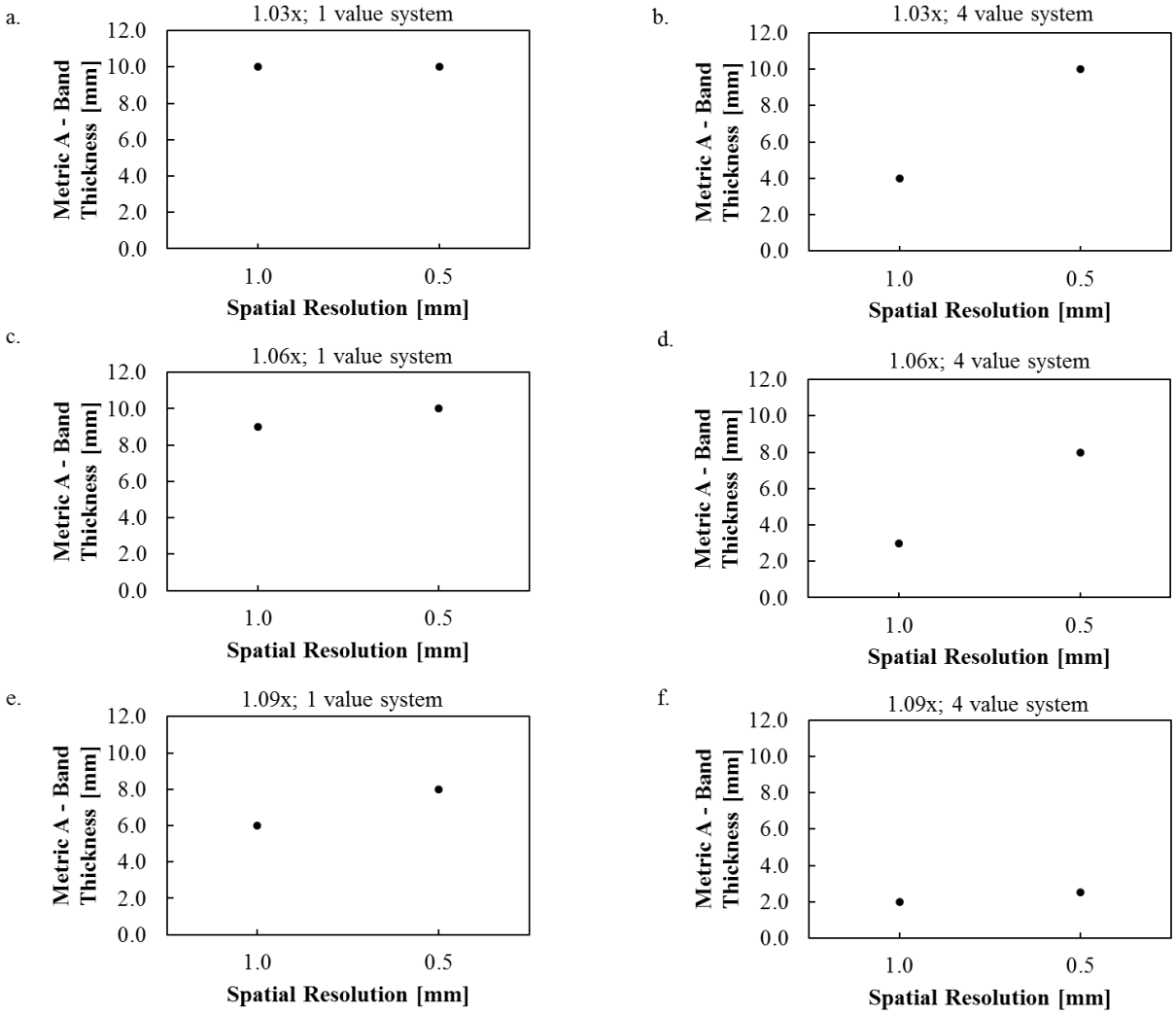

Figure 112: Metric A using 1 mm and 0.5 mm spatial resolution scans with factors 1.03x, 1.06x, 1.09x and 1 and 4 value system

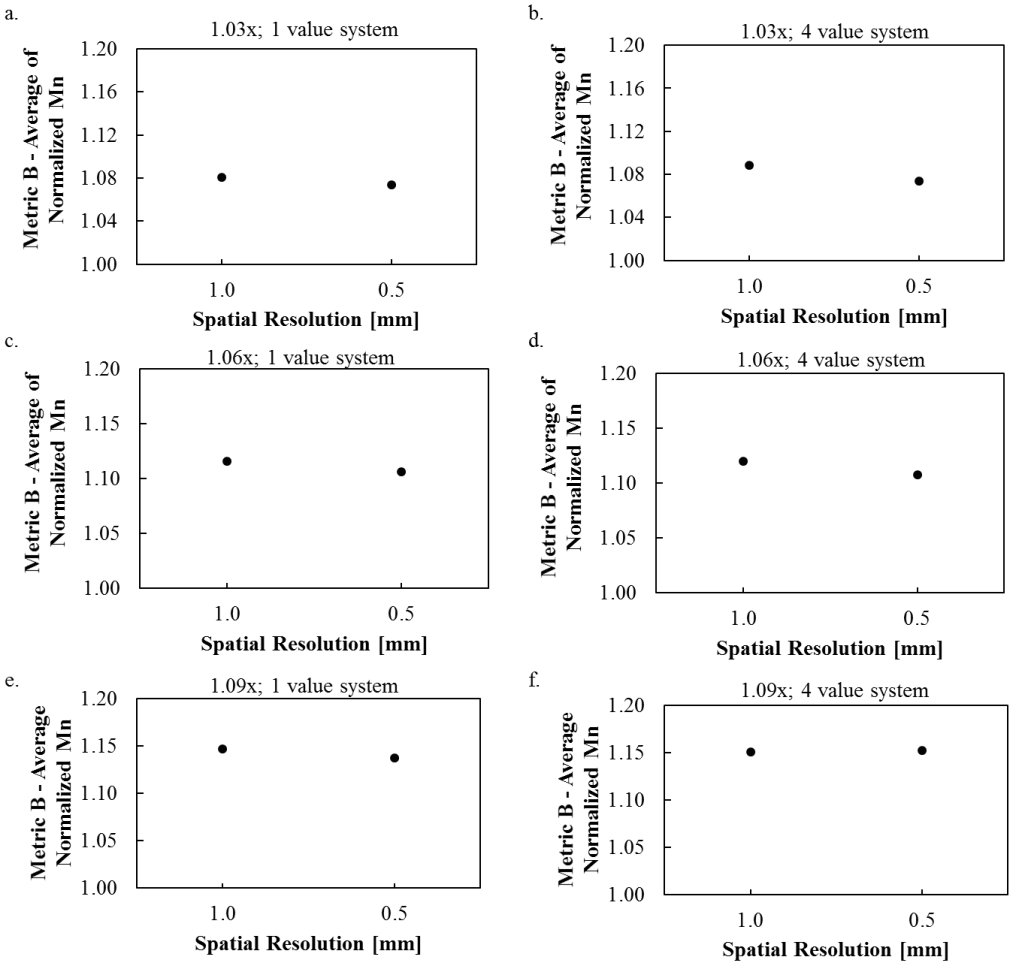

Figure 113: Metric B using 1 mm and 0.5 mm spatial resolution scans with factors 1.03x, 1.06x, 1.09x and 1 and 4 value system

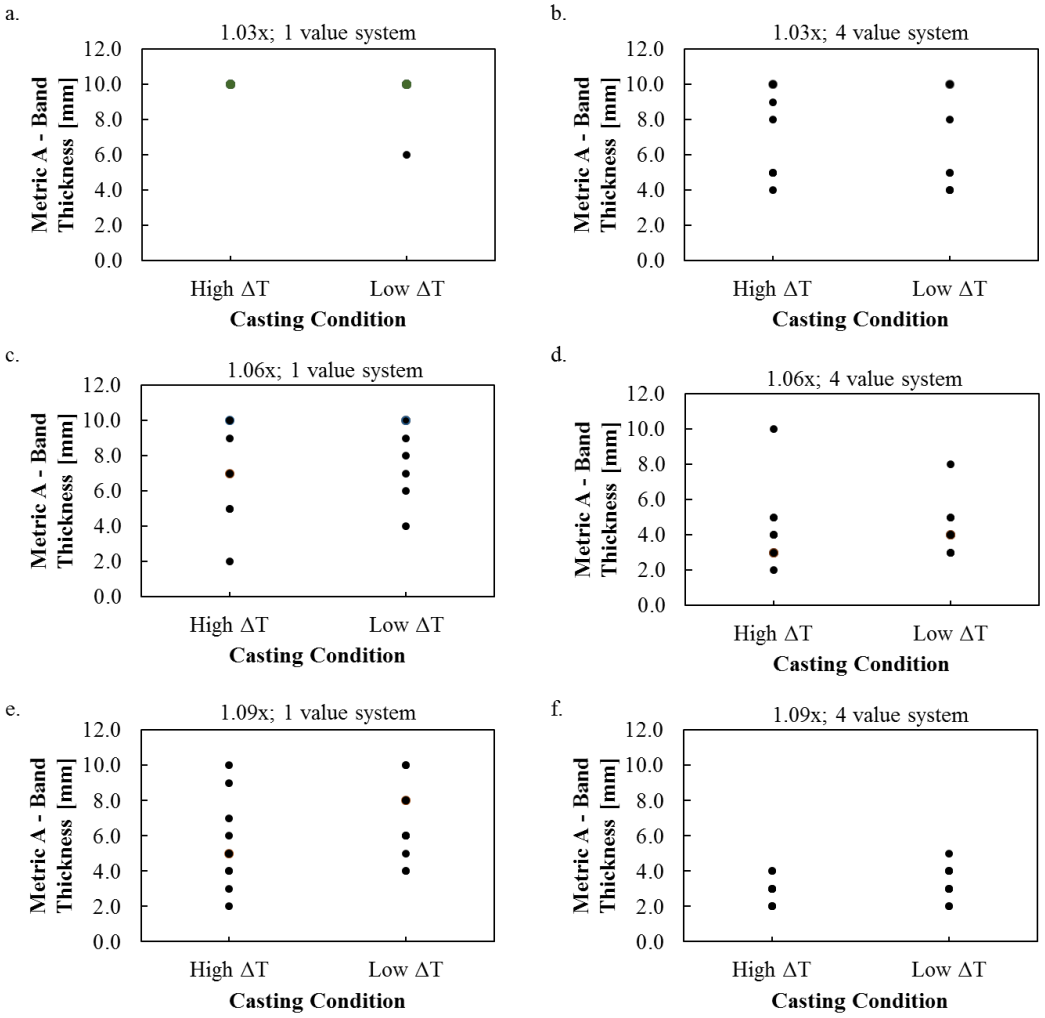

Figure 114: Method 2 and Metric A as a function of superheat for 1.5 Mn wt% using factors 1.03x, 1.06x, 1.09x and 1 and 4 value systems

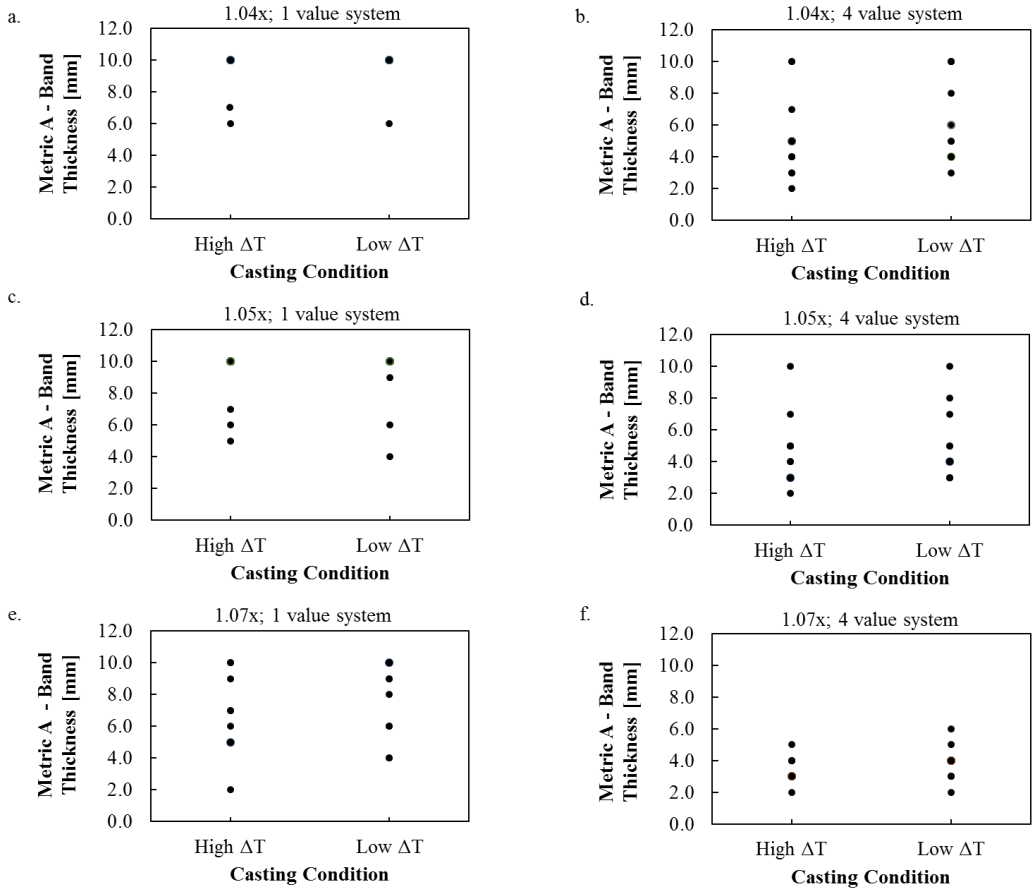

Figure 115: Method 2 and Metric A as a function of superheat for 1.5 Mn wt% using factors 1.04x, 1.05x, 1.07x and 1 and 4 value systems

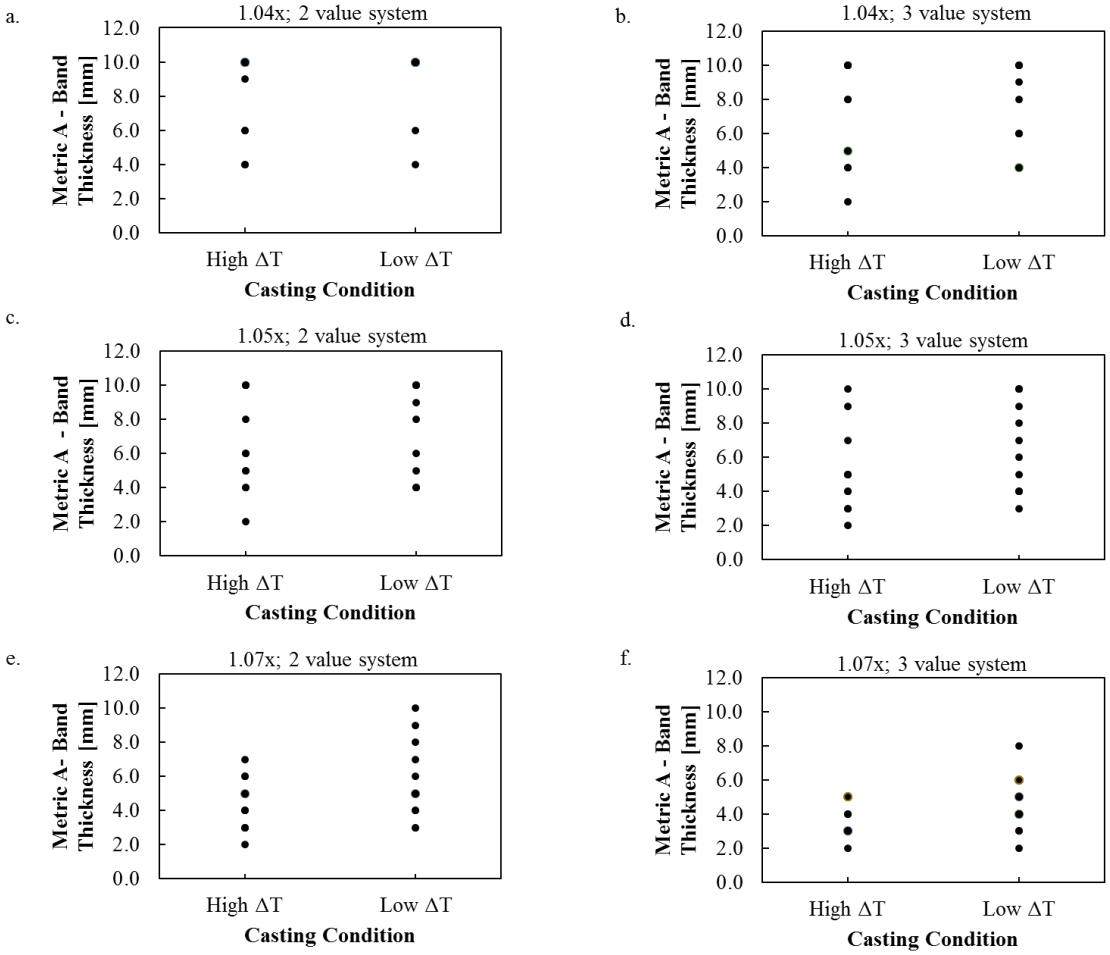

Figure 116: Method 2 and Metric A as a function of superheat for 1.5 Mn wt% using factors 1.04x, 1.05x, 1.07x and 2 and 3 value systems

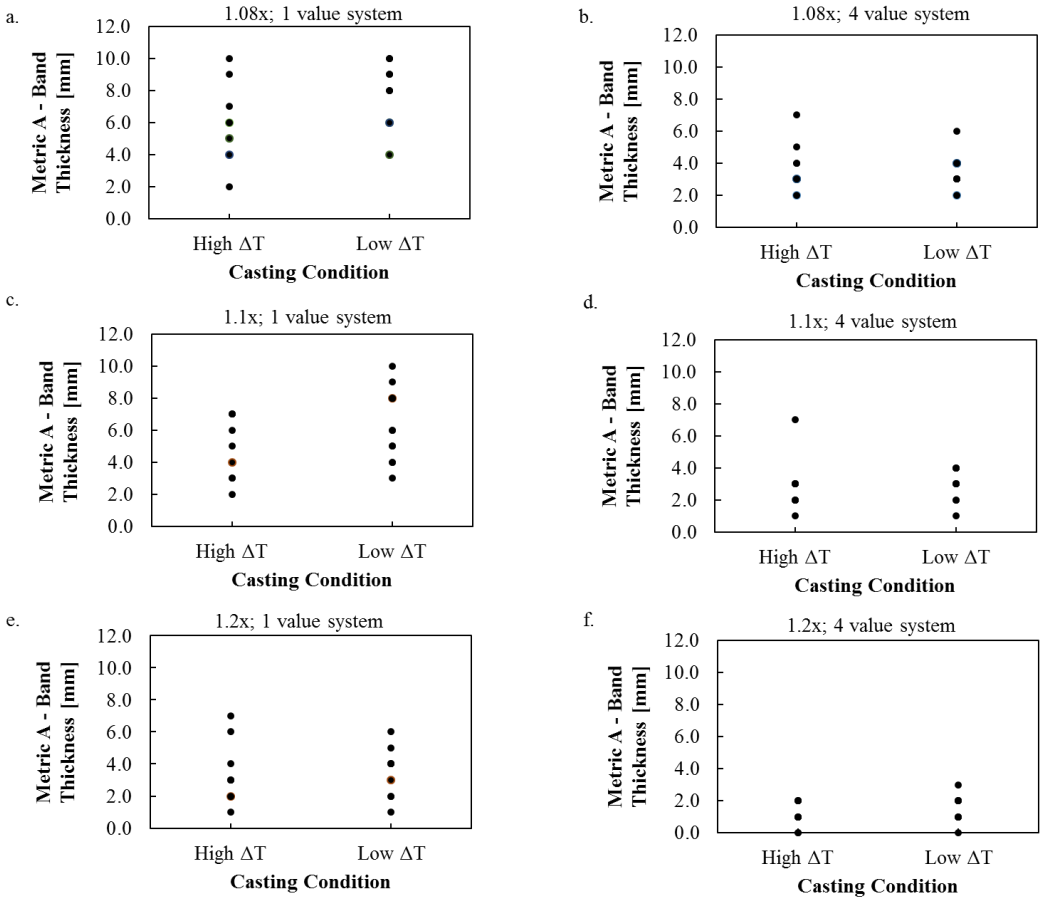

Figure 117: Method 2 and Metric A as a function of superheat for 1.5 Mn wt% using factors 1.08x, 1.1x, 1.2x and 1 and 4 value systems

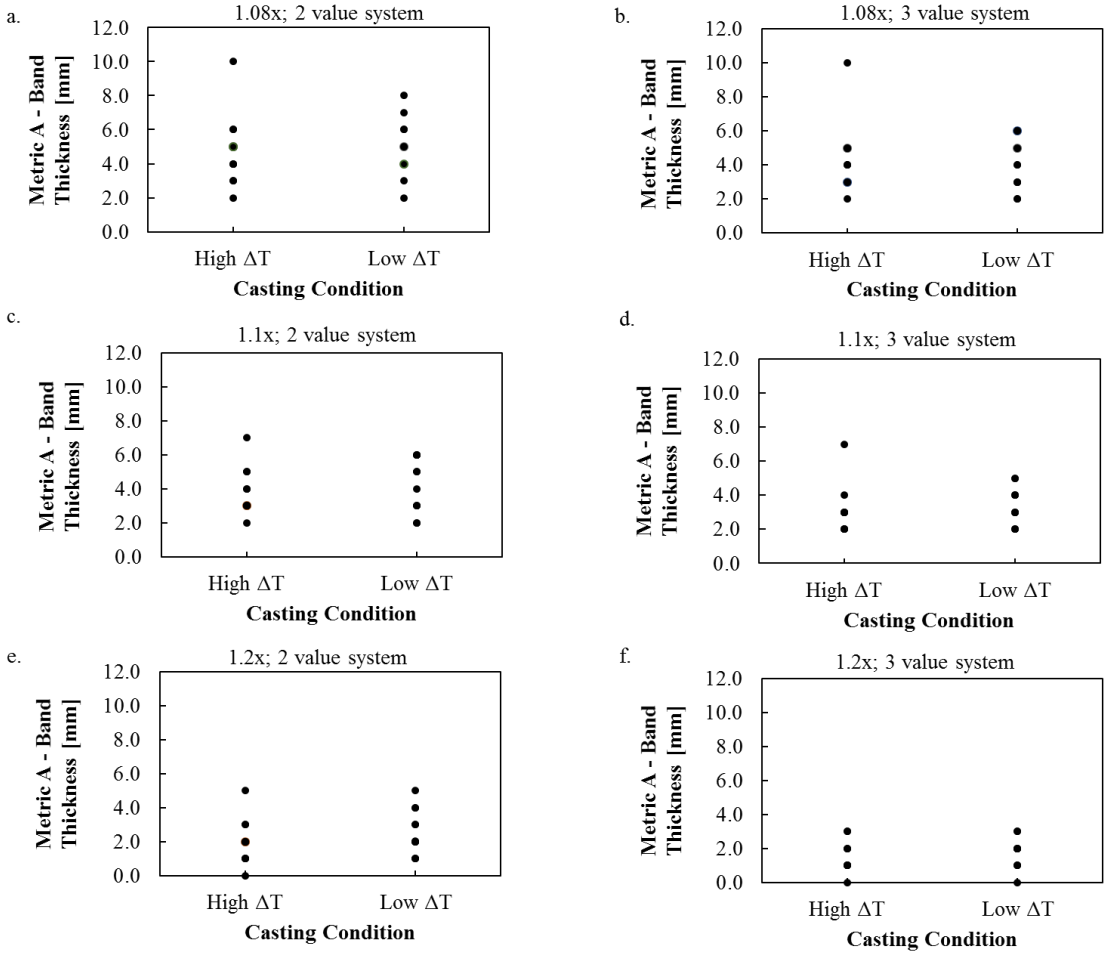

Figure 118: Method 2 and Metric A as a function of superheat for 1.5 Mn wt% using factors 1.08x, 1.1x, 1.2x and 2 and 3 value systems

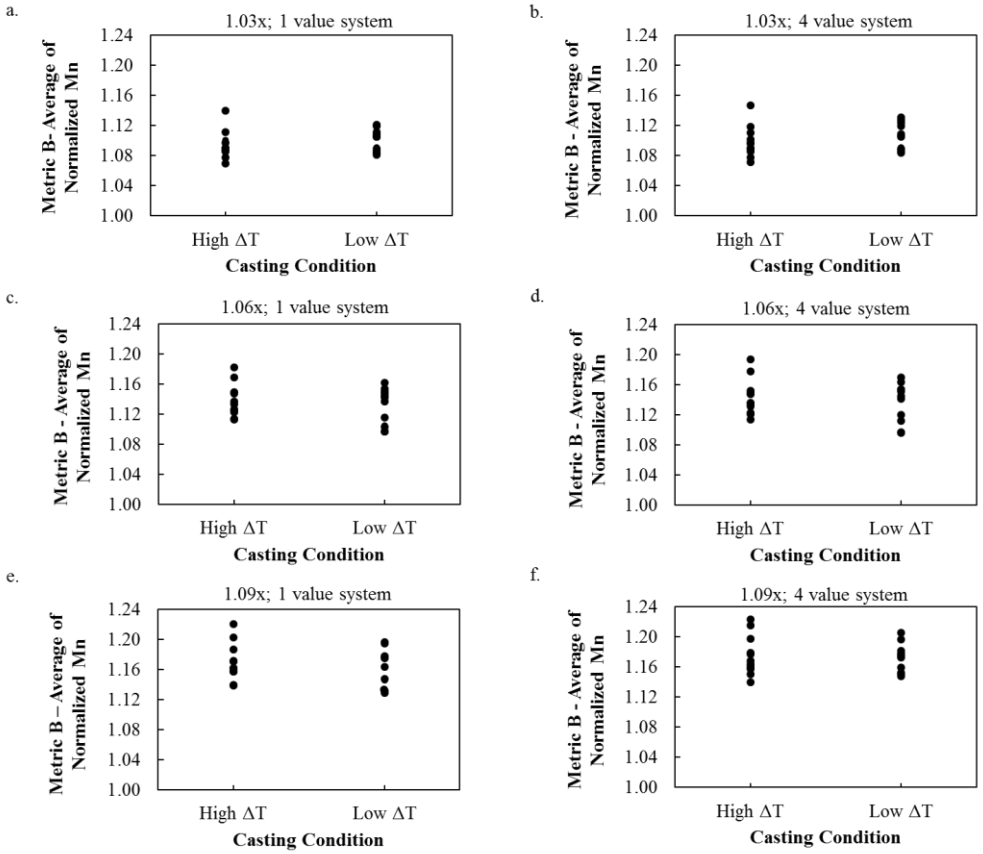

Figure 119: Metric B as a function of superheat for 1.5 Mn wt% using factors 1.03x, 1.06x, 1.09x and 1 and 4 value systems

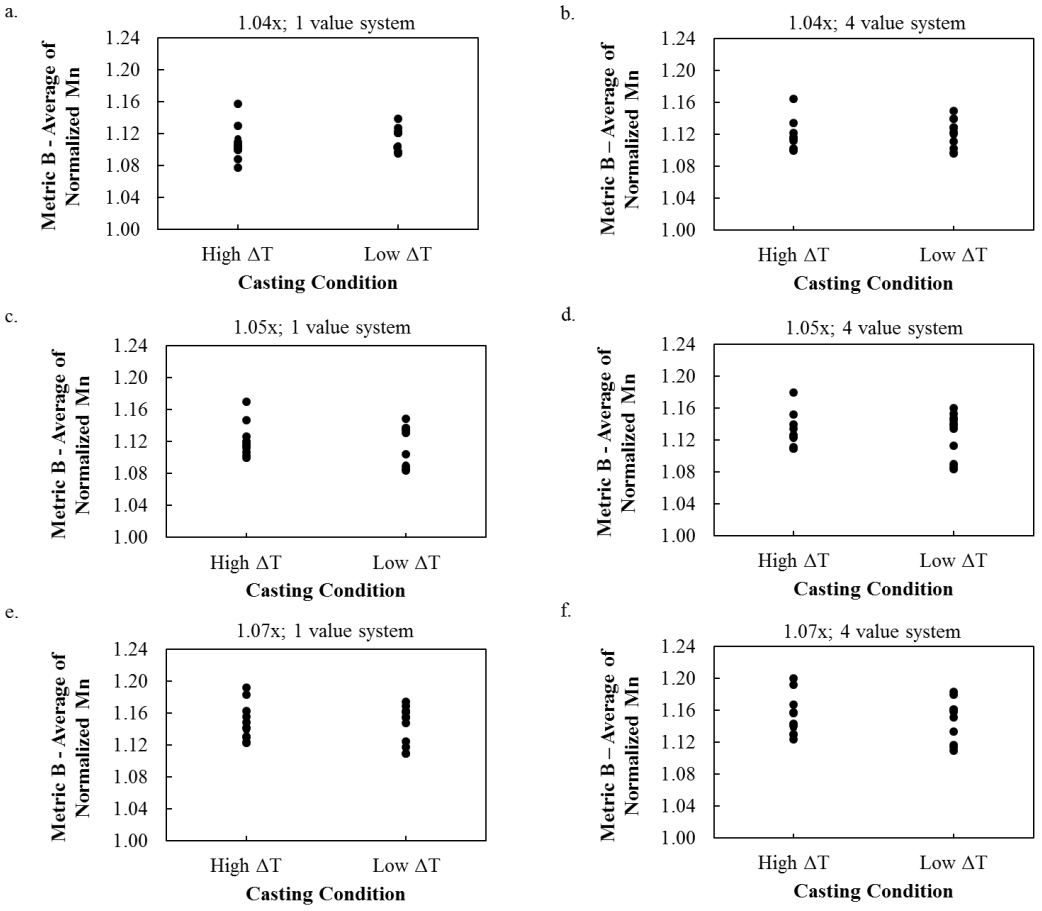

Figure 120: Metric B as a function of superheat for 1.5 Mn wt% using factors 1.04x, 1.05x, 1.07x and 1 and 4 value systems

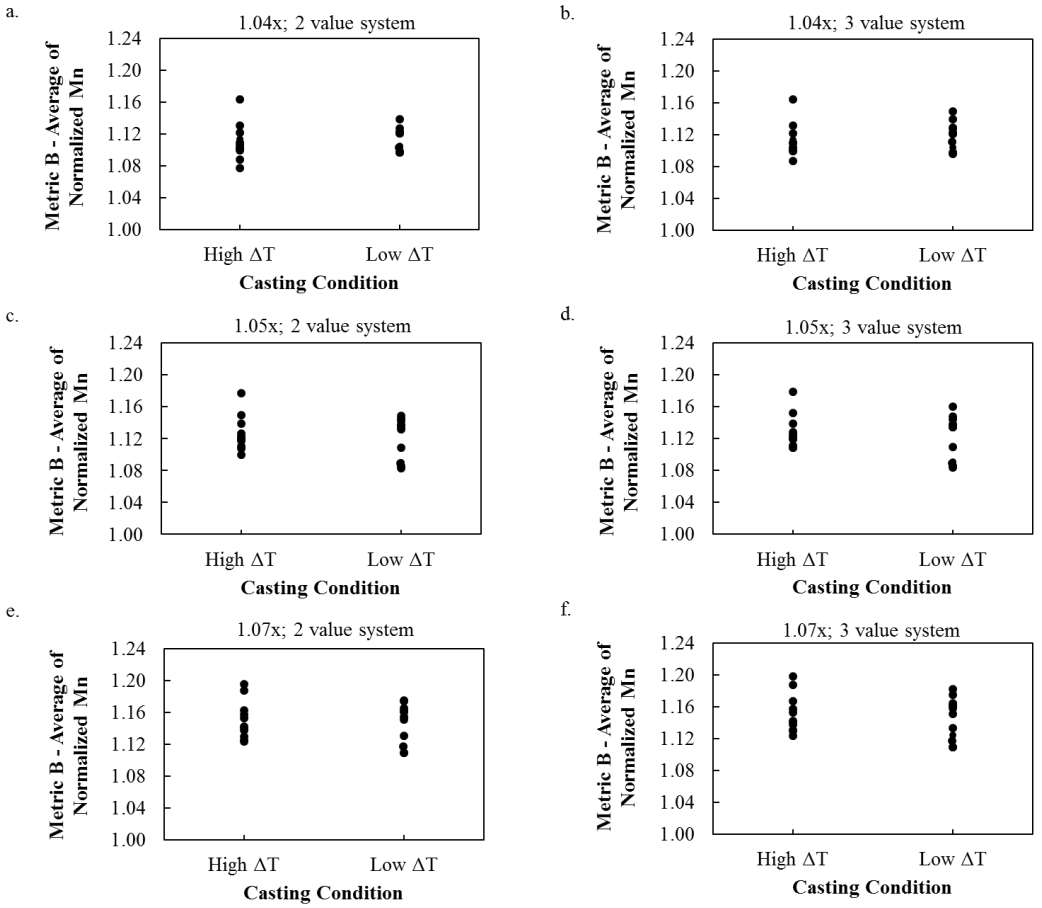

Figure 121: Metric B as a function of superheat for 1.5 Mn wt% using factors 1.04x, 1.05x, 1.07x and 2 and 3 value systems

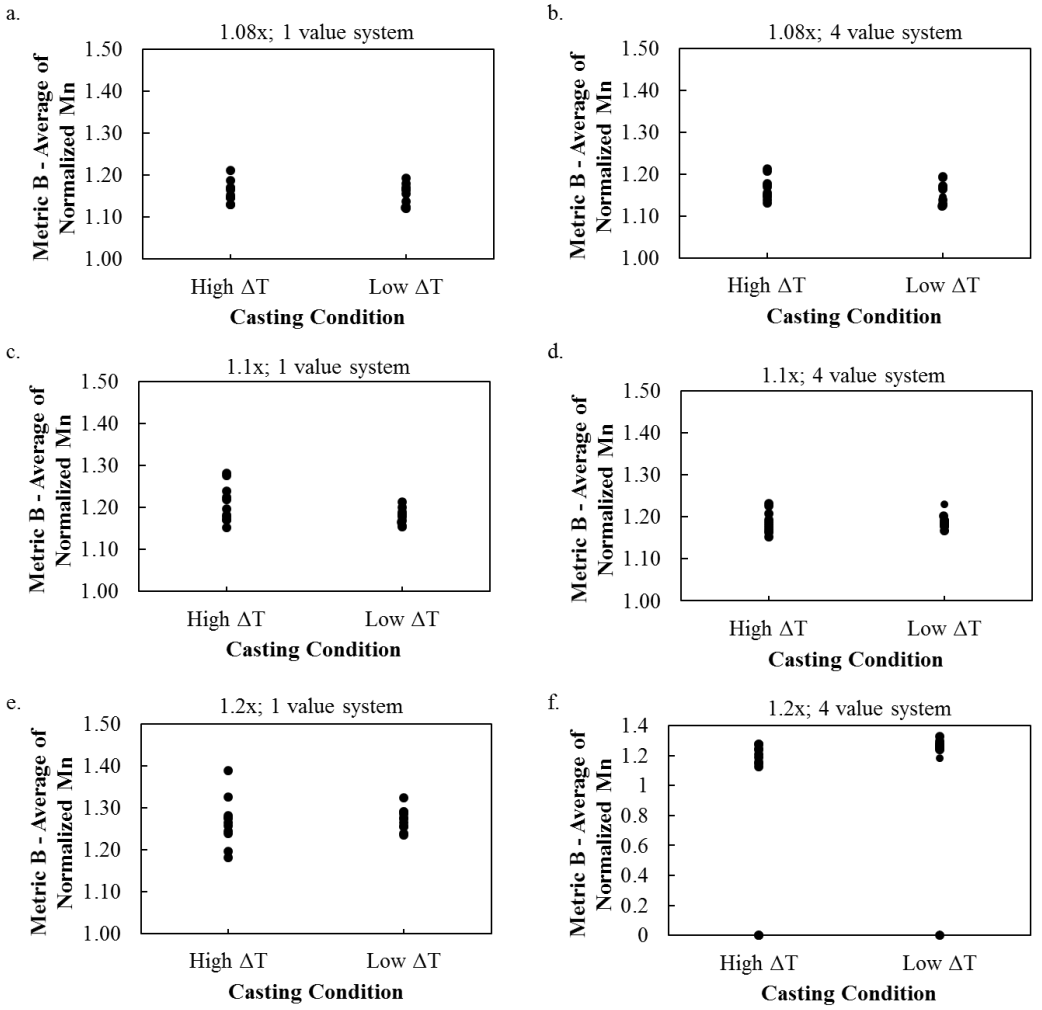

Figure 122: Metric B as a function of superheat for 1.5 Mn wt% using factors 1.08x, 1.1x, 1.2x and 1 and 4 values

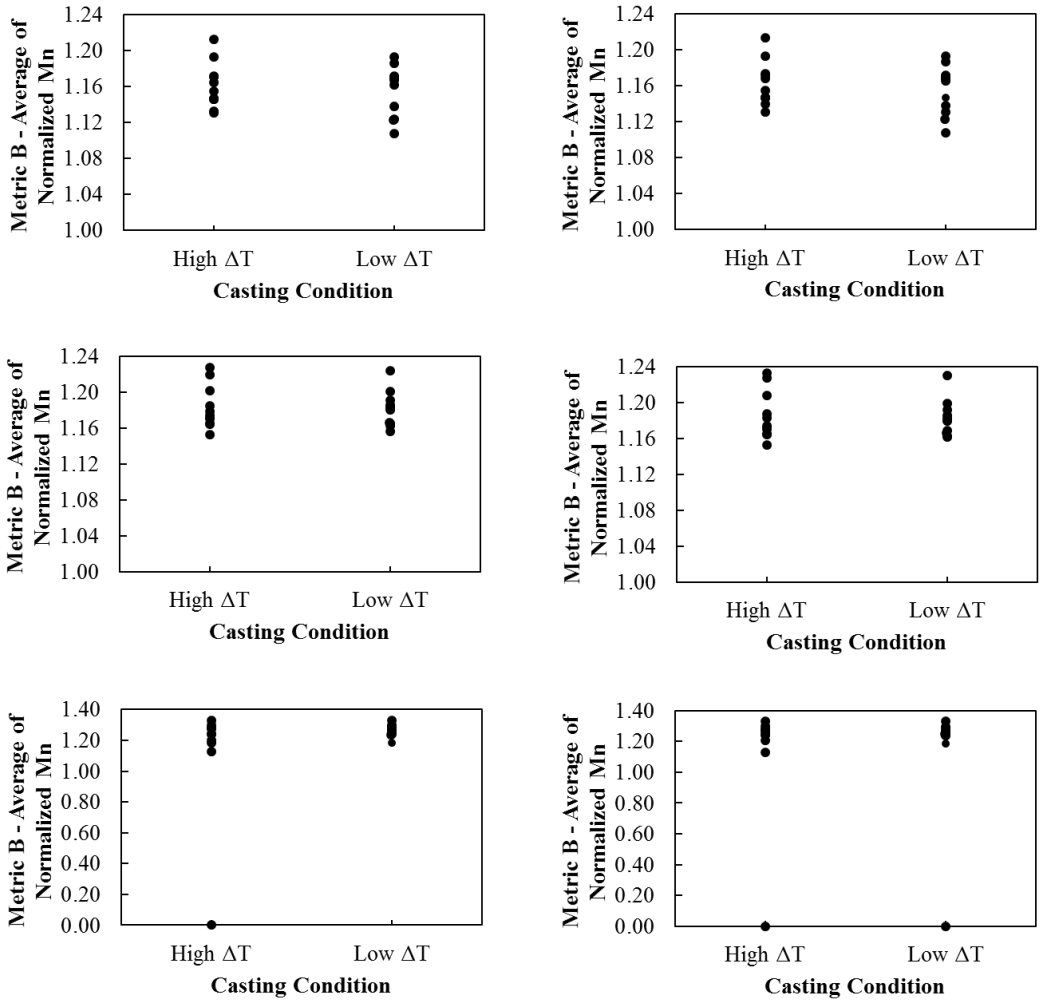

Figure 123: Metric B as a function of superheat for 1.5 Mn wt% using factors 1.08x, 1.1x, 1.2x and 2 and 3 values

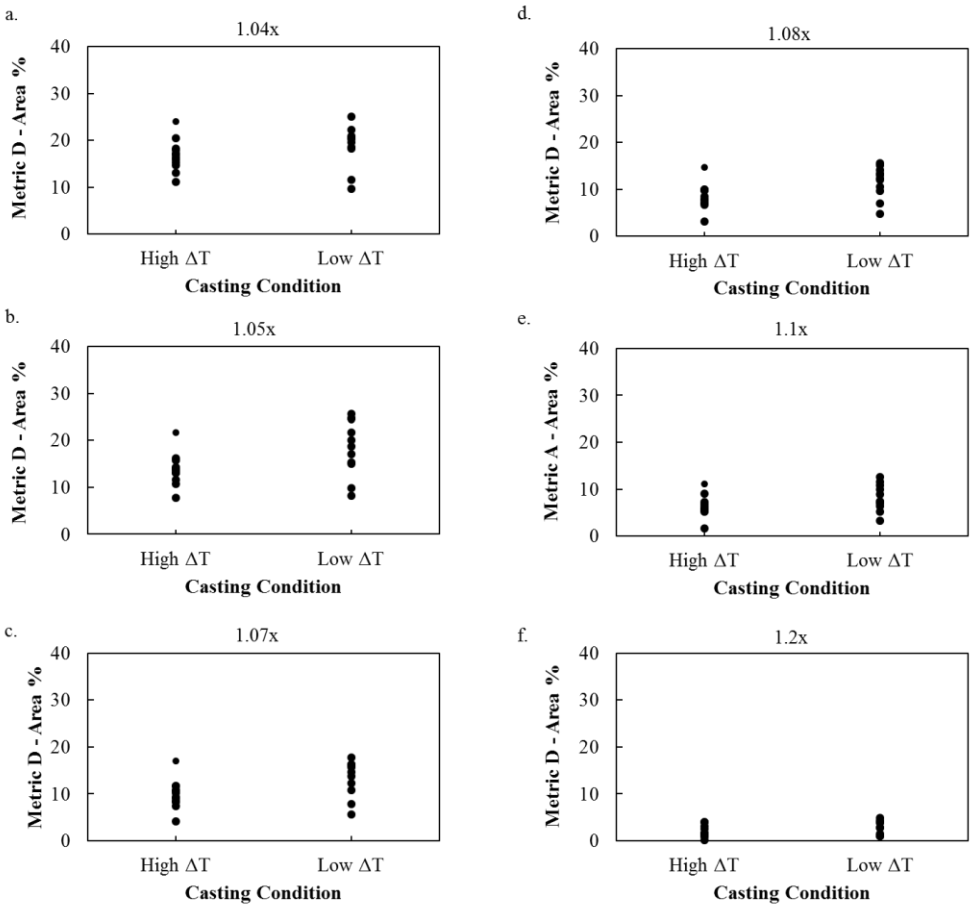

Figure 124 Metric D as a function of superheat for 1.5 Mn wt% using factors 1.04x, 1.05x, 1.07x, 1.08x, 1.1x and 1.2x